Communications Research Centre Canada
An Agency of Industry Canada

Centre de recherches sur les communications Canada
Un organisme d'industrie Canada

Compact Dielectric-Loaded Patch Antennas For L-Band Mobile Satellite Applications

by Sara M. Stout

Advanced Antenna Technology

CRC Report No. CRC-RP-2000-003
January 27, 2000

Canada

CRC

Compact Dielectric-Loaded Patch Antennas For L-Band Mobile Satellite Applications

By Sara M. Stout

Advanced Antenna Technology

CRC Report No. CRC-RP-2000-003
January 27, 2000

Abstract

In this work, a novel dielectric-loaded patch antenna is presented as a technique to miniaturize a microstrip antenna while maintaining a fairly wide impedance bandwidth. It consists of an aperture-coupled microstrip patch suspended above a ground plane and loaded with high permittivity dielectric pieces. The dielectric loading enhances the coupling from the aperture and perturbs the fields beneath the patch. Its resonant frequency is reduced therefore resulting in a smaller patch at lower frequencies. This configuration was developed at L-band frequencies for use in mobile satcom applications.

A detailed characterization of a linearly polarized prototype was performed and the effect of varying the dimensions, permittivity, and location of the dielectric load pieces was investigated. Experimental results revealed that frequency reductions on the order of 30% compared to the conventional patch antenna could be achieved with impedance bandwidths greater than 8%. A circularly polarized prototype was also developed and the effect of loading on the quality of the CP was investigated. Testing this structure revealed that frequency reductions on the order of 35% were possible with impedance bandwidths just under 8%.

This investigation demonstrates the potential for the dielectric-loaded patch antenna as a suitable candidate for mobile satcom applications.

Table of Contents

List of Tables

List of Figures

List of Abbreviations and Acronyms

Chapter 1:

INTELSAT	International Telecommunications Satellite System
satcom	Satellite Communications
ICO	Intermediate Circular Orbit Satellite Based Mobile
MSAT	North American Mobile Satellite System
INMARSAT	International Maritime Satellite Organization
GHz	Gigahertz

Chapter 2:

GEO	Geostationary Earth Orbiter
GPS	Global Positioning System
EIRP	Effective Isotropically Radiated Power
RHCP	Right Hand Circular Polarization
DRA	Dielectric Resonator Antenna
MMIC	Monolithic Microwave Integrated Circuits

Chapter 3:

EM	Electromagnetic
TM	Transverse Magnetic
AF	Array Factor
CP	Circular Polarization
LHCP	Left Hand Circular Polarization

Chapter 4:

HP HFSS	Hewlett Packard High Frequency Structure Simulator
3D	Three Dimensional
2D	Two Dimensional
VSWR	Voltage Standing Wave Ratio
CCW	Counter-Clockwise
CW	Clockwise
HP	Hewlett Packard
CoPol	Co-polarization
Xpol	Cross-polarization

Chapter 5:

DUT	Device Under Test
ADS	Advanced Design System

List of Symbols

Chapter 2:

C/No	Carrier-to-noise power density ratio
G/T	Ratio of system gain to system noise temperature

Chapter 3:

λ_o	Free space wavelength
h	Thickness of patch substrate
E_r	Relative permittivity
E_x	x-component of electric fields
H_y	y-component of magnetic fields
H_z	z-component of magnetic fields
R	Radial coordinate
θ	Elevation coordinate
ϕ	Azimuthal coordinate
Q	Quality factor of antenna
δ_{eff}	Effective loss tangent
TM^x	Transverse magnetic to the x direction
A_{mnp}	Constant resulting from solution of homogeneous wave equation
k_x, k_y, k_z	Wavenumbers in the x, y, z directions respectively
μ	Permeability
ω	Radian frequency
E_y	y-component of electric fields
E_z	z-component of electric fields
H_x	x-component of magnetic fields
$\mathbf{J}_s$	Equivalent electric current density (vector)
$\mathbf{M}_s$	Equivalent magnetic current density (vector)
J_t	Equivalent electric current density on top surface of patch
J_b	Equivalent electric current density on bottom surface of patch
n	Unit vector normal to the surface
E_ϕ	Phi component of electric field
E_R	Radial component of electric field
E_θ	Azimuthal component of electric field
j	Complex number symbol: $j = (-1)^{0.5}$
k_o	Propagation constant
Y_1	Equivalent admittance at slot #1
B_1, B_2	Susceptance
G_1, G_2	Conductance
Z_c	Characteristic impedance
R_{in}	Input resistance

E_{reff}	Effective relative permittivity
L_{eff}	Effective length
f_r	Resonant frequency
μ_o	Permeability of Free Space
E_o	Permittivity of Free Space
Y_b	Admittance due to back radiation
Y_a	Antenna admittance
Y_S	Total admittance
Y_e	Admittance of higher order modes
Z_L	Impedance of the matching stub
Z_{in}	Input impedance
N	Turns ratio
τ	Loss free region
$\mathbf{E}_1$	Electric fields of original cavity (vector)
$\mathbf{H}_1$	Magnetic fields of original cavity (vector)
$\mathbf{E}_2$	Electric fields of perturbed cavity (vector)
$\mathbf{H}_2$	Magnetic fields of perturbed cavity (vector)
ΔEr	Small change in relative permittivity
$\Delta\mu$	Small change in permeability
ω_1	Radian Frequency of original cavity
ω_2	Radian Frequency of perturbed cavity
$\mathbf{E}_1^*$	Conjugate of E_1 (vector)
$\mathbf{H}_1^*$	Conjugate of H_1 (vector)

Chapter 4:

t	Thickness of substrate
tan δ	Loss tangent
Ω	Ohm
S_{11}	S-parameter indicating forward reflection (return loss)
r	Normalized resistance on the Smith Chart

Chapter 5:

f_o	Desired operating frequency of the loaded patch
f_x	Frequency required to achieve desired one
f_{feed}	Frequency to design feed network
mil	Thousandth of an inch

CHAPTER 1: Introduction

1.1 Target Application and Current Challenges

1.1.1 Overview

Since the launch of INTELSAT I, nearly 35 years ago, the world has witnessed an explosive growth in the area of satellite communications (satcom). As technological innovations progressed, the global satcom market expanded and it is now capable of providing access to all types of information from virtually anywhere on the planet.

Many of the proposed satellite systems today, such as ICO and Ellipso, are focused on personal mobile communications, where individuals will be able to access a satellite with a very small handset. The system targeted for this research work, however, is more related to vehicle satcom applications where the mobile terminals are mounted on cars, trucks, ships, airplanes, or trains. These applications most commonly involve geostationary satellites, as used in the MSAT and INMARSAT systems, and are aimed at improving the navigation, tracking, and safety of the vehicles.

1.1.2 Vehicle Antenna Design Challenges

The vehicle-mounted antenna constitutes one of the weakest links in mobile satcom systems and is therefore an area of considerable research. These antennas, operating at L-band frequencies (between 1.5 and 1.6 GHz), must meet stringent mechanical and electrical specifications.

The mechanical requirements are straight-forward; the antenna must not disturb the aesthetics or the aerodynamics of the vehicle which forces it to be very low-profile,

have a compact size, and be light-weight. Electrically, the most difficult task is to combine circular polarization with a wide impedance bandwidth and low-angle beam coverage. Achieving the mechanical and electrical requirements simultaneously is particularly difficult since a number of the electrical parameters are dependent on the physical dimensions of the antenna. Electrical performance is thus often sacrificed to make the antennas smaller.

There are several possible candidates for vehicle antennas including the quadrifilar helix, the crossed-drooping dipole, and the microstrip patch. The helix and the dipole both have excellent electrical performance but are far too tall to be mounted on a vehicle. The microstrip patch antenna, although it satisfies the low profile requirement in its conventional form, suffers from a poor bandwidth and tends to be quite large at L-band frequencies.

1.1.3 Motivation for Dielectric-Loaded Patch Structure

Microstrip patch antennas offer a number of attractive advantages over the previously mentioned candidates. They are the lightest-weight, the lowest-profile, and can be easily conformed to different surfaces. Manufacturing is relatively simple and integration with other printed circuits makes them low-cost. For these reasons, many researchers have tried to develop innovative ways to both reduce the size of the microstrip patch as well as increase the bandwidth.

The most common method of miniaturization has been by shorting the patch in the plane where the electric fields are minimum. This was successful at reducing the patch dimensions by about half but obtaining circular polarization was quite difficult since the orthogonal mode cannot exist on the shorted boundary. The research carried out

in this thesis was focused on dielectric-loading the patch antenna to achieve miniaturization in such a way that circular polarization would still be possible and the impedance bandwidth would meet the satcom requirement.

The idea was to decrease the resonant size of the patch by strategically loading the patch cavity with small pieces of dielectric material. The resulting dielectric-loaded patch structure overcomes both the dimension and bandwidth problems of the conventional patch antenna and, as such, is a viable candidate for mounting on a vehicle in mobile satcom applications.

1.2 Thesis Objective

The overall objective of this thesis was to investigate dielectric-loading as a technique to miniaturize a microstrip patch antenna and hence make it a more suitable alternative to helices and crossed dipoles for mobile satcom applications.

A detailed characterization of a linearly polarized dielectric-loaded patch antenna was to be performed to determine the effects of each physical parameter in the structure. Emphasis was to be placed on observing how the frequency reduction, matching ability, and bandwidth could be controlled and used to enhance the antenna's performance. Design guidelines were to be developed from the trend information and tested to assess their practicality.

In order to ensure that this antenna would be viable for mobile satcom applications, the effect of dielectric-loading on the quality of the circular polarization was also to be evaluated, though not investigated in detail.

1.3 Thesis Organization

The thesis is organized in the following manner. The second chapter briefly outlines the important background information leading into a detailed discussion of the motivation for the development of this novel antenna. Mobile satcom applications are reviewed as well as the current antenna candidates under consideration. This chapter concludes by introducing the dielectric-loading concept.

The third chapter presents the theory behind the dielectric-loaded patch antenna. Microstrip patch radiation mechanisms are reviewed and the cavity model is presented in significant detail. Current methods of achieving patch miniaturization are outlined followed by a description of perturbation theory and how it relates to dielectric-loading.

The fourth chapter encompasses the main body of the work in this thesis. It describes, in detail, the experimental characterization of the dielectric-loaded structure. Details on how the prototype was designed and fabricated are outlined and the measurement methodology is presented as well as the observed trends. This chapter concludes with a comparison between some of the simulated and measured results.

The fifth chapter begins with the development of a set of guidelines for designing a linearly polarized dielectric-loaded patch. Using these guidelines, a prototype antenna was developed and measured. The results of this design are presented and the validity of the guidelines is discussed. The remaining half of the chapter focuses entirely on the circular polarization investigation.

CHAPTER 2: Background

2.1 Introduction

This chapter will provide an introduction to mobile satellite communications and outline some of the major challenges and technical difficulties in the development of vehicle antennas. After a review of the satellite services in operation today, the discussion will focus on the antennas currently under consideration for these systems with a detailed examination of their advantages and disadvantages. Finally, the dielectric-loaded patch antenna structure will be revealed and presented as a future candidate for mobile satcom applications.

2.2 Current Mobile Satellite Communication Services

Mobile satellite services relay communications through satellites to and from mobile vehicles such as cars, trucks, ships, and airplanes. Unlike cellular telephone technology, where a user moves through cells, mobile satellite services rely on satellites overhead of a user. The satellite thus functions as a "cellular tower" in the sky where, in the case of geostationary Earth orbiters (GEOs), at least three satellites are required to provide coverage over the entire planet, excluding the polar regions. The goal of these systems is to have communication capability for anyone at anytime and from anywhere with any kind of information.

The concept of mobile satellite services is not new. Ships, airplanes and trucks have relied on GEOs to provide these services for years. With the rapid growth of wire-

less communications, many new avenues are opening for mobile satellite applications. The following are some examples of applications currently under consideration [1]:

- On-board navigation systems for vehicles,
- Embedded GPS systems (GPS in other systems such as cell phones),
- Air traffic management systems [2],
- Global tracking services [3].

The three current satellite contenders for these types of applications are MSAT, INMARSAT, and Iridium. MSAT is the North American geostationary mobile satellite system that began providing the United States and Canada with an unprecedented range of innovative mobile services in 1995. This satellite is dedicated to providing service for mobile telephone, radio, facsimile, paging, position location, and data communications for users on land, at sea, and in the air. Communications between mobile users and the satellites are accomplished at L-band frequencies while terrestrial feeder stations use Ku-band frequencies to communicate.

INMARSAT, originally known as the International Maritime Satellite Organization, is now a group in control of an international mobile satellite communication system [4]. The INMARSAT system became operational in 1981 and, with its nine geostationary satellites, it now provides mobile communications world-wide. INMARSAT's primary interests have been in providing services in the area of maritime safety including the distress call for ships at sea. The communications link between the mobile terminal and the satellite is at L-band frequencies.

The Iridium system, designed by Motorola, is one of the newer commercial satellite systems launched in 1997. It comprises a constellation of 66 low-Earth-orbit satellites

and uses L-band frequencies to provide global communications services through portable handsets. The Iridium phones and pagers are intended to work anywhere in the world by communicating with both terrestrial wireless networks as well as the satellites in orbit.

2.3 Current Antenna Candidates for Mobile Satcom

2.3.1 Vehicle Antenna Requirements

In implementing mobile satellite communications, the vehicle antenna is one of the most important technologies to consider. The system requirements for these antennas can be classified as follows [5,6]:

- Mechanical characteristics,
- Electrical characteristics,
- Propagation and environmental conditions.

2.3.1.1 Mechanical Characteristics

The mechanical requirements for vehicle antennas vary depending on the actual vehicle under consideration but, in general, they must be compact and light-weight. The mechanical strength of the installation is also an important factor and should be considered carefully in the design and evaluation of such antennas.

Although antennas intended for ships are subject to a harsh sea environment, they have far less stringent installation requirements than antennas intended for aircraft or cars. Ships generally have ample space to install relatively large antennas and aerodynamics is not a major concern. In the case of cars, however, the antennas must be low-profile and light-weight in order to disturb neither the aesthetics nor the aerodynamics of the car. Antennas designed for aircraft must satisfy more stringent standards than most

other vehicles due to the severe conditions they encounter and the need to minimize air drag.

2.3.1.2 Electrical Characteristics

The electrical characteristics of vehicle antennas are restricted by the mechanical requirements. A compact antenna implies that its gain will be low since the gain of an antenna is theoretically determined by its physical dimensions. Also, a more compact antenna will have a wider radiation pattern beamwidth. This means that the antenna is susceptible to interference from undesired signals.

To meet the mechanical requirements of being compact and light-weight, the vehicle antenna's electrical weaknesses must be compensated by having a large antenna with high power located on the satellite. The electrical requirements for vehicle antennas are thus determined primarily by the capability of the antenna on the satellite in orbit. A high gain satellite with a large effective isotropically radiated power (EIRP) and good receiver sensitivity would permit the fabrication of compact and light-weight antennas in mobile terminals.

MSAT, as well as INMARSAT-C (third generation), both provide higher satellite capability than older systems thus allowing for the design of relatively compact vehicle antennas. Since the characteristics of these two systems are similar, each demands similar requirements for vehicle antennas. These specifications are outlined in Table 2.1 [6].

L-band frequencies are used in almost all present systems for the communication link between the satellite and the mobile terminal on earth. Since the signal is transmitted at 1.6 GHz and received at 1.5 GHz, an 8% impedance bandwidth is required to cover

both bands. This is a difficult specification to meet with most compact antennas and is an area of significant research.

Specification	MSAT/INMARSAT-C
Frequency	L-band
Impedance Bandwidth	8%
Gain	12-15 dBi (voice/high-speed data) 0-4 dBi (low-speed data)
Elevation Coverage	0-90 degrees (tracking required for high gain case)
Azimuth Coverage	0-360 degrees (tracking required for high gain case)
Polarization	RHCP
Axial Ratio	<5 dB

Table 2.1: Mobile Terminal Antenna Specifications

The required antenna gain is determined by a link budget which takes into account the satellite capability and the required channel quality. The channel quality is represented mathematically as the carrier-to-noise power density ratio (C/N_o) and depends on the receiving capability and EIRP of both the satellite and the mobile terminal.

Depending on the satellite system, different levels of gain are required ranging from 24 dBi in high gain systems to less than 4 dBi in low gain systems. There are no exact definitions to differentiate between low, medium, and high gains, but present and upcoming L-band mobile satcom systems will have gains classified as shown in Table 2.2.

Gain Class	Antenna	Typical Gain (dBi)	Typical Antenna (el. = elements)	Typical Service
High	Directional	20-24	Dish (1 m)	Voice/high-speed data
High	Directional	17-20	Dish (0.8 m)	Ship (INMARSAT-A,B)
Medium	Semi-directional (only in azimuth)	8-16	Short Backfire (0.4 m) Phased array (20 el.)	Voice/high-speed data Aircraft (INMARSAT)
Medium	Semi-directional (only in azimuth)	4-8	Array (2-4 el.) Helix, patch	Ship (INMARSAT-M) Landmobile
Low	Omnidirectional	0-4	Quadrifilar Drooping dipole Patch	Low-speed data Ship (INMARSAT-C) Landmobile

Table 2.2: Classification of L-band Antennas [5]

Since the satellites in these systems are in a geostationary orbit, they appear to have a stationary location in the sky with respect to the mobile user. In northern and southern latitudes, the satellite will appear at low elevation angles requiring that the vehicle antennas provide adequate gain at these angles. In order to avoid tracking, low gain antennas with hemispherical pattern coverage are required. Higher gain antennas, for improved link margins, have narrower beam patterns and therefore require tracking capabilities.

To avoid polarization tracking, mobile satellite communication systems use circularly polarized waves. The reason for this becomes clear by considering briefly a linearly polarized system. If both the satellite and the mobile vehicle terminal were linearly polarized, either vertically or horizontally, the vehicle antenna would have to keep the exact same polarization as the antenna on the satellite. If the direction of the electric-fields generated by the vehicle antenna rotate by 90 degrees with respect to the polarization of the satellite, then the mobile will not receive any signals from the satellite. Using circularly polarized antennas avoids this problem for the most part but polarization mismatch loss must be taken into account. To keep the mismatch loss below 0.5 dB, the axial ratio of vehicle antennas must be kept under 5 dB in all directions.

Other factors to consider include the ratio of system gain to system noise temperature (G/T), which determines the level of the weakest signal that can be received, and the antenna's EIRP, defined as the sum of the antenna gain and output power of the high power amplifier. However, since this thesis is focused on the antenna and not the entire system, these two parameters were not included in the investigation.

2.3.1.3 Propagation and Environmental Considerations

The location of the vehicle antenna is important in mobile satellite communication systems. Having line-of-sight capability and avoiding signal degradation through the propagation environment are both serious considerations that must be accounted for in any vehicle antenna design.

Maritime applications, for example, suffer from sea reflections and blocking caused by superstructures such as masts and other antennas. In aeronautical applications, fading caused by the fuselage was found to be more significant than even the sea reflection fading. Land mobile applications, on the other hand, are limited by shadowing and blocking effects caused by trees, buildings, and the shape of the terrain. Research is thus currently being conducted in these areas and is focused on methods of minimizing the effects [7,8].

2.3.2 Current Omnidirectional Antenna Candidates

High performance vehicle antennas are needed to provide the required satellite communications link. If the vehicle antenna has a high gain then it has to track the satellite following both the vehicular and orbital motions. This is both difficult and expensive. On the other hand, if the vehicle antenna has low gain it will inevitably have less performance such as radiation power and receiving capability. This limits the overall communications link.

A significant amount of research over the last decade has been concentrated on the development of low gain omnidirectional antennas with improved capability and better performance [4, 5, 6, 9, 10]. The purpose of developing these antennas is to provide users with solutions that are simple, reliable, and low-cost. As discussed in section

2.3.1.2, these types of antennas provide gains from 0 to 4 dBi and do not require satellite tracking capability. There are four basic antenna types in the omnidirectional family which have been considered as possible candidates for vehicle antennas:

- Quadrifilar helix,
- Crossed-drooping dipole,
- Microstrip patch antenna,
- Dielectric resonator antenna (DRA).

2.3.2.1 Quadrifilar Helix

The quadrifilar helix antenna [11] is composed of four identical helices wound, equally spaced, on a cylindrical surface as illustrated in Figure 2.1. The helices are fed with signals that have equal amplitude but are 0, 90, 180, and 270 degrees in relative phase. Generally, for mobile satcom applications, the quadrifilar helix stands about 40 cm high and provides a minimum gain of –4 dBi and a 3-dB maximum axial ratio over continental United States, from zenith to the horizon [12].

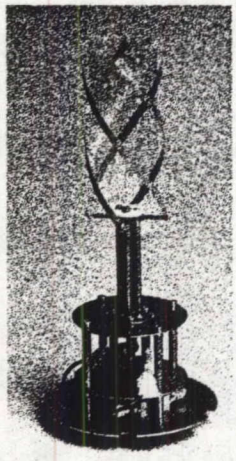

Figure 2.1: Quadrifilar Helix (from [12])

The quadrifilar helix builds on the benefits of the unifilar helix which inherently generates circularly polarized waves without an external feed network and has a wide impedance bandwidth due to its travelling-wave mode of operation. The quadrifilar helix is more advantageous since it has an even larger impedance bandwidth and the axial mode of operation occurs at a lower frequency. The main disadvantages of the quadrifilar helix, however, are that the feed network requires extra complexity and that the ground plane must be larger.

2.3.2.2 Crossed-Drooping Dipole

The crossed-drooping dipole antenna is well suited to land mobile satellite applications where the required angular coverage is narrow in elevation and is almost constant in azimuth. The crossed-dipole configuration consists of two half-wave dipoles which are set in a cross formation geometrically orthogonal to one another as shown in Figure 2.2(a). Since a single dipole antenna radiates linearly polarized waves, two crossed-dipole antennas, fed in phase quadrature, are used to generate circularly polarized waves.

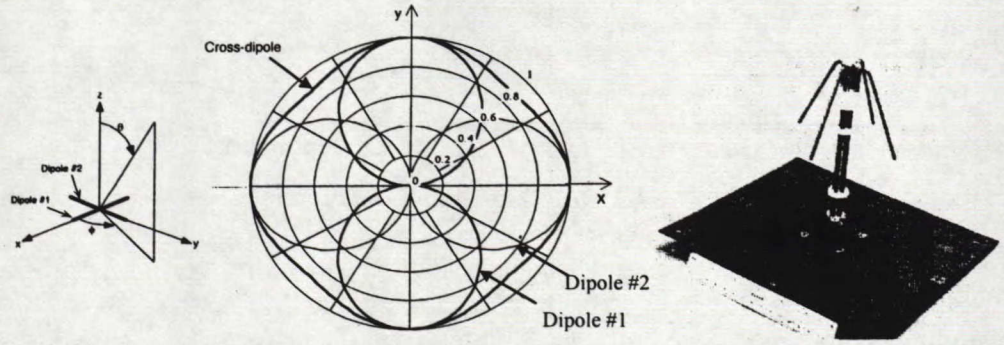

(a) (b) (c)

Figure 2.2: (a) Crossed Dipole, (b) Patterns, (c) Crossed-Drooping Dipole (from [1,6])

The radiation pattern of the crossed-dipole, shown in Figure 2.2(b), is nearly omnidirectional in the horizontal plane. The maximum gain of this structure is at boresight

(z-axis) but can be optimized to have higher gains at lower elevations by bending the dipoles toward the ground as shown in Figure 2.2(c). This also helps to increase the circular polarization at low elevations. The distance between the ground plane and the dipoles affects the pattern shape of the overall antenna. By adjusting this height and the bending angle of the dipoles, the designer has control over both the gain and elevation patterns. Generally, for mobile satcom applications, the dipole stands about 15 cm above the ground and achieves a minimum gain of 4 dBi and a maximum axial ratio of 6 dB over continental United States, between zenith and the horizon [12].

2.3.2.3 Microstrip Patch Antenna:

Microstrip antennas are also being considered for mobile satellite communication systems. This type of antenna, as shown in Figure 2.3, consists of a metallic patch, most commonly square or circular, supported by a dielectric substrate over a ground plane.

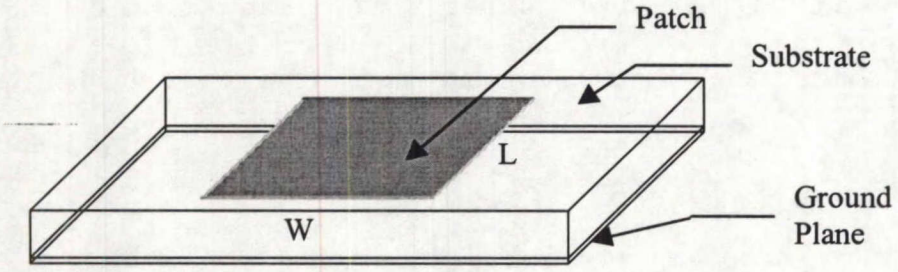

Figure 2.3: Microstrip Patch Antenna

The main advantage of microstrip antennas is that they are very low-profile and light-weight as compared to the helix and dipole discussed above. These antennas can be designed to produce a wide-broadside beam (like the dipole) or an omnidirectional beam depending on the mode of excitation.

In order to produce circular polarization, the patch antenna is generally excited at two points orthogonal to each other and fed with signals equal in amplitude and 90 degrees out of phase. A typical circular microstrip antenna used in satcom applications will stand about 1 cm above the ground and achieve a minimum gain of 3.5 dBi and a maximum axial ratio of 4 dB over continental United States, between zenith and the horizon [12].

Simple microstrip patch antennas have relatively narrow impedance bandwidths (2-3%) and are thus not operational over both the transmit and receive bands of mobile satellite systems. Many attempts have been made to increase the bandwidth of these antennas. Three ways that have been successful are increasing the dielectric thickness, decreasing the dielectric constant, and stacking one patch above the other. Using a thick-air dielectric substrate of about 7 mm in height will yield an impedance bandwidth close to 8%. However, the dimensions of such an antenna at L-band frequencies are L=W=80 mm, which is fairly large. Another problem with this bandwidth enhancement technique is that probe-coupling is required to feed the patch on the thick-air substrate. The probe tends to radiate under these conditions which leads to high cross-polarization levels and a degradation in the circular polarization.

Significant size reductions have been accomplished by strategically placing shorting posts [13,14] and using high dielectric constant substrates [15]. However, these methods tend to make the impedance bandwidth even smaller and do not lend well to generating circular polarization. Researchers have proposed many ways to reduce the size of the patch and still maintain the required impedance bandwidths. Suggestions range from an annular-ring loaded, shorted-patch antenna [16, 17] to dielectric-

resonator-loaded patch configurations [18] in which a dielectric resonator is strategically placed on top of a patch. Other configurations have also been suggested but, to date, a compact microstrip patch antenna that meets all of the required electrical specifications has not been achieved.

2.3.2.4 Dielectric Resonator Antenna (DRA):

Dielectric resonator antennas [19] are relatively new alternatives to the conventional technologies described above. As illustrated in Figure 2.4, they are open resonant radiating structures fabricated from low-loss dielectric materials (tan δ = 0.0001 to 0.002) which are formed into any one of a number of shapes including rectangular, circular disk, ring, cross, triangular, or hemispherical.

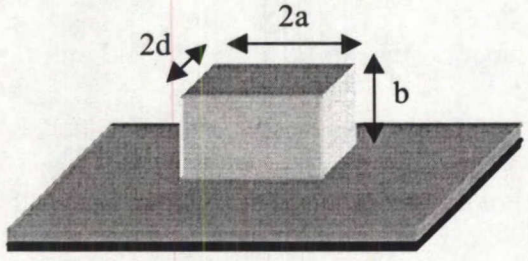

Figure 2.4: Rectangular Dielectric Resonator Antenna

The resonant frequency of the DRA is determined from its size, aspect ratio, and the relative permittivity of the dielectric material. DRAs are free from conduction losses since they are non-metallic, thus yielding higher radiation efficiencies. Another advantage is that they have inherently wide impedance bandwidths (5-15%) which can be achieved without exciting surface waves.

DRAs offer more flexibility than microstrip patches in that a wide range of relative permittivities can be selected to optimize their size. At L-band frequencies, however,

a permittivity of about 10 is required to achieve an impedance bandwidth of 8%. This forces the DRA dimensions to be on the order of 2a=50 mm, 2d=50 mm, b=32 mm [20] which is clearly not as low-profile as the microstrip patch dimensions detailed above. The height can be reduced to some degree but that comes at the expense of much larger width and transverse dimensions. The DRA calculations and associated design equations leading to the values above are outlined in Appendix 1.

2.4 Novel Antenna for Low Gain Applications

Since satellite tracking is both undesirable and expensive, the design focus of recent years has been directed primarily towards low gain omnidirectional antennas. As outlined above, the design of these structures is an interesting challenge at L-band frequencies and current candidates do not satisfy simultaneously all of the system requirements.

The quadrifilar helix and the crossed-drooping dipole meet most of the electrical parameters but are far too high in profile. DRAs can also satisfy the electrical specifications but they too are excessively high and large at L-band frequencies. Microstrip patch configurations, on the other hand, are the only antennas that meet the low-profile requirement. They are also the lightest-weight of all the proposed candidates and are easily fabricated and used with monolithic microwave integrated circuit (MMIC) technology. To achieve the required impedance bandwidth of 8% they require thick substrates with low dielectric constants. This forces both the transverse dimensions and the height of the patch to be larger and leads to radiation problems when fed with a probe.

Given the many advantages of the microstrip patch, much research has been devoted to developing creative ways to both reduce the dimensions and widen the band-

width of the patch. The work of this thesis focused on one such innovative patch miniaturization method, that being dielectric-loading.

Preliminary investigations on the novel dielectric-loaded patch antenna have produced results of particular interest. The structure is effectively a miniaturized microstrip patch antenna which overcomes the dimension and bandwidth problems of the current candidates. Miniaturization is accomplished by placing pieces of dielectric in strategic locations underneath a patch that is fed via aperture-coupling, as illustrated in Figure 2.5.

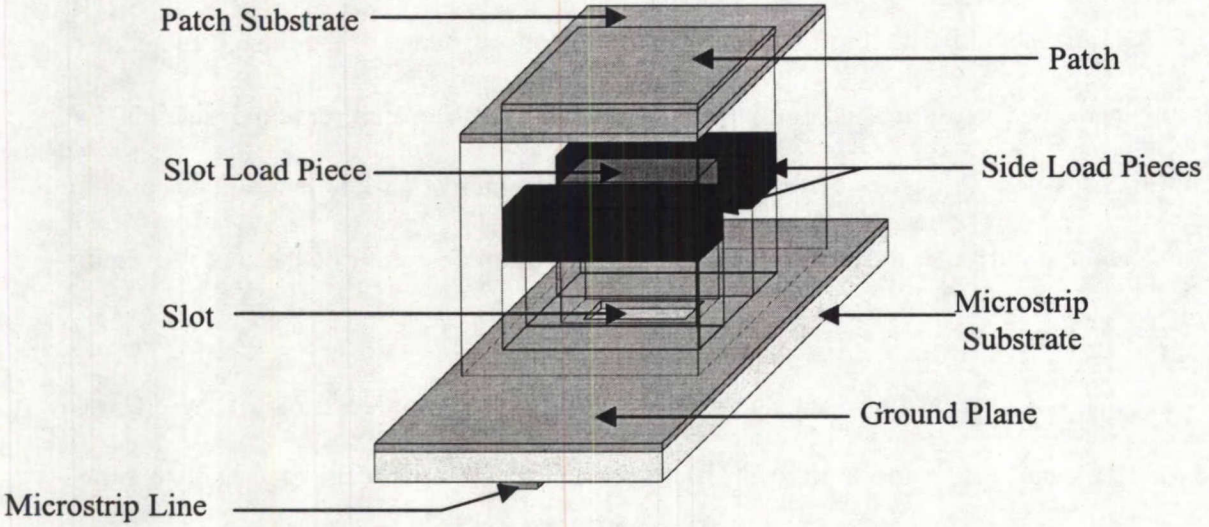

Figure 2.5: The Dielectric-Loaded Patch Antenna Basic Configuration

In this way, the fields between the patch and the ground plane are perturbed and the operating frequency of the patch antenna is lowered, thus enabling a smaller patch size to be used at lower frequencies. This novel antenna makes use of the low-profile and light-weight advantages of microstrip antennas and is theoretically capable of good circular polarization performance.

CHAPTER 3: Theory

3.1 Introduction

The intent of this chapter is to examine the theoretical background information required for the design and analysis of the dielectric-loaded patch antenna described at the end of the second chapter. Since this novel structure builds on the advantages of microstrip antenna technology, a detailed presentation of microstrip patch theory will be presented with an emphasis on the cavity model as outlined by Balanis [21] and Bahl & Bhartia [22].

Current methods of achieving patch miniaturization will then be presented with an outline of their advantages and disadvantages. Finally, cavity perturbation theory will be described followed by an explanation of how it can be used to achieve a frequency reduction and hence a miniaturized microstrip patch.

It is important to realize that, due to the complexity of the structures under consideration, the theory presented in the following sections is approximate and dependent on several underlying assumptions. The insight gained in this process, however, is valuable and serves to better comprehend the problem.

3.2 Microstrip Patch Antenna Theory

Although the concept of microstrip radiators was first proposed as early as 1953 by Deschamps [23], it was not until the early 1970s that practical microstrip antennas were designed and implemented by Howell [24] and Munson [25]. Since then, theoretical models, photoetching techniques, and good low loss dielectric materials have been developed and the microstrip patch antenna has now reached an age of maturity. There are

many well tried techniques that can be relied upon and there are few mysteries left to discover about its behavior.

The topic of microstrip antennas is not static as the quest for more innovative designs coupled with reliable manufacturing methods is very much alive. The driving forces behind the active research is the thirst for lower-cost, lighter-weight, and more compact structures.

3.2.1 Microstrip Patch Antenna Basics

3.2.1.1 General Structure

A microstrip antenna consists of a very thin (thickness<<λ_o, the free space wavelength) metallic strip (patch) placed a small fraction of a wavelength (h<<λ_o) above a ground plane, as shown in Figure 3.1. The strip and the ground plane are separated by a low loss insulating material, the dielectric substrate, and the radiating patch element is usually photo-etched.

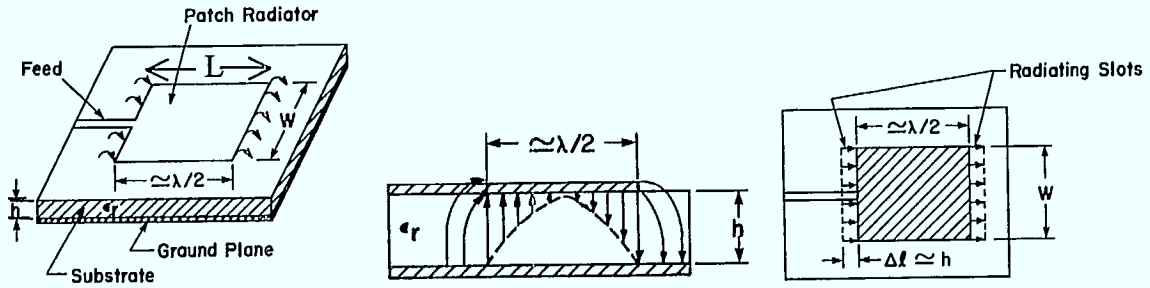

(a) *(b)* *(c)*

Figure 3.1: Microstrip Patch Structure (a) 3D, (b) Side, (c) Top views (from [22]) (Note that the arrows indicate the direction and magnitude of the electric fields.)

Although patches can take on many shapes such as square, rectangular, triangular, and circular, only the square patch will be discussed in the remaining part of this work. The square shape was chosen since it was well suited to the available dielectric-load pieces, as will become obvious in Chapter 4. The microstrip antenna is very low in pro-

file and, as such, can be used in applications where small size, light-weight, low cost, ease of installation, and high performance are required.

The dielectric substrate of the microstrip patch provides a stable support for the conductor strip and fulfills an electrical function by concentrating the electromagnetic fields beneath the patch. The degree of field concentration depends on the type of substrate since dielectric constants can vary in the range of $1 < E_r < 12$. Generally, it is more desirable in radiation problems to have limited field concentration so low permittivity substrates would be preferred. However, microstrip transmission-lines require a higher level of field concentration and therefore would perform better on substrates with higher permittivities. The microstrip antenna and the microstrip transmission-line have opposing requirements and, when used together on the same substrate, a compromise in the performance of both is necessary.

Thick substrates with dielectric constants in the lower end of the range provide good antenna efficiency with larger bandwidth but result in larger patch dimensions. The patch dimensions can be reduced by increasing the substrate permittivity but surface waves can become significant.

3.2.1.2 Surface Waves

Surface waves propagate along an interface between two different media and essentially deteriorate the microstrip antenna's performance. The surface waves that diffract off the edges of the microstrip structure contribute to increasing both side lobe and cross-polarization levels. Since they use up part of the signal's energy, they lead to a decreased antenna efficiency. Surface waves should therefore be suppressed wherever possible.

Due to its structure, consisting of a dielectric substrate together with a ground plane, the microstrip patch antenna can support dielectric slab-type modes with zero cut-off frequencies [26]. This means that, at any frequency of operation and at any discontinuity in the conducting strip of a microstrip line, such as an open circuit termination, the substrate surface waves will be launched.

The surface wave power typically decays at a rate slower than that of the space wave (radiated) since its phase velocity is less than that of the surrounding medium. The slow decay rate leads to phasing issues with the space waves when the surface waves are diffracted from the edges of the substrate, therefore contributing to increased cross-polarization levels and unwanted side lobes. Substrates that are thick with very high relative permittivities will support a higher number of surface waves that have a much lower speed of propagation than the space waves and will seriously affect the antenna's performance.

3.2.1.3 Basic Radiation Mechanism

The basic radiation mechanism of the microstrip patch antenna is best understood by considering the structure in Figure 3.1. Assuming that there is no variation of the electric fields along the width and thickness of the structure, the electric fields along the remaining dimension of the radiator are as indicated in Figure 3.1(b). This dimension is the patch length and, for efficient radiation, it should be about a half-wavelength long such that the fields are fringing at the open-circuited edges of the patch.

By resolving the fringing fields into normal and tangential components with respect to the ground plane, it becomes clear that the normal components will be out of phase with each other due to the half-wave dimension of the patch length and thus cancel

in the far field. The tangential components (those parallel to the ground plane) will be in phase with one another and thus combine in the far field to give a maximum radiated field normal to the surface of the patch. This principle is approximately illustrated in Figure 3.2.

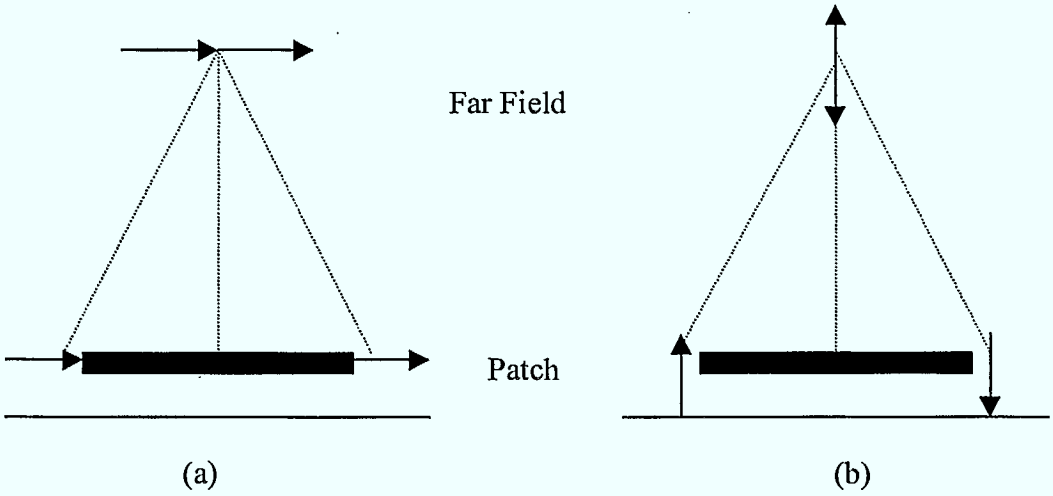

Figure 3.2: Components of the Fringing Fields (a) Tangential, (b) Normal

The microstrip patch can therefore be represented as two slots, spaced a half wavelength apart (Figure 3.1(c)) and excited in phase, such that radiation is broadside into the half space above the ground plane. The patch antenna can also be designed to have an end-fire radiation pattern where the pattern maximum is in the plane of the patch. The direction of the pattern maximum is dictated by the mode of excitation or field configuration beneath the patch.

3.2.2 Microstrip Patch Models

3.2.2.1 Overview

The electromagnetic (EM) fields of the microstrip structure are determined by solving Maxwell's equations subject to the appropriate boundary conditions. Though mi-

crostrip patches appear to be simple structures, the determination of the EM fields is made difficult by the following three complexities:

- The fields extend over different propagation media (air and dielectric), each having different properties.
- Different boundary conditions apply at different points on the surface due to the patch conductor being in one area and not in others.
- The dimensions of the structure are finite so that the edge effects caused by the surface waves cannot be neglected.

It is these complexities that make the microstrip antenna nearly impossible to solve analytically. Many simplified models were developed to ease the analysis and comprehension of the microstrip antenna behavior, each with underlying assumptions. Most of these models are only partially successful in predicting microstrip antenna performance and require considerable calculations [22].

Both the transmission-line and cavity models were used extensively in this work. The transmission-line model leads to adequate results for most design purposes and, although it is only applicable to rectangular or square patch geometries, it provides a set of useful design equations. The cavity model is not as simple as the transmission-line model but it provides more insight into the fields and radiation capability of the microstrip antenna. The cavity model will be described in significant detail. The transmission-line model will then be outlined, based on the interpretation of Balanis [21], and typical design equations will be presented.

3.2.2.2 Cavity Model Basics

3.2.2.2.1 Background

It was found that the fields within the dielectric of a microstrip antenna can be more accurately determined by treating the region as a *cavity* bounded by electric walls on the top and bottom and magnetic walls on the sides. The cavity model hinges on the basic assumption that the substrate thickness is much smaller than a wavelength so that the field variations along the height (*x*-directed as illustrated in Figure 3.3) will be considered constant. This assumption implies that the electric fields are nearly normal to the surface of the patch since the fields along the edges of the patch will be very small. The fields existing in the cavity are thus transverse magnetic (TM) to *x*, having only the E_x, H_y, and H_z components.

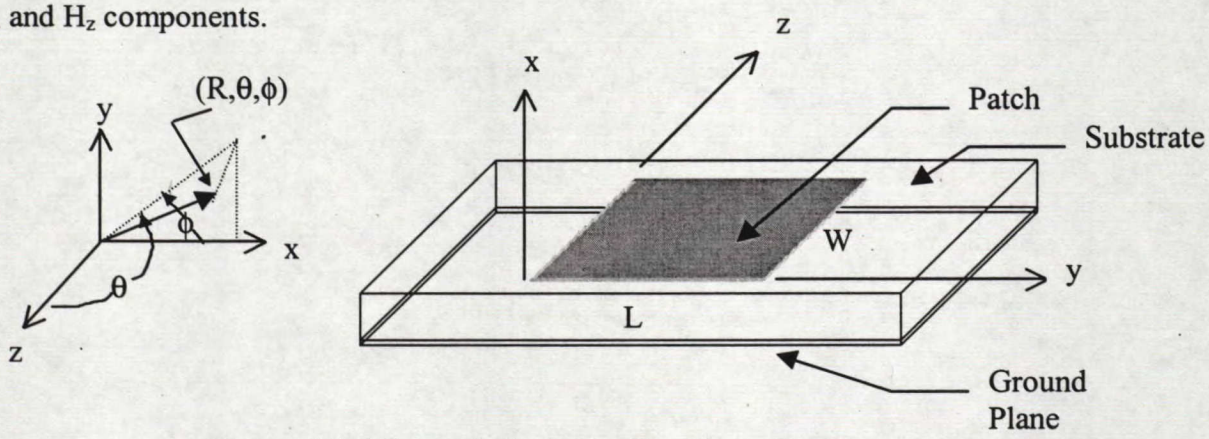

Figure 3.3: Microstrip Antenna Coordinate System

In this way, the fields in the antenna are assumed to be the same as those of a cavity and thus can be evaluated in a more simple manner. However, there is a problem with modeling the antenna as a cavity in that a lossless cavity does not radiate. The cavity model implies that the input impedance will be purely reactive and that it will not radiate any power. The model must therefore be modified to account for the radiating ability of

the antenna by including a loss component in the form of an effective loss tangent. This loss tangent is related to the quality factor of the antenna (Q) by the following equation:

$$\delta_{eff} = 1/Q \qquad (3\text{-}1)$$

3.2.2.2.2 Field Configurations

Considering only the TM^x modes within the cavity and assuming that the dielectric material comprising the substrate of the microstrip antenna does not extend past the edges of the patch, the vector potential approach [27] can be used to derive the field configurations. These resulting field equations are as follows where A_{mnp} is a constant and k_x, k_y, k_z, are the wavenumbers in the x, y, z directions respectively.

$$\begin{aligned}
E_x &= \frac{-j(k^2 - k_x^{\,2})}{\omega\mu E_r} A_{mnp} \cos(k_x x)\cos(k_y y)\cos(k_z z) \\
E_y &= \frac{-j(k_x k_y)}{\omega\mu E_r} A_{mnp} \sin(k_x x)\sin(k_y y)\cos(k_z z) \\
E_z &= \frac{-j(k_x k_z)}{\omega\mu E_r} A_{mnp} \sin(k_x x)\cos(k_y y)\sin(k_z z) \\
H_x &= 0 \\
H_y &= \frac{-k_z}{\mu} A_{mnp} \cos(k_x x)\cos(k_y y)\sin(k_z z) \\
H_z &= \frac{k_y}{\mu} A_{mnp} \cos(k_x x)\sin(k_y y)\cos(k_z z)
\end{aligned} \qquad (3\text{-}2)$$

Fringing fields were not taken into account in this cavity model. Their effect can be included when determining the resonant frequency of the cavity as will be done in Section 3.2.2.5 with the transmission-line model.

3.2.2.3 Equivalent Current Densities

Based on the cavity model, the four side walls of the truncated patch substrate can be thought of as slots or narrow apertures through which radiation occurs. Using Huygens' field equivalence principle [27], these slots can be represented by an equivalent electric current density ($\mathbf{J}_s$) and an equivalent magnetic current density ($\mathbf{M}_s$) which are related to the electric and magnetic fields at the slots by:

$$\begin{aligned} \boldsymbol{J}_s &= \hat{n} \times \boldsymbol{H}_a \\ \boldsymbol{M}_s &= -\hat{n} \times \boldsymbol{E}_a \end{aligned} \qquad (3\text{-}3)$$

Similarly, the patch can be represented by an equivalent current density, $\mathbf{J}_t$ on the top surface, and $\mathbf{J}_b$ on the bottom surface. When the ratio h/W is small, $\mathbf{J}_t$ is much smaller than $\mathbf{J}_b$ and so it can be set to zero. Also the tangential magnetic fields along the edges of the patch are ideally zero thus leading to having the side walls represented by magnetic walls. With these tangential magnetic fields very small, $\mathbf{J}_s$ will also be very small such that it too can be set to zero. $\mathbf{M}_s$ will therefore be the only remaining current density on the sides of the patch cavity.

Thus far, it has been assumed that the patch has been sitting on a ground plane. Using image theory [27] the presence of the ground plane can be accounted for by effectively doubling the magnetic current density such that $\mathbf{M}_s$ now radiates into an unbounded free space and is represented by:

$$\boldsymbol{M}_s = -2\hat{n} \times \boldsymbol{E}_a \qquad (3\text{-}4)$$

Since this equivalent magnetic current density is along all sides of the cavity, there are a total of four slots on the patch antenna. Based on the equivalence principle

[27], each slot radiates the same fields as a magnetic dipole having a current density defined by (3-4).

As illustrated in Figure 3.4, the current densities on slots #1 and #2 on the two walls separated by length L are both of the same magnitude and phase. They form a two element array of magnetic dipoles with a separation of L equal to about a half wavelength from each other. In the far field, these two sources will add in a direction normal to the patch and form a broadside pattern in the principal E-plane.

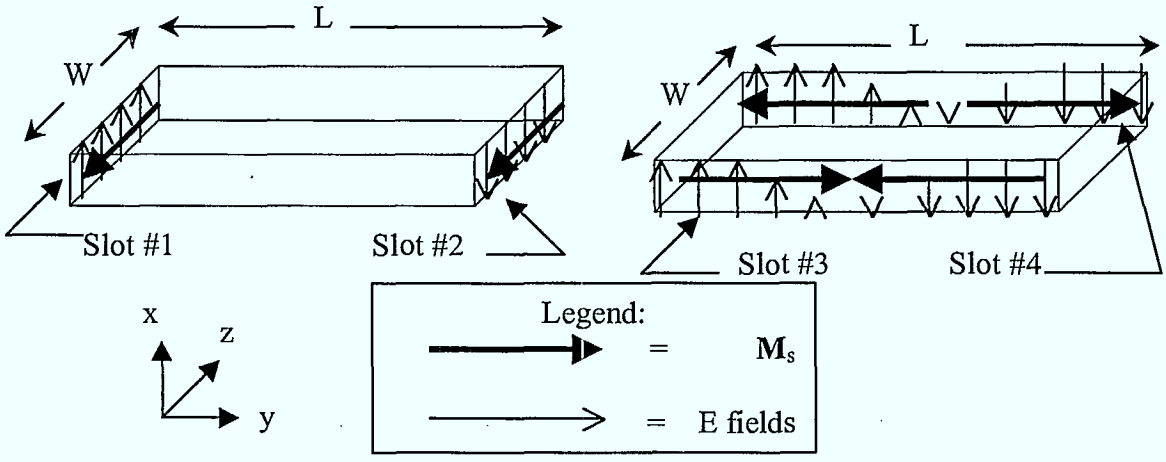

Figure 3.4: Radiating Slots on the Microstrip Patch

Different from slots #1 and #2, slots #3 and #4 *each* consist of two magnetic current densities that are of the same magnitude but are opposite in direction. The fields radiated from one side (say the left) of each slot will be canceled in the far field H-plane by the fields radiated from the other side (say the right) of the same slot. Also, since the slots on opposite walls are 180 degrees out of phase with each other, their radiation will cancel in the E-plane as well. It is for this reason that slots #3 and #4 are considered to be non-radiating. Figure 3.5 illustrates the typical E-plane and H-plane patterns.

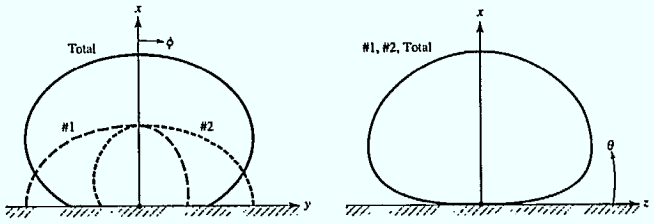

Figure 3.5: Typical E and H Plane Radiation Patterns (from [21])

3.2.2.4 Radiated Fields and Patterns

Although the slots #3 and #4 in Figure 3.5 are considered non-radiating, they do radiate away from the principal planes. This field intensity is very small, however, compared to the fields radiated by slots #1 and #2 so their effect will be neglected in this analysis. The total radiated field from the microstrip patch antenna is therefore the sum of the fields generated by the two elements in the array of magnetic dipoles representing the radiating slots. An array factor can be used for this calculation since the two slots are considered to be identical.

The phi (ϕ) component of the electric fields (E_ϕ) radiated by each slot in the far field, using the equivalent current density as in (3-4) and assuming that the radial and azimuthal components of the electric field (E_R and E_θ respectively) are approximately zero, is defined as follows [21]:

$$E_\phi = -j\frac{k_o h W E_o e^{-jk_o r}}{\pi r}\left[\sin\theta\left(\frac{\sin(\frac{k_o h}{2}\sin\theta\cos\phi)}{\frac{k_o h}{2}\sin\theta\cos\phi}\right)\left(\frac{\sin(\frac{k_o W}{2}\cos\theta)}{\frac{k_o h}{2}\cos\theta}\right)\right] \qquad (3\text{-}5)$$

From array theory, the array factor (AF) for two magnetic dipoles separated by a distance L in the y direction can be written as [21]:

$$AF = 2\cos\left(\frac{k_o L}{2}\sin\theta\sin\phi\right) \qquad (3\text{-}6)$$

To include the effects of fringing, an effective length can be used in (3-6) instead of the physical length as discussed in section 3.2.2.5. The total electric field of the array is obtained by multiplying (3-5) and (3-6) which yields the following equation for small values of h ($k_o h << 1$):

$$E_\phi = -j\frac{4hE_o e^{-jk_o r}}{\pi r}\left[\sin\theta\frac{\sin\left(\frac{k_o W}{2}\cos\theta\right)}{\cos\theta}\right]\cos\left(\frac{k_o L}{2}\sin\theta\sin\phi\right) \qquad (3\text{-}7)$$

From (3-7), E_ϕ can be determined in both the E and H planes by setting θ equal to 90 degrees, and ϕ equal to 0 degrees respectively. Plotting the resulting expressions will lead to the patterns shown previously in Figure 3.5. It should be noted that the cavity model does not take into account either the edge effects or the position of the feed.

3.2.2.5 Transmission-Line Model and Patch Design Equations

3.2.2.5.1 Model Basics

The transmission-line model is based on the microstrip antenna being represented as an array of two radiating slots each having a width (W) and a height (h) and the two being separated by a distance (L). The electric field in the slots is assumed to be constant and is characterized by the equivalent conductance of an open parallel plate waveguide.

The two slots are connected by a section of low characteristic impedance transmission-line one half guided wavelength long. For a square patch, the transmission-line equivalent model is depicted in Figure 3.6. B_1 and B_2 represent the susceptance of slots #1 and #2 respectively while G_1 and G_2 represent the associated conductances.

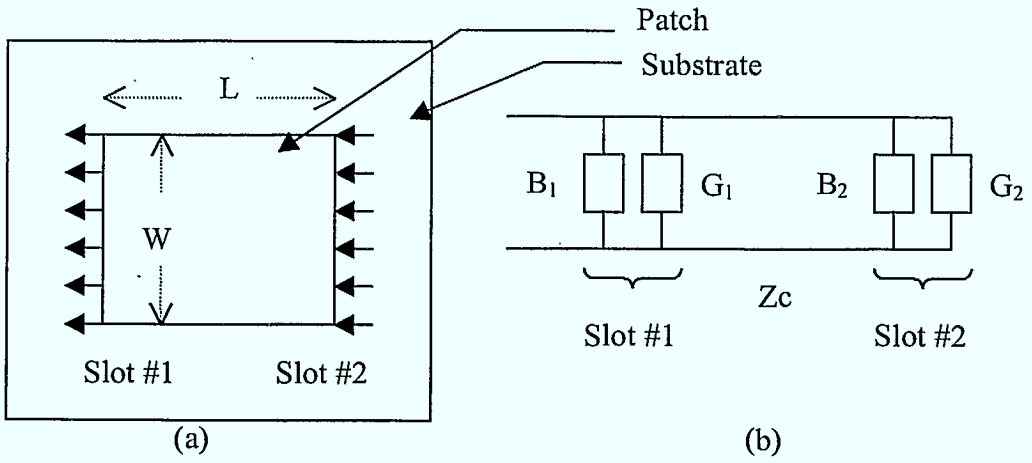

Figure 3.6: (a) Square Microstrip Patch and (b) Equivalent Transmission-line Model

The equivalent admittance of slot #1 is:

$$Y_1 = G_1 + jB_1 \qquad (3\text{-}8)$$

where, for a slot of finite width and assuming base metric units, the equations for G_1 and B_1 are [21]:

$$G_1 = \frac{W}{120\lambda_o}\left[1 - \frac{1}{24}(k_o h)^2\right] \quad \text{for } h/\lambda_o < 0.1 \qquad (3\text{-}9)$$

$$B_1 = \frac{W}{120\lambda_o}\left[1 - 0.636\ln(k_o h)\right] \quad \text{for } h/\lambda_o < 0.1 \qquad (3\text{-}10)$$

Since slot #2 is identical to slot #1, the two admittances are the same. An approximate value of G_1 can be found by using the field expressions derived in the cavity model [21]:

$$G_1 = \frac{1}{90}\left(\frac{W}{\lambda_o}\right)^2 \quad \text{for } W \ll \lambda_o \qquad (3\text{-}11)$$

$$G_1 = \frac{1}{120}\left(\frac{W}{\lambda_o}\right) \quad \text{for } W \gg \lambda_o \qquad (3\text{-}12)$$

3.2.2.5.2 Input Resistance

The resonant input resistance of the patch (R_{in}), as derived in [21] and neglecting mutual coupling effects, is obtained by transferring the admittance of slot #2 from the output terminals to the input terminals using standard transmission-line transformation equations. It is then given by:

$$R_{in} = \frac{1}{2G_1} \qquad (3\text{-}13)$$

The resonant input resistance can be changed by altering the width of the patch or by using an inset feed recessed a certain distance from slot #1. This method can be used to obtain a better match between a microstrip feedline and the patch antenna [21].

3.2.2.5.3 Design Equations that Account for Fringing

Because the dimensions of the patch are finite, the fields at the edges of the patch undergo fringing. The amount of fringing is a function of the dimensions of the patch and the height of the substrate. The effect of the fringing is to make the patch appear to be electrically longer than its physical dimensions. Accounting for the fringing is accomplished by introducing two quantities in the transmission-line model, the effective dielectric constant (E_{reff}), and the effective length (L_{eff}).

Since the microstrip antenna is non-homogeneous with fields propagating in both air and dielectric, the effective dielectric constant will have values in the range of $1 < E_{reff} < E_r$. As the frequency increases, the fields are more constrained in the substrate which means that the effective dielectric constant is independent on frequency. E_{reff} can be calculated using (3-14) with W/h>1 [21]:

$$E_{reff} = \frac{E_r + 1}{2} + \frac{E_r - 1}{2}\left[1 + 12\frac{h}{W}\right]^{-1/2} \qquad (3\text{-}14)$$

The effect of fringing on the electrical length of the patch is taken into account by increasing the effective dimensions of the patch by a distance ΔL on each end. This increase in length is a function of E_{reff} and the width-to-height ratio. An approximation to this extension is [21]:

$$\Delta L = 0.412(h)\frac{\left(E_{reff}+0.3\right)\left(\frac{W}{h}+0.264\right)}{\left(E_{reff}-0.258\right)\left(\frac{W}{h}+0.8\right)} \qquad (3\text{-}15)$$

The effective length of the patch thus becomes [21]:

$$L_{eff} = L + 2\Delta L \qquad (3\text{-}16)$$

where L is given by 3-17 and f_r is the resonant frequency.

$$L = \frac{1}{2f_r\sqrt{E_{reff}}\sqrt{\mu_o E_o}} \qquad (3\text{-}17)$$

For the dominant TM_{010} mode, the resonant frequency of the microstrip antenna, taking into account the above effects, is calculated using the following relationship [21]:

$$f_r = \frac{1}{2L_{eff}\sqrt{E_{reff}}\sqrt{\mu_o E_o}} \qquad (3\text{-}18)$$

Finally, a practical width that leads to good radiation efficiencies is [21]:

$$W = \frac{1}{2f_r\sqrt{\mu_o E_o}}\sqrt{\frac{2}{E_r+1}} \qquad (3\text{-}19)$$

where f_r is the resonant frequency of the antenna and E_r is the relative permittivity of the microstrip substrate.

The transmission-line model, though not as accurate as the cavity and perhaps other models, provides good physical insight into the design parameters. More elaborate

transmission-line models have been developed that account for substrate and conductor losses, aperture-coupling, and reactive effects [28,29]. These models enable the initial calculated results to better approximate the actual values.

3.2.3 Methods of Excitation

There are many configurations that can be used to feed microstrip antennas but the three most popular are the following [21]:

- Microstrip line,
- Coaxial probe,
- Aperture-coupling.

Each have some advantages and disadvantages which were weighed in the design decisions of this thesis. Aperture-coupling was the final chosen method of excitation and a more lengthy description will be presented for this type of feed.

3.2.3.1 Microstrip Line Feed

The microstrip line feed consists of a microstrip line extending from a connector to the patch and actually making contact with the patch. The microstrip line has a very small width compared to that of the patch and is generally simple to fabricate. Matching with this type of feed is achieved by insetting the microstrip line into the patch until the desired impedance is reached. Figure 3.7 illustrates the microstrip line feed configuration.

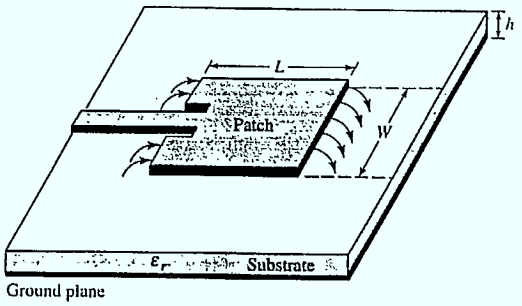

Figure 3.7: Microstrip Line Feed Configuration (from [21])

The primary disadvantage of this type of feed is that the microstrip line must often be on the same type of substrate as the patch antenna. As noted in section 3.2.1.1, the microstrip feedline and the microstrip patch require opposing substrate thickness and dielectric constant values in order to be optimal. For example, if the antenna requires a thick substrate, this will cause the surface waves in the feedline to increase and lead to spurious radiation. Another disadvantage is the inherent asymmetry since the feed network makes contact with only one side of the patch. Clearly, this type of feed will sacrifice the performance of the antenna.

3.2.3.2 Coaxial Probe Feed

Coaxial probe structures are configured such that the inner conductor of the coax is connected to the patch and the outer conductor connected to the ground plane as shown in Figure 3.8. This type of feed is also straight-forward to fabricate and matching is achieved by adjusting both the location and the width of the probe.

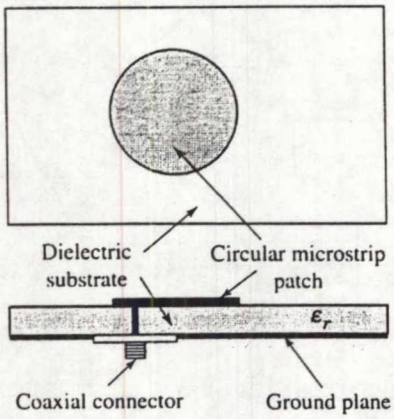

Figure 3.8: Coaxial Probe Feed Configuration (from [21])

The coaxial probe, however, suffers from similar asymmetries as the microstrip line feed since the probe will be located wherever the match is best. This can cause higher order modes to be generated, producing unwanted cross-polarized radiation. Another disadvantage of probe-coupling is that the probe can radiate thus making the H-plane cross-polarization levels quite high and causing a null to occur in the E-plane co-polarized patterns. This effect ultimately degrades the quality of circular polarization and is especially noticeable at L-band frequencies with patches sitting on thick-air substrates.

3.2.3.3 Aperture-Coupled Feed

3.2.3.3.1 Basics

Aperture-coupled feed configurations, originally proposed by Pozar [30], eliminate the asymmetry problems present in both the microstrip line and coaxial probe feed structures. This type of feed consists of two substrates separated by a ground plane. On the bottom side of the lower substrate, there is a microstrip feedline which has the form of an open-circuit stub while the top side of the upper substrate contains the microstrip

patch element. The energy is electromagnetically coupled from the feedline to the patch through an aperture cut in the ground plane as shown in Figure 3.9.

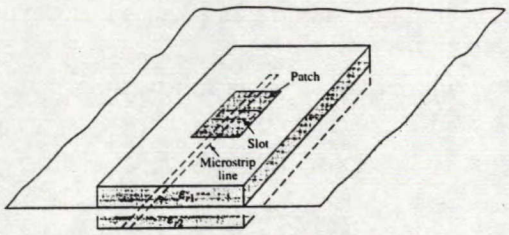

Figure 3.9: Aperture-coupled Feed Configuration (from [21])

There are several advantages of this configuration, the most important being that the feed network and the patch are well isolated from one another. In this way, no radiation from the feed network can interfere with the main radiation pattern since a ground plane separates the two mechanisms. Back radiation from the feed network is an issue but it can be minimized by carefully sizing the slot. Another advantage of the aperture-coupling feed is that surface wave excitation can be better controlled by choosing different substrate materials for the feed and radiating elements. The feed circuit layer can also be easily integrated with MMICs and there is plenty of room for active devices or phase shifters.

The aperture is most often modeled using magnetic current densities. This model is based on the equivalence principle which effectively replaces the coupling aperture with a magnetic surface current ($\mathbf{M}_s$) both above and below the aperture. The magnitude of the two currents is the same but they are opposite in direction to ensure the continuity of the tangential electric field through the aperture.

3.2.3.3.2 Design Parameters

The design of an aperture-coupled feed for a patch antenna configuration involves the careful selection of parameters such as the length of the open-circuited feedline beyond the aperture (stub length), the length and width of the slot, the substrate thickness, and the dielectric constants of both substrates [31]. Many experiments have shown the general effect of these parameters [32] to be as follows:

- *Stub Length*: If the input impedance at a single frequency is plotted for various stub lengths, the Smith chart locus follows a constant resistance contour. This implies that the aperture and antenna act like a series load along an open circuited transmission-line.
- *Slot Length*: Reducing the aperture length effectively decreases the coupling factor between the feedline and the patch antenna.
- *Feed Substrate Permittivity (E_r)*: Increasing the dielectric constant of the feed substrate results in an increased coupling factor with very little effect on the resonant frequency of the antenna.
- *Feed Substrate Thickness*: Increasing the thickness of the feed substrate causes the coupling factor to decrease with very little effect on the resonant frequency of the antenna.
- *Patch Position*: The input impedance of the structure is relatively insensitive to small variations in patch position over the aperture. It is generally desirable to have the slot centered under the patch as this is where the electric fields are zero and the magnetic fields are maximum for the dominant mode. Thus, this yields the greatest coupling factor.

- *Matching*: Matching with the aperture-coupled structure is achieved by choosing the length of the slot to match the resistive part of the input impedance and then using the open-circuit stub to tune out (eliminate) the reactive component. In this way, designers have far more flexibility than with other feed configurations.

3.2.3.3.3 Methods of Analysis

The overall aperture-coupled microstrip antenna has been analyzed using several different methods, but was originally based on the cavity model of the patch combined with small-hole coupling theory as presented by Pozar. Sullivan and Schaubert performed a rigorous analysis using the method of moments [33] and Ittipiboon later analysed the structure using a modal expansion method [34]. This method is of particular interest since it provides significant insight into the coupling mechanism and general operation of the structure.

The modal expansion method makes use of the cavity model to describe the patch, the dynamic planar waveguide model to represent the feedline, and the magnetic current density model described earlier to represent the aperture. From the field expressions of the entire structure including the boundary conditions imposed by the aperture, the circuit model shown in Figure 3.10 can be constructed.

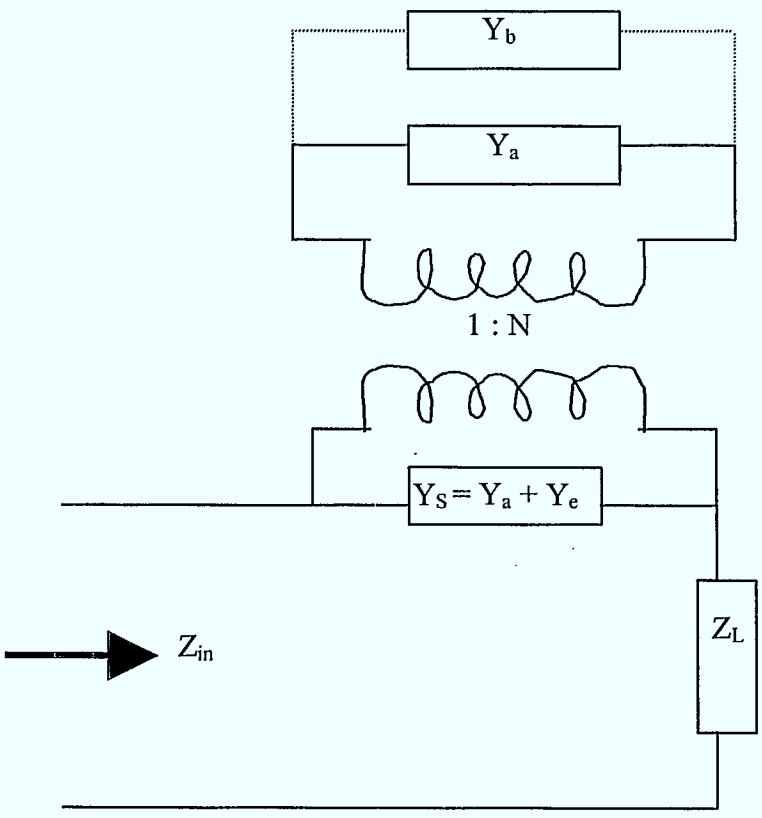

Figure 3.10: Equivalent Circuit for the Aperture-Coupled Patch Structure

Y_b is the admittance due to back radiation, Y_a is the antenna admittance, Y_S is the total admittance given by (3-20), Y_e is the admittance of the higher order modes inside the guide, Z_L is the impedance of the matching stub as seen by the slot, and Z_{in} is the input impedance as seen by the microstrip line at the slot. Through use of the above circuit model, this method relates the effect of the slot to that of an impedance transformer having a *turns ratio* (N):

$$Y_S = N^2(Y_e + Y_a) \qquad (3\text{-}20)$$

$$Z_{in} = Z_L + Z_S$$

$$Z_{in} = Z_L + \frac{Z_a}{N^2} \qquad (3\text{-}21)$$

If the back radiation and the admittance due to the higher order modes are assumed to be small, the relationships of (3-21) result from basic circuit analysis. In this way, the total input impedance of the structure can be found.

3.2.4 Circularly Polarized Patch Theory

Polarization describes the time-varying direction and relative magnitude of the electric field vector. The microstrip patch antenna with conventional feeds and no modifications radiates primarily linearly polarized waves wherein the electric field vector is always directed along a line. Circularly polarized waves can be obtained by either making slight changes to the patch elements or by using a special feed configuration that forces the electric field vector to trace out (rotate in) a circular path.

Fundamentally, in order to obtain circular polarization (CP), two orthogonal modes must be excited with a ±90 degree time-phase difference between them. The 'plus' and 'minus' indicate that the electric field vector could trace out a circle either counter-clockwise (right hand circularly polarized, RHCP), or clockwise (left hand circularly polarized, LHCP) respectively. The quality of a circularly polarized wave is represented by the ratio of the ellipse's major axis to its minor axis, called the axial ratio [27].

The most direct approach to obtain CP with a microstrip patch structure is to use a symmetrical patch element, such as a square, in conjunction with a feed configuration which consists of either a quarter-wave power divider or a 90-degree hybrid [21] as shown in Figure 3.11. CP is obtained by the two separate and spatially orthogonal feeds which have a relative phase shift of 90 degrees.

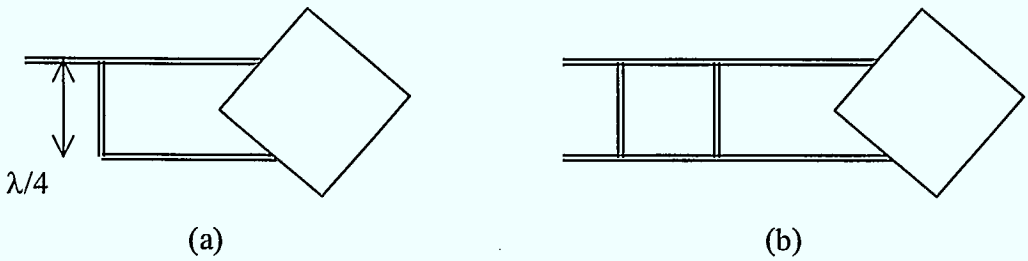

Figure 3.11: Square Patch Driven with a: (a) Power Divider, (b) 90-Degree Hybrid

Another approach is to attach a feed such as a microstrip line or coaxial probe to the patch at a specific location to excite two equal amplitude degenerate orthogonal modes. Some sort of asymmetry must then be applied to the patch element such that the degeneracy is removed. If the asymmetry is properly applied, the phase of one mode can lead by 45 degrees with the other mode lagging by 45 degrees at a given frequency, thus producing CP as illustrated in Figure 3.12.

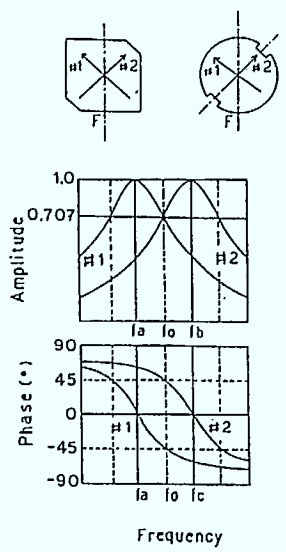

Figure 3.12: Achieving CP with Degenerate Mode Excitation (from [22])

This single feed method has a disadvantage in that phase and amplitude errors rapidly degrade the axial ratio off the center frequency leading to narrow band CP performance. Examples of antennas making use of this technique are the corner-fed rectan-

gular patch, the slightly elliptical patch, and the square patch with a 45-degree center slot [35].

Circular polarization with an aperture-coupled microstrip antenna can be accomplished by making the patch slightly asymmetric and then rotating it 45 degrees with respect to the slot. The two orthogonal modes of the patch will be excited and their degeneracy will be removed. However, this method has a very narrow axial ratio bandwidth and, for this reason, the direct feed methods described above are more often used. Using a direct feed method with an aperture-coupled configuration requires two slots as shown in Figure 3.13, meaning that neither will be located at the center of the patch. Isolation between the two feeds is an important issue as the slots are not only located close together but they have open-circuited microstrip stubs that extend past the slot and will likely be in very close proximity.

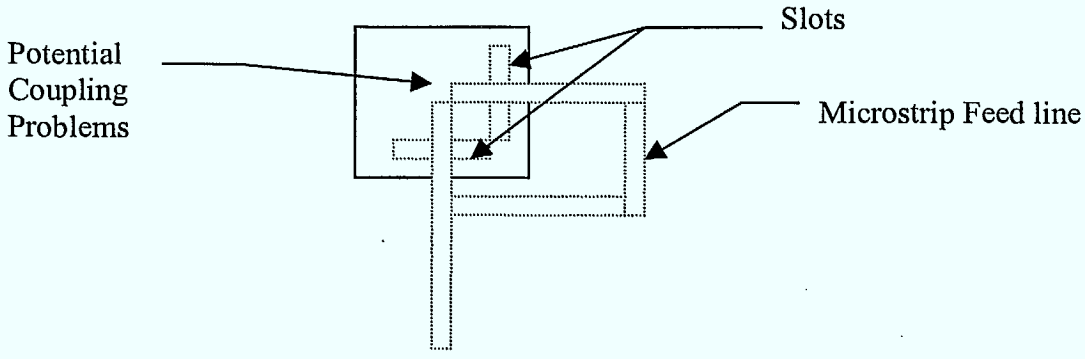

Figure 3.13: Aperture-Coupled Direct CP Method

3.3 Current Antenna Miniaturization Techniques

A significant amount of research over the last few years has been dedicated to making microstrip patch antennas more compact for mobile satcom applications at L-band frequencies. Researchers have been able to achieve certain degrees of miniaturi-

zation mainly by one or a combination of the following four methods with each having significant disadvantages:

- use of substrates and/or superstrates of higher permittivity,
- use of short-circuiting techniques,
- use of chip resistor loading,
- modification of the basic patch shape.

The word *miniaturized* is used most commonly in the literature to denote a patch which, for a given frequency, has its largest linear dimension smaller than that of a reference patch operating at the same frequency. However, in this thesis the term *miniaturized* is used to denote a patch having constant dimensions that is made to operate at a lower frequency. Both definitions lead to the same result which is a smaller patch at lower frequencies. They are simply two different ways of approaching the problem.

3.3.1 Patches with Substrate and/or Superstrates of High Permittivity

The most straight-forward method of miniaturizing a principle-shaped patch antenna (shapes, like circles or rectangle, that can be defined on the principal coordinate systems) is to use a substrate of high permittivity. Since the resonant length of the antenna and the substrate permittivity are inversely related, as shown in (3.17) of Section 3.2.2.5, a high permittivity substrate will shrink the size of the patch. This miniaturization technique has the disadvantage of causing extremely narrow bandwidths as well as significant reductions in gain. Therefore it is not suitable for mobile satcom applications.

It was demonstrated in a planar inverted-F antenna [36] that the gain reductions incurred with high permittivity substrates can be recovered by adding superstrates having high dielectric constants. A superstrate is a substrate layer that is placed directly on top

of a patch covering the entire layer. The inverted-F configuration, consisting of a probe-fed short-circuited plate, incorporated a superstrate having a dielectric constant of 80 with an optimized thickness such that, at 1.8 GHz, a size reduction of up to four times was achieved. The same technique has been applied to an aperture-coupled microstrip antenna resonating at 1.66 GHz [37]. In this case, the patch size was reduced to about one fifth of that of a conventional microstrip antenna. The advantage of superstrate layers is that they can also be used as covers to protect the antennas from the environment [38].

3.3.2 Shorted Patches

The short-circuited patch antenna is constructed by short-circuiting the zero potential plane of an ordinary microstrip antenna that is excited in the dominant mode. Physically, this short-circuit may be achieved in either a complete way by wrapping a copper strip around the edge of the antenna or in an approximate way by using a series of shorting posts. From a manufacturing point of view, the construction of shorting posts is easier and is more widely used.

A short-circuited patch antenna can realize the same resonant frequency as a standard microstrip antenna but at about half the size. Further reductions can be achieved by varying the shorting parameters such as the number of posts, the radius of each post, and the post length which is primarily determined by the thickness of the microstrip antenna. It was found that by using a very small number of thin shorting posts, the antenna size could be reduced to less than a quarter-wavelength [39].

The use of a single shorting post has also been shown to reduce the conventional patch size to less than half in both probe [40] and aperture-coupled [41] feeding configu-

rations. Other similar structures such as superposing two quarter-wavelength patches and connecting them with a short-circuit plane have been shown to halve the size of the patch and also enable bandwidths that are about two times wider to be achieved [42]. Stacking patch antennas and shorting the two with the same post is another technique that provides patch miniaturization as well as a wider bandwidth [43-45].

There are fundamental problems associated with shorting the microstrip patch antenna. First, fabrication of the structure with shorting posts is not simple and requires a high degree of accuracy. Second, the shorted patch generates a high level of cross-polarized fields in the H-plane which is unsuitable for mobile satcom. Recently, however, a novel balanced shorted patch configuration [46] has been shown to significantly reduce these cross-polarized fields. This new structure consists of two feed/shorting post combinations positioned at symmetrically opposite locations on the patch which provides the benefits of a traditional balanced feed structure. The third and most important disadvantage of the shorted patch for mobile satcom applications is that it is difficult to achieve circular polarization. The shorting posts are an approximation to an electric wall which inherently cannot support the tangential electric fields necessary for circular polarization.

3.3.3 Chip Resistor Loading

Building on the benefits of the patch antenna shorted with a single post, chip resistor loading has been proposed as a method to reduce the patch size as well as increase the bandwidth. The basic structure consists of replacing the shorting post with a chip resistor having a low resistance ($\approx 1\Omega$).

Wong showed that chip resistor loading can reduce the patch size further than with the single shorting post while also achieving a bandwidth of about 9%, five times better than that of a conventional patch and about six times better than the shorted post configuration [47]. However, the gain of the chip resistor loaded antenna suffers due to the ohmic loss of the resistor loading. Adding a high permittivity superstrate has been proposed [48] to increase this gain back to the level of a conventional patch but this is at the expense of the antenna height which went from about 1 mm to nearly 5 mm.

3.3.4 Patches with Modification to Basic Shape

Modifying the principle-shaped patch itself can allow substantial size reductions without requiring shorting posts or high-permittivity substrates and/or superstrates. This can be accomplished by either changing the shape of the patch or by perturbing the shape with slits or slots.

There are a wide range of shapes that have been proposed to achieve patch miniaturization, the most popular of which seem to be the H and the Bow-tie shapes. The H-shaped half-wavelength patch antenna was first proposed by Palanisamy [49] and later implemented in a quarter-wavelength configuration with shorting posts along one side of the H-shape [50]. The resonant frequency of this patch was reduced by about 42% (from 5 GHz to 2.86 GHz) but the impedance bandwidth was reduced from 0.77% to 0.39%. This configuration does not meet the mobile satcom bandwidth requirements.

The bow-tie shaped patch antenna [51] achieves a 60% size reduction while maintaining comparable antenna characteristics to those of a conventional rectangular patch. Despite these results, shape modification is not a suitable solution for two reasons; it can introduce out-of-phase radiating edges which lead to a reduction in the overall ef-

ficiency of the antenna and it is debatable whether or not these shapes can support circularly polarized operation.

Perturbing the shape of the patch antenna with slits or slots is a miniaturization method that lends very well to circular polarization. When the slits are cut in orthogonal directions, they provide a size reduction by effectively lengthening the surface current path. This lowers the resonant frequency of the patch and hence reduces the size at a given frequency. A pair of diametrically opposed slits cut into a circular patch has shown to be a convenient way to control the size of the patch and enable a reduction of about 15% [52]. Cutting the slits into a square patch enables a 30% reduction in the patch size and, combined with a high permittivity superstrate layer, yields a gain that is 5 dB greater [53]. With proper adjustment of the slit lengths and strategic probe locations, circular polarization can be easily achieved [54].

Cutting slots inside the patch boundaries also leads to a more compact patch design. A circular patch with a crossed slot can achieve a 36% size reduction while also providing circularly polarized operation [55]. Four bent slots arranged symmetrically around the center of a square patch have also been successful at reducing the size of the patch with overall reductions of 50% being achieved in [56]. In both cases, however, the axial ratio bandwidth was reduced as well as the gain.

3.4 Cavity Perturbation Theory

Perturbation theory is a method of obtaining an approximate solution to an integral equation problem that cannot be otherwise solved. The method is based on having an unperturbed problem in which a solution is known and then changing (perturbing) the problem slightly and approximating the effect of the change. Perturbational methods are

therefore most useful for calculating changes in a given quantity due to small changes in the overall problem.

There are many types of perturbations that can be analyzed, the selection of which depends on the desired outcome. Harrington [57] outlines a number of different types including perturbations of cavity walls, cavity-material perturbations, waveguide perturbations, and others. Since the objective of this thesis was to achieve a miniaturized microstrip patch by using dielectric-loading techniques, the cavity-material perturbation method would be a good way to approximate the effect of perturbing the microstrip cavity with dielectric.

3.4.1 Cavity-Material Perturbation Method

The cavity perturbation method will approximate the change in resonant frequency of the microstrip cavity due to a perturbation of the material inside the cavity. The method begins by assuming that an arbitrary resonant cavity is formed by a conductor covering a surface (S) and enclosing a loss-free region (τ) which contains matter having relative permittivity (E_r) and permeability (μ). Figure 3.14(a) illustrates the cavity.

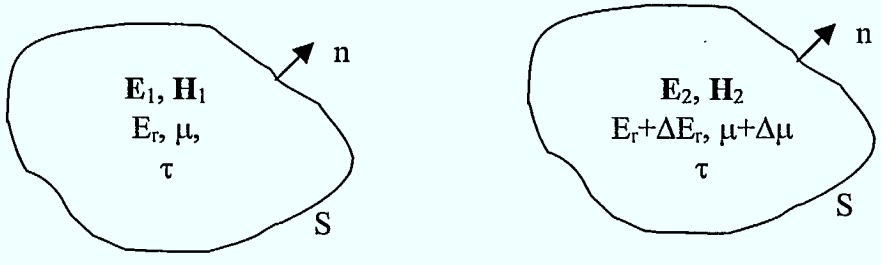

Figure 3.14: (a) Original Cavity, (b) Perturbed Cavity

The cavity material is then perturbed such that a small change in both the permittivity and permeability occurs. The perturbed cavity is shown in Figure 3.14(b) where the

matter permittivity has been changed to $E_r+\Delta E_r$ and $\mu+\Delta\mu$. The fields of the original problem will be represented by $\mathbf{E}_1$ and $\mathbf{H}_1$ while the corresponding fields of the perturbed cavity will be represented by $\mathbf{E}_2$ and $\mathbf{H}_2$. The resonant frequency of the original problem is similarly ω_1 while the resonant frequency of the perturbed cavity is ω_2.

Within S, the following field equations apply:

$$\begin{aligned} -\nabla\times\boldsymbol{E}_1 &= j\omega_1\mu\boldsymbol{H}_1 & -\nabla\times\boldsymbol{E}_2 &= j\omega_2(\mu+\Delta\mu)\boldsymbol{H}_2 \\ \nabla\times\boldsymbol{H}_1 &= j\omega_1 E_r\boldsymbol{E}_1 & \nabla\times\boldsymbol{H}_2 &= j\omega_2(E_r+\Delta E_r)\boldsymbol{E}_2 \end{aligned} \qquad (3\text{-}22)$$

As outlined in [57], the last equation of (3-22) is scalarly multiplied by $\boldsymbol{E}_1^*$ and the conjugate of the first equation is multiplied by $\boldsymbol{H}_2$. The two equations resulting from this operation are added. The analogous operation is performed on the second and third equations of (3-22), with the two resulting equations also being added. The final equations from each are then added and integrated throughout the cavity. After applying the divergence theorem, the final result can be rearranged into the form of (3-23) which represents the exact formula for the change in resonant frequency due to a change in the permittivity and/or permeability in the cavity.

$$\frac{\omega_2-\omega_1}{\omega_2} = -\frac{\iiint(\Delta E_r\boldsymbol{E}_2\cdot\boldsymbol{E}_1^* + \Delta\mu\boldsymbol{H}_2\cdot\boldsymbol{H}_1^*)d\tau}{\iiint(E_r\boldsymbol{E}_2\cdot\boldsymbol{E}_1^* + \mu\boldsymbol{H}_2\cdot\boldsymbol{H}_1^*)d\tau} \qquad (3\text{-}23)$$

In the limiting case, when $\Delta E_r\rightarrow 0$ and $\Delta\mu\rightarrow 0$, the resonant frequency and the electric and magnetic fields of the perturbed cavity can be approximated by the resonant frequency, electric, and magnetic fields of the original problem such that (3-23) can be re-written as (3-24).

$$\frac{\omega_2-\omega_1}{\omega_1} \approx -\frac{\iiint(\Delta E_r|E_1|^2 + \Delta\mu|H_1|^2)d\tau}{\iiint(E_r|E_1|^2 + \mu|H_1|^2)d\tau} \qquad (3\text{-}24)$$

From this equation, it can be seen that any small increase in E_r and/or μ can only decrease the resonant frequency of the cavity. This is because the term ω_2-ω_1 will always be less than zero due to the negative sign on the right-hand-side of (3-24), thus making ω_2 always less than ω_1. Since a large change in E_r and/or μ can be viewed as a succession of many smaller changes, it can be said that any increase in E_r and/or μ within the cavity can only decrease the cavity's resonant frequency.

3.4.2 Patch Miniaturization

The perturbation method discussed above revealed that any increase in E_r and/or μ within the cavity can only decrease the cavity's resonant frequency. This knowledge can be applied to the microstrip cavity by viewing the dielectric-loading of the patch antenna as a permittivity perturbation in the cavity in which $\Delta\mu$ is zero.

. Equation (3-24) reveals that, if the perturbation is made in a location where the electric fields are at a maximum, ω_2 will be less than ω_1 by the largest amount, yielding the best possible frequency reduction. In the case of the patch antenna, the location of the maximum electric field intensity is at the radiating edges of the patch. A very miniaturized patch can thus be achieved by placing dielectric-loading at the radiating edges of the patch. The resonant frequency of the patch will decrease significantly, allowing it to operate at a lower frequency but have the dimensions of a higher frequency patch.

Unfortunately, this method cannot predict the exact amount of frequency reduction that is achievable since it can only predict the trend. Other antenna parameters such as bandwidth and matching cannot be determined either. Experimental work is required to characterize the results of this perturbation theory analysis.

CHAPTER 4: Dielectric-Loaded Patch Antenna Characterization

4.1 Introduction

Dielectric loading of a microstrip patch antenna, in the context of this thesis, consisted of placing pieces of dielectric in strategic locations beneath a microstrip patch. The idea is that the fields in the cavity are perturbed such that the operating frequency of the patch is reduced without altering the dimensions of the patch itself, thus yielding a more compact antenna at lower frequencies.

A significant amount of effort was devoted to acquiring an understanding of the various design parameters and their effect on the overall performance of the antenna. To highlight the progression of this understanding, this chapter will describe in detail the systematic characterization of a linearly polarized dielectric-loaded patch prototype. The design and fabrication techniques will be presented as well as an outline of the measurement process. The major results will be summarized from which important trends will be discussed. The chapter will end with a brief comparison between simulated and measured results.

Although not the original intention, most of the above described process was conducted experimentally. The initial idea was to electromagnetically model the structure in HP HFSS [58] and systematically analyze it until the effect of each design parameter was understood. This would have reduced the fabrication costs and material usage and also saved time. However, due to the problems discussed in Appendix 2, modeling of

these structures generated inconclusive results and required lengthy simulation times. As a result, the systematic analyses had to be performed experimentally.

4.2 Prototype Design and Fabrication

4.2.1 Overview

The concept of dielectric-loading a patch antenna and achieving a lower resonant frequency for the same size patch was verified in a preliminary investigation. This initial set of measurements revealed that at least a 20% reduction in frequency could be reasonably achieved while maintaining an impedance bandwidth on the order of 8%. As will be discussed, important physical parameters of the structure were identified as requiring further examination and several dielectric permittivities and sizes were eliminated from consideration.

Based on these initial results, a linearly polarized prototype was developed. The structure was designed and fabricated such that the effect of each important parameter could be isolated and observed in a controlled manner. This required taking into account both patch and loading alignment issues as well as establishing an accurate method to suspend the patch above the dielectric pieces by a controllable amount. The following sections will outline in detail the entire design process.

4.2.2 Structure Design

Due to problems with the HFSS software and the lack of an alternative 3D simulation tool, the approach taken to design the structure was to simulate the patch and feed network, separate from the loading, in the 2D software package Ensemble [59]. This design was performed at a frequency higher than the desired one to leave enough room

for the dielectric-loading to reduce the frequency to the proper range. Given that the desired frequency band of operation was between 1.5 and 1.6 GHz and that a 20% reduction in frequency was found to be achievable, the initial resonant frequency of the patch was chosen to be 2 GHz.

4.2.2.1 Patch and Feed Structure Design

The patch shape was chosen to be a simple square such that it would lend itself well to being loaded with the available rectangular dielectric pieces. A circular or other odd-shaped patch would have required dielectric pieces that involved a more specialized and lengthy fabrication.

The patch substrate was chosen to have a relatively low loss tangent and be a firm material that would guarantee minimal sagging problems. This substrate was Rogers 4003 with a dielectric constant (E_r) of 3.38, a thickness (t) of 0.762 mm (0.030"), and a loss tangent (tan δ) of 0.0027.

The feed network design required some forethought into the eventual dielectric-loading plan. First, the preliminary investigation showed that, to get the required impedance bandwidth, the patch would likely have to be raised above the ground plane by 5 to 8 mm. This is illustrated in Figure 4.1 where x represents the height above the ground plane. Second, the load pieces would be placed under the radiating edges of the patch, where the electric fields are maximum, since perturbation theory indicated that this would produce the greatest reduction in frequency. Third, this loading would have to be symmetrical with respect to the patch and feed to avoid skewing the radiation pattern. Finally, there would have to be room for both the height of the dielectric pieces and the

height of air above the pieces to vary since both were deemed important design parameters to investigate.

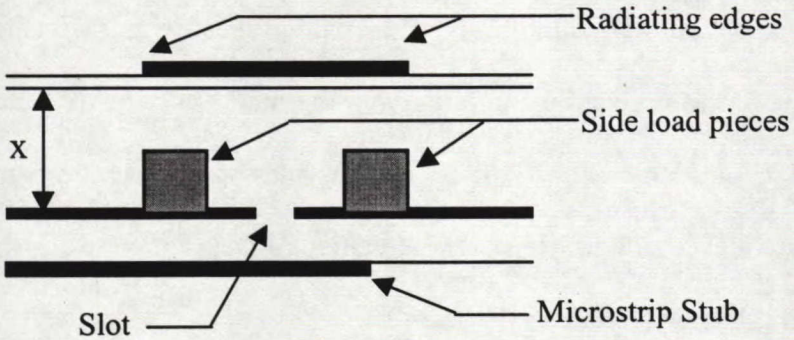

Figure 4.1: Pictorial Diagram of Side Loading

With this in mind, consideration was given to each of the feed methods described in Chapter 3, these being probe-coupling, microstrip feed line, and aperture-coupling. Traditionally, probe-coupling has been the feed mechanism of choice for patches at L-band frequencies due to the thick-air substrates required to get the 8% impedance bandwidths. However, this is not an ideal feeding technique since the probe radiates, contributing to high cross-polarization levels and a degradation in the quality of the circular polarization. The coaxial probe feed would also require that the patch have a fixed height above the ground plane since the probe must be physically soldered to the patch and ground. This would make it very difficult to work with the dielectric load pieces and vary both the height of the pieces as well as the height of air above the pieces. Finally, since the coaxial probe would have to be placed in a location where the match is closest to 50 Ω, it would likely interfere with the symmetric placement of the dielectric load pieces.

Microstrip line feeding was eliminated from consideration due to the likelihood of surface wave generation with the feed line being on a thick-air substrate. Another

eliminating factor was that this type of feed would not be symmetrical about the patch due to the fact that it contacts only one of the patch edges.

The aperture-coupling feed technique has many advantages over the other methods. It has inherent symmetry about the major axes of the patch (assuming that the slot is in the center of the patch), it provides unlimited room to vary the height of dielectric pieces and air, it has a high degree of isolation between the feed and the patch, and it is relatively simple to fabricate.

This feed method, despite its many advantages, has not been used in L-band applications since it typically cannot provide enough coupling through large amounts of air (required to get the bandwidth) to the patch. However, with the realization that the slot effectively behaves as an impedance transformer as described in Chapter 3, placing dielectric over the slot would have an effect on the match of the antenna and possibly provide the required coupling from the slot to the patch. The preliminary investigation indicated that matching could indeed be accomplished in this way and therefore aperture-coupling was chosen as the patch feed configuration.

The feed substrate was chosen to have the same properties as that of the patch, these being Rogers 4003, E_r=3.38, t=0.762 mm (0.030"), tan δ=0.0027. On this substrate, at 2 GHz, the 50 Ω microstrip line was 1.764 mm wide, the effective dielectric constant was 2.672 and the guided wavelength was 91.8 mm.

4.2.2.2 Patch and Feed Optimization

The basic structure described above was modeled in the Ensemble software and the patch dimensions were estimated to be 41.12 mm by 41.12 mm at 2 GHz, assuming a voltage standing wave ratio (VSWR) of 2 and a 50 Ω system. The slot length and width

were chosen to be non-resonant at L-band frequencies and the slot was placed directly in the center of the patch, where the horizontal magnetic fields are maximum, to allow the greatest amount of coupling. The other benefit of having the slot centered was that the vertical magnetic fields on each end of the slot would cancel with each other. Figure 4.2 illustrates this idea.

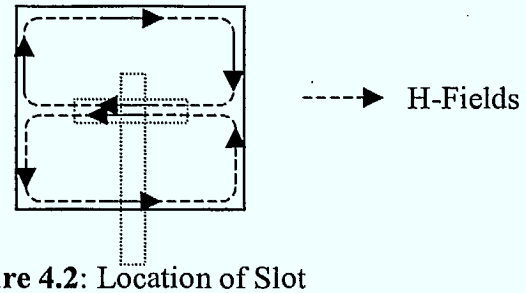

Figure 4.2: Location of Slot

The microstrip line stub (past the slot) was given an initial length of about a quarter wavelength to ensure that the standing wave in the line would yield minimum electric fields at the slot. Substrate dimensions were not necessary in the simulation since Ensemble assumes they are infinite, an assumption that will have a slight effect on the amount of ripple in the radiation patterns.

The patch and feed network dimensions were adjusted to obtain a good impedance match at the resonant frequency and to limit the front-to-back ratio of the radiation pattern to less than 10 dB. Achieving these criteria was relatively simple and involved varying primarily the slot dimensions and the microstrip stub length. The resulting patch characteristics are outlined in Table 4.1 and the simulated return loss (S_{11}) is shown overlaid with measured results in Figure 4.5 of section 4.2.4.

Note that the gain of the patch was much lower than the typical 6 dB. The reason for this was initially of concern, but upon further investigation, it was determined that the majority of the loss occurred entirely in the substrate. This was confirmed because the

structure was re-simulated without including the substrate loss and the antenna was found to have a gain of more than 5 dB.

Patch Dimension	37 mm
Slot Width	1.05 mm
Slot Length	13.4 mm
Stub Length	7.5 mm
Resonant Frequency	2.03 GHz
Impedance Bandwidth	0.78%
Gain	3.7 dB
Front to Back Ratio	17 dB

***Table 4.1**: Ensemble Simulated Patch Results*

4.2.2.3 Design of Dielectric Load Pieces

The preliminary investigations revealed that the following physical parameters of the dielectric pieces had an effect on the frequency reduction, impedance matching ability, and bandwidth of the dielectric-loaded patch structure and thus would be important in the characterization:

- length (L),
- width (w),
- height (h),
- permittivity (E_r),
- height of air above the dielectric pieces.

Figure 4.3 provides a visual interpretation of these parameters. In order to accurately observe the trends involved in varying these dielectric sample parameters, over 200 specially sized dielectric pieces were fabricated. Among these, about 175 pieces were

intended for placement only over the slot while about 25 pieces were for loading the edges of the patch.

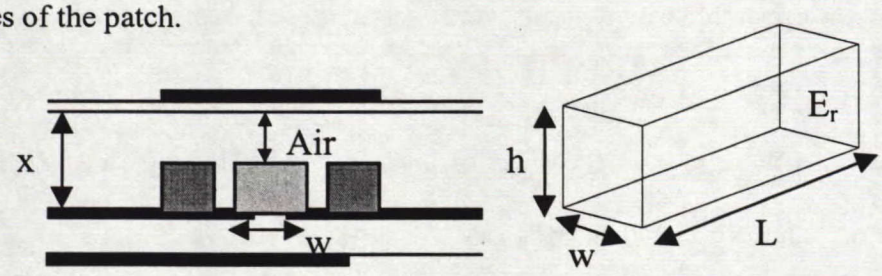

Figure 4.3: Important Design Parameters

4.2.2.3.1 Slot Load Pieces

The dimensions of the pieces that were to be covering only the slot consisted of five different widths, four lengths, and three thicknesses, with each having three permittivities as listed below:

- E_r: 20, 40, 100
- Length (L): 13.5 mm,15.5 mm, 20 mm, 30 mm
- Width (w): 1.5 mm, 2.5 mm, 3.5 mm, 5 mm, 10 mm
- Thickness (h): 2 mm, 3 mm, 4 mm

The relative permittivities were chosen based on the preliminary results. It was found that dielectrics having large dimensions and permittivities greater than 100 resonated on their own and thus were not useful in providing either coupling or loading. Also, dielectrics with small dimensions and relative permittivities of ten or less were not able to provide enough coupling and had very little effect while loading the slot. Dielectric constants of 20, 40 and 100 performed well and were readily available for fabrication.

The dimensions were chosen by starting with a sample that was slightly bigger than the slot (13.4 mm x 1.05 mm) and then increasing them to a reasonable size. The

previous measurements had indicated that the width and thickness of the sample would be of most importance so smaller increments were used in these cases.

4.2.2.3.2 Side Load Pieces

The pieces that were to load the sides of the patch consisted of varying widths, thicknesses and dielectric constants as described above but all were 37 mm long, the length of a side on the square patch. This decision was based on perturbation theory which predicts that the greatest reduction in frequency would occur when the entire region of maximum electric fields is perturbed. For this same reason, only the largest two widths, 5 mm and 10 mm, were fabricated.

4.2.2.3.3 Dielectric Resonant Frequency Check

To ensure that the dielectric pieces would not be resonant in the band of interest, the resonant frequency of each piece was calculated assuming that it was a dielectric resonator antenna. A sample calculation is shown in Appendix 1. The pieces that were to be located over the slot were of most concern due to their proximity to the source of excitation. The pieces that were to be located under the sides of the patch would see very little coupling from the slot and were not expected to be a concern.

The calculation revealed that the samples with dielectric constants of 100 and thicknesses of 4 mm would resonate just under 2 GHz when placed over the slot. These cases were eliminated from the list of pieces that would load the slot since they were deemed to resonate too close to the desired band.

4.2.3 Structure Fabrication Issues

The optimized patch and feed network structures from Ensemble were exported to a .DXF file and then imported into DW2000, a commercial mask layout software

package. The substrates and ground plane were given dimensions of 15 cm by 15 cm which corresponded to about 0.8 wavelengths away from the patch on all sides. The microstrip line had to be extended to meet the edge of the substrate such that its total length was 54 mm. Figure 4.4 depicts the planar representation of the final structure of the patch and feed network where the dimensions of both views are exaggerated..

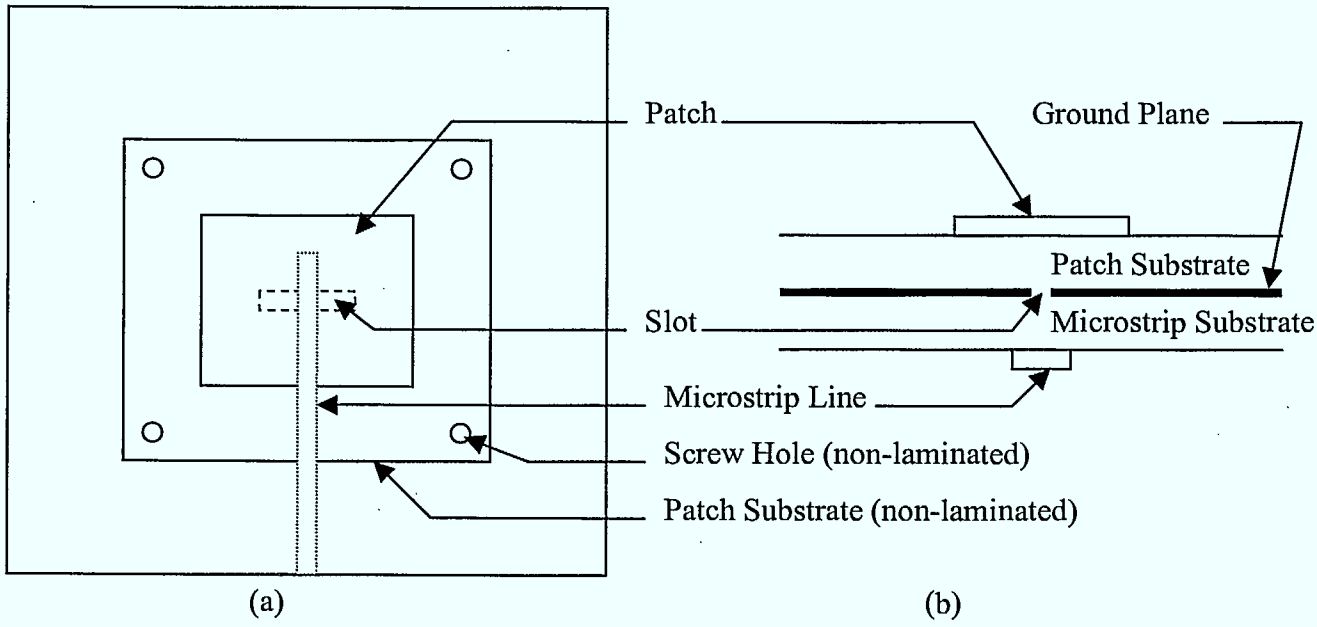

Figure 4.4: Aperture-Coupled Microstrip Patch Antenna, a) top view and b) side view

Two versions of the patch were prepared for fabrication. The first one consisted of the patch and microstrip substrates being laminated together where both substrates were of the same dimensions (15 cm x 15 cm). This case was designed to ensure that there would be no air gap between the two substrates and that it would resonate as predicted by Ensemble. The second version of the patch involved the two substrates not being laminated together. In this case, the patch substrate was cut smaller (7 cm x 7 cm) and aligned over the slot with plastic screws which extended from the patch substrate

through to the microstrip substrate. These alignment screws were to also be used as a means of accurately controlling the height of the patch above the dielectric load pieces. The exact height would be specified by the specially sized spacers through which the screws would be placed.

To guarantee accuracy with the alignment of the dielectric load pieces under the patch, a number of alignment (grid) lines were drawn on the structure in DW2000. The original idea was to silk-screen the grid directly onto the ground plane but, since this might influence the operation of the antenna as the silk contains a small amount of dielectric, the lines were instead printed onto a transparency. In this way, the transparency would be fixed over the ground plane with tape and a hole would be cut in the location of the patch substrate to ensure that it would not interfere with the operation of the antenna.

4.2.4 Laminated and Non-Laminated Patch Return Loss Measurements

The return loss of both the laminated and non-laminated versions of the patch antenna were measured on a network analyzer to confirm operation at 2 GHz. The laminated patch was observed to resonate at 2.01 GHz with a return loss at that frequency of –20 dB thus yielding an impedance bandwidth of about 0.9%. These results were very close to those predicted in Ensemble.

The non-laminated patch antenna, which was fabricated to have the smaller patch substrate, was found to resonate at 2.5 GHz with a return loss of about –16 dB. This operating frequency was significantly higher than what was measured with the laminated antenna, an effect that was assumed to be due to the slight air gap present between the patch and the microstrip layers. To confirm this, nuts were used on the alignment screws

to push the two layers together and eliminate as much of the air gap as possible. With the nuts tight, the resonant frequency reduced to 2.1 GHz, a value that more closely approximated the results achieved with Ensemble and the laminated antenna. Figure 4.5 shows a comparison between the Ensemble and non-laminated (with nuts tight) return loss characteristic (the magnitude of S_{11} is plotted on the vertical axis). The smaller size of the patch substrate appeared to have little effect on the overall operation of the antenna.

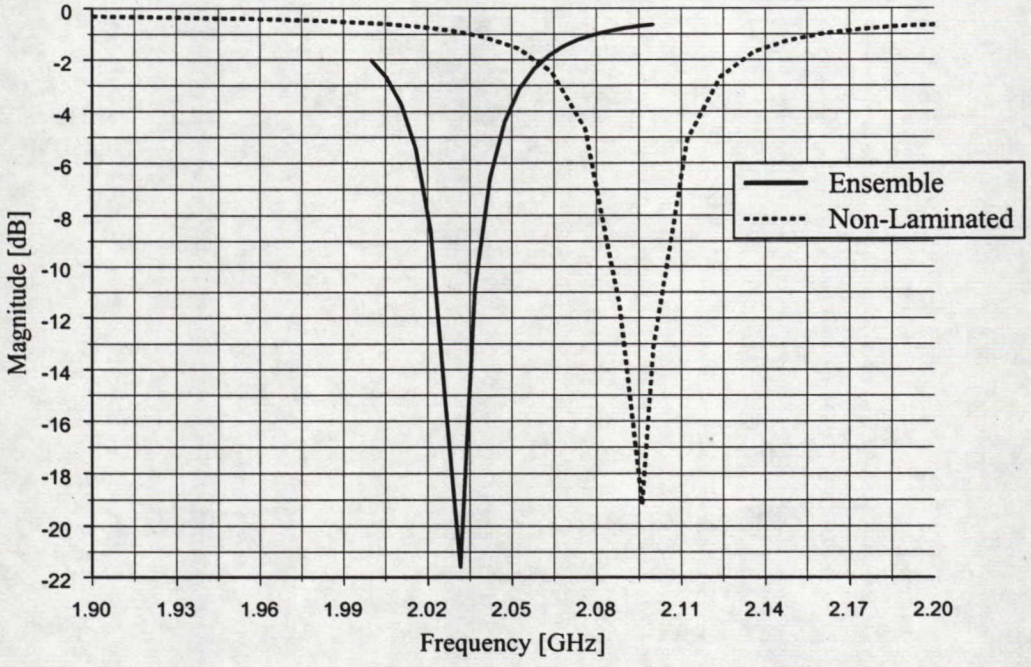

Figure 4.5: Measured (non-laminated) and Simulated Patch Return Loss Characteristic

4.3 Return Loss Measurement Process

4.3.1 Overview

The overall dielectric-loaded patch structure is shown in Figure 4.6. An illustrative diagram is displayed in Figure 4.6(a), and photographs of the actual antenna are shown in Figure 4.6(b) and (c).

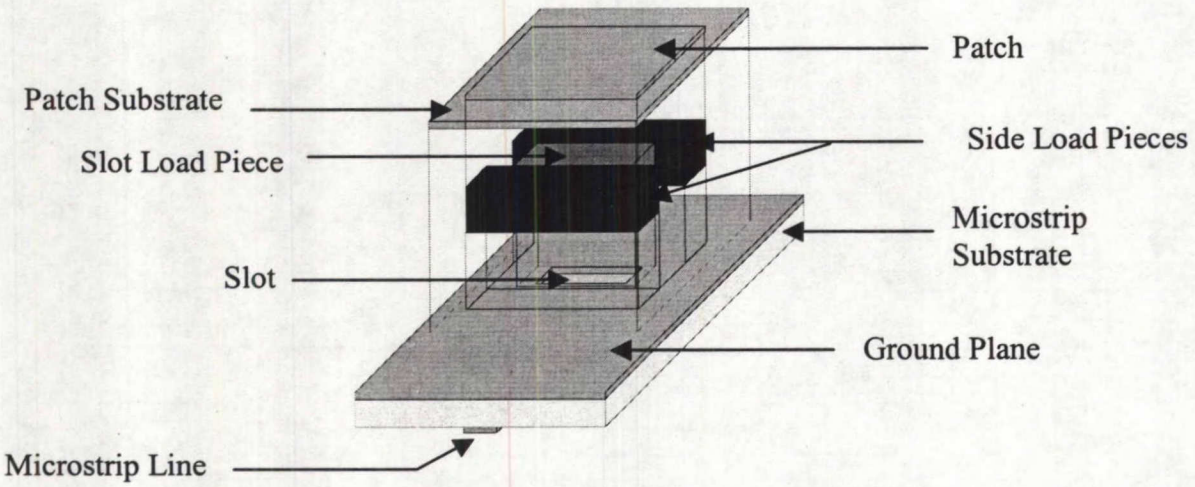

Figure 4.6(a): Diagram of Dielectric-Loaded Patch Structure

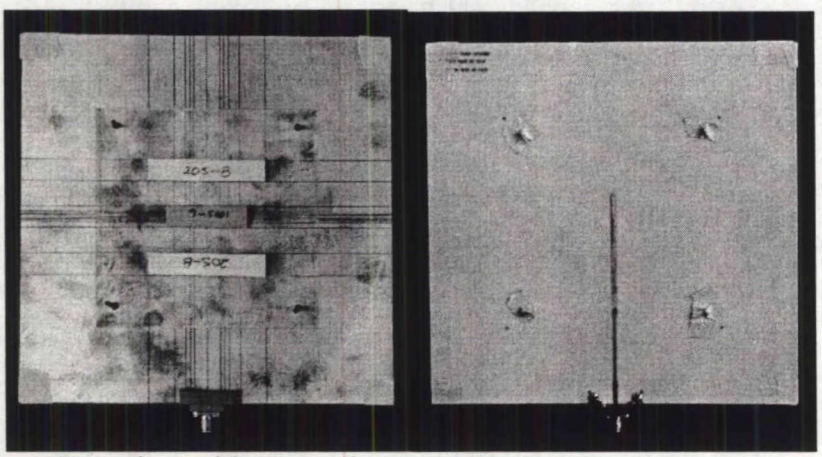

Top view without patch Bottom view

Figure 4.6 (b): Photographs of Dielectric-Loaded Patch Structure

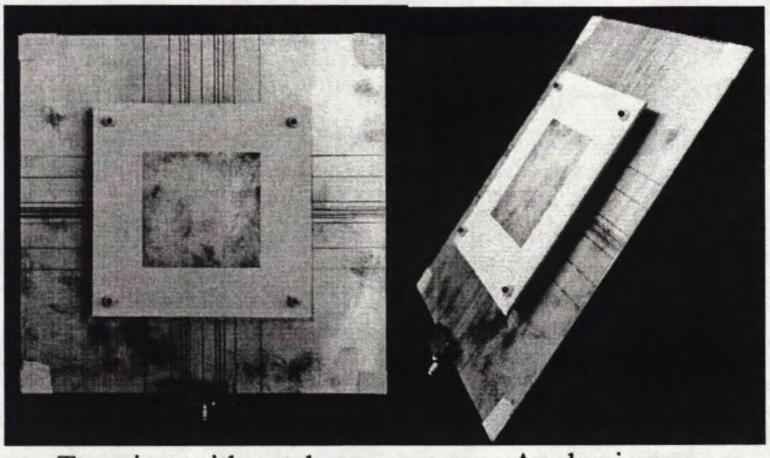

Top view with patch Angle view

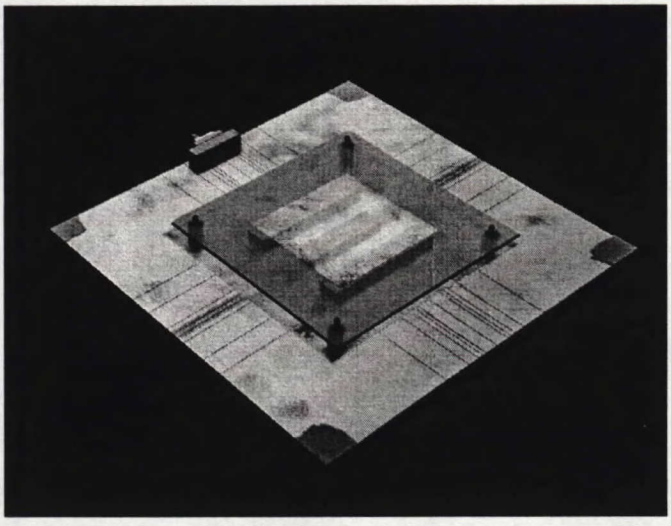

Whole structure

Figure 4.6 (c): Photographs of Dielectric-Loaded Patch Structure

The slot load piece was placed directly over the slot with its longest dimension aligned with that of the slot. The side load pieces, were placed parallel to the slot just under the two radiating edges of the patch. The reasoning behind this arrangement will be reviewed in the next section.

4.3.2 Dielectric Loading Review

Since the electric fields are minimum near the middle of the patch where the slot is located perturbation theory predicts that loading in this area (provided the dielectric is

relatively thin and short) will not affect the resonant frequency of the patch. The purpose of loading the slot is to provide a better match from the slot to the patch. Without this loading, the fields must couple through the air to the patch decreasing in strength as they propagate. At the heights required in this investigation the fields reaching the patch were weak and thus not useful.

The loading on the sides of the patch does affect the resonant frequency of the antenna since the loading is located where the electric fields are maximum. Looking at this type of loading alone shows the extent to which the frequency can be reduced even though the matching will be poor. These observed trends will enable future designers to estimate the parameters for the side loading dielectric pieces (E_r, thickness, width) that are required for a given frequency reduction.

4.3.3 Measurement Purpose and Process

The overall idea was to first load the sides of the patch with the dielectric pieces that produced a desired frequency reduction. Then, using the trends observed from the slot-loaded cases, attempts were made to obtain a match with a bandwidth greater than 8%.

The measurement process was divided into three main stages, these being slot loading only, side loading only, and matching (side loading with slot loading). The first stage of measurements, shown pictorially in Figure 4.7, was to focus on the way that the resonant loop moved on the Smith chart as the many parameters were varied. Although these trends apply only to the slot loaded cases, it was assumed that they would not change once the side loading was in place and thus could be used to obtain a match in the third stage.

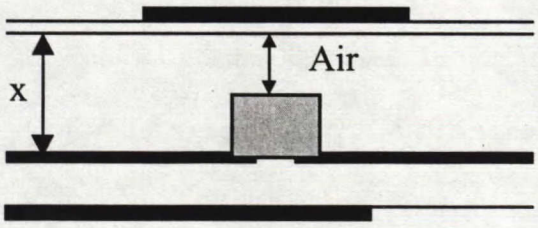

Figure 4.7: Pictorial Diagram of Slot Loading

The second stage of measurements, shown pictorially in Figure 4.8, was to determine the effect of side loading the patch on the resonant frequency. The quality of the impedance match and the bandwidth were of secondary concern at this stage. These measurements would give an indication as to the lowest frequency reduction possible for the dielectric pieces under investigation.

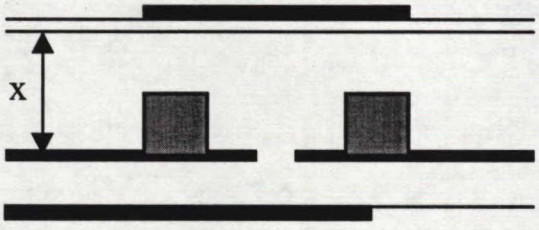

Figure 4.8: Pictorial Diagram of Side Loading

The final stage of the measurement process, shown pictorially in Figure 4.9, was carried out to determine the amount of frequency reduction possible while still maintaining a reasonable impedance bandwidth. This stage involved loading both the slot and the sides of patch and would make use of the trends observed in the first stage to obtain a better match for the best side-loaded cases observed in the second stage.

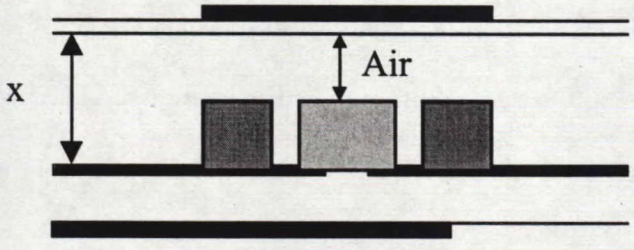

Figure 4.9: Pictorial Diagram of Slot and Side Loading

In all cases the dielectric pieces were attached to the ground plane of the structure with a silicone epoxy to ensure that they remained securely in place.

4.3.4 Additional Measurement Notes

With regard to the trend analysis that follows, each measurement was compared to a *reference* case where the dielectric loading was removed and the patch was kept at the same height above the ground plane as illustrated in Figure 4.10.

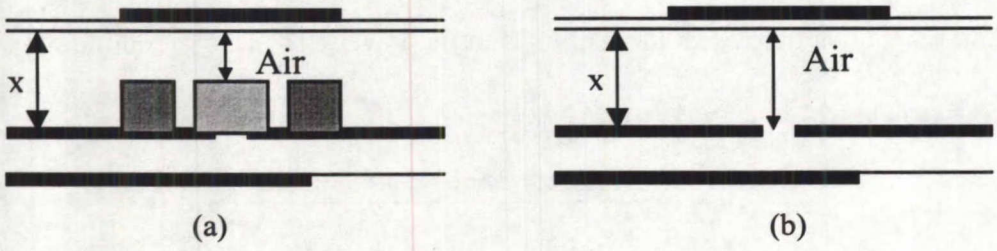

Figure 4.10: Pictorial Diagram of (a) Loaded Structure, (b) Reference Case

The reference case was different for each structure since the total amount of air differed depending on the thickness of the dielectric sample and the height of the patch required to get the desired bandwidth. For this reason it was important to know the return loss characteristic for the structure having a thickness of air from 2 to 8 mm between the patch and the ground plane. These cases were simulated in Ensemble but only the characteristics of the first three heights were obtained, since above 4 mm the coupling to the patch was unacceptably degraded. For the remaining heights, the reference resonant frequency was calculated using the estimator tool in Ensemble.

The curves of Figure 4.11 represent the Ensemble simulated return loss results for the patch with a layer of air added between the ground plane and the patch substrate. The

results showed that the resonant frequency was just above 3 GHz for heights 2, 3, and 4 mm.

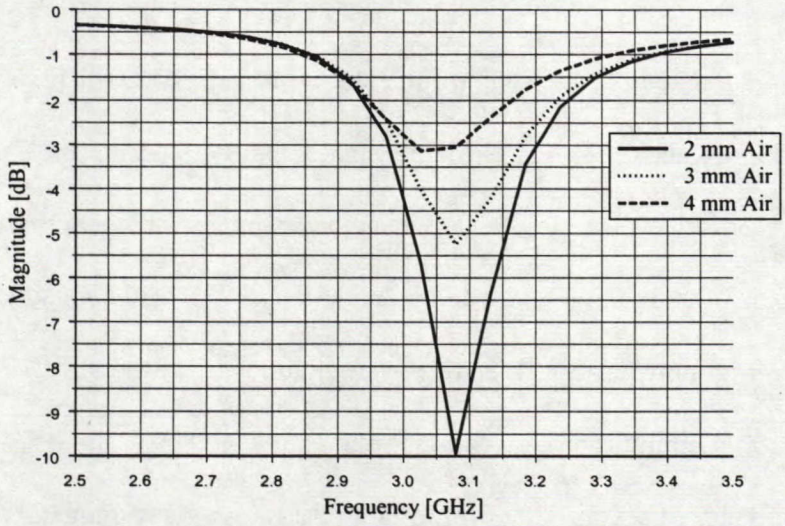

Figure 4.11: Ensemble Return Loss Results for a Patch on an Air Substrate

Assuming a matched condition, Table 4.2 displays the reference resonant frequencies of a patch sitting on 5, 6, 7, and 8 mm of air. These resonant frequency results were obtained from the Ensemble estimator tool, given VSWR=2 and Z_{in}=50 Ω. These values were required by the estimator tool and were presumed to be realistic. However, since the resonant frequencies obtained from this tool were the reference frequencies used for comparison purposes and for determination of the frequency reduction in all of the proceeding measurements, experimental confirmation of the assumptions should be obtained to confirm the accuracy of the results.

Total Height of Air (mm)	Resonant Frequency (GHz)
5	3.43
6	3.33
7	3.24
8	3.16

Table 4.2: Characteristics of the Patch on an Air Substrate

4.4 Return Loss Trend Analysis

4.4.1 Overview

The trends related only to loading the slot with dielectric will first be investigated followed by the trends observed with only side loading. Many measurements were recorded but only a select few will be shown as they represent the general trends.

Prior to discussing how the loaded patch antenna was matched, a brief section will explain the required network analyzer reference plane shift to the slot. Two sections are then devoted to explaining the observations related to matching. The discussion will end with a brief summary of several other important return loss measurements.

4.4.2 Trends Observed with Slot Loading Only

This set of return loss measurements was intended to determine the effect of varying the length, width, height, and relative permittivity of the dielectric pieces loading the slot. All cases were measured with 1 mm of air between the sample and the patch substrate, a decision based on the initial measurements which indicated that a significant bandwidth improvement could be achieved. Adding more than 1 mm of air was shown to cause the match to degrade. The implications of this decision were that the trends observed when changing the height of the dielectric samples would not be entirely accurate since the patch height above the ground plane was not kept constant.

The major observations for the effect of each parameter are described below with graphs shown to illustrate the general trends.

4.4.2.1 Dielectric Height

With increasing height, the Smith chart resonant loop moved counter-clockwise (CCW) on a constant radius circle centered about a point near the r = 2 location (normalized resistance) on the horizontal axis. The rotation was away from the middle of the chart, often moving from the inductive region into the capacitive region. As the relative permittivity increased, this movement became more spread out and covered a larger distance. It was also observed that the match would degrade and the Smith chart resonant loop would often disappear as the height increased. Figures 4.12 through 4.14 illustrate these effects by showing the same dielectric sample over the slot for each relative permittivity.

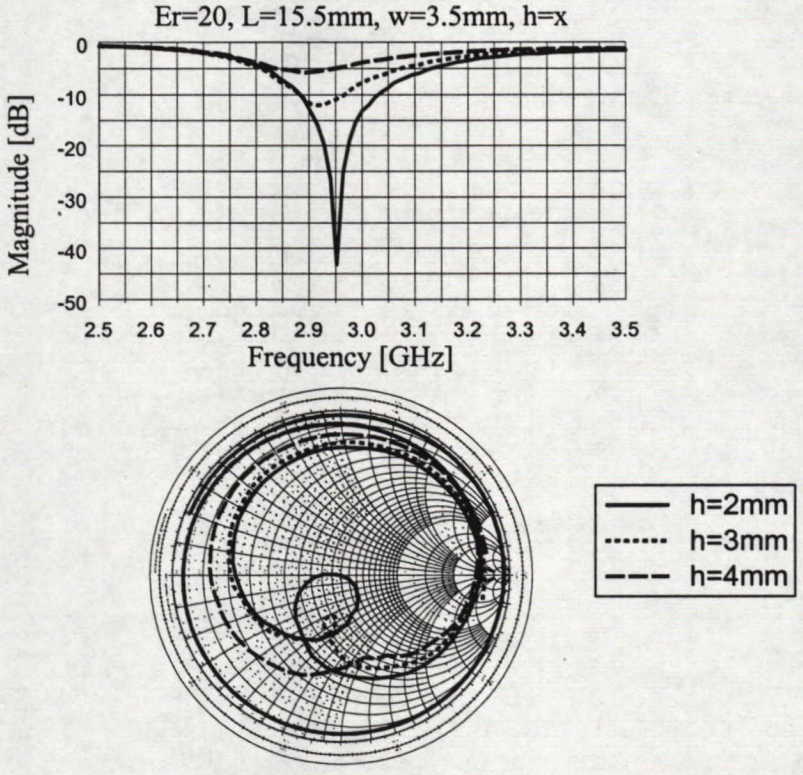

Figure 4.12: Measured Results of Varying Dielectric Height with E_r=20

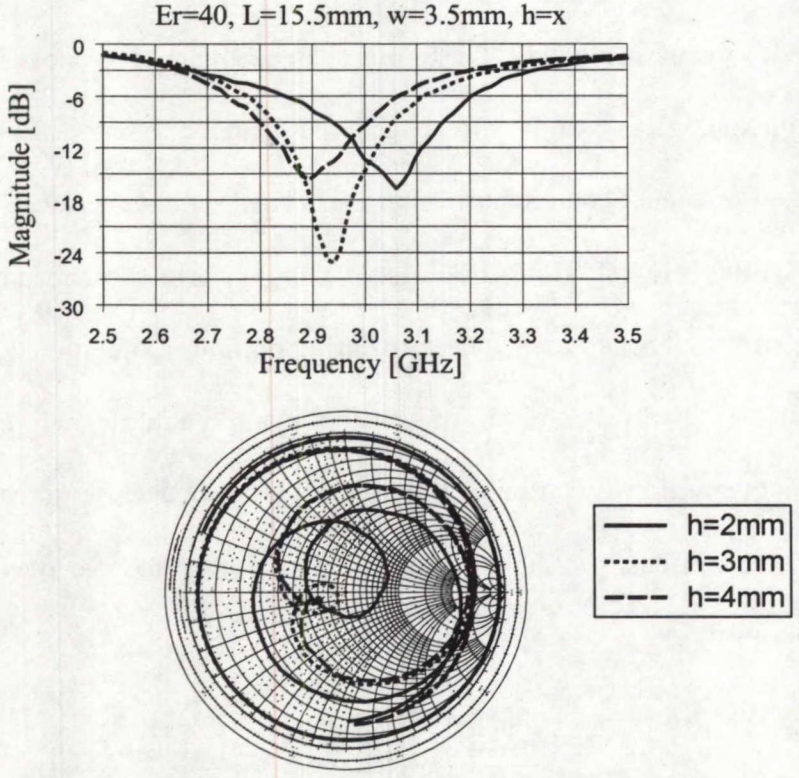

Figure 4.13: Measured Results of Varying Dielectric Height with E_r=40

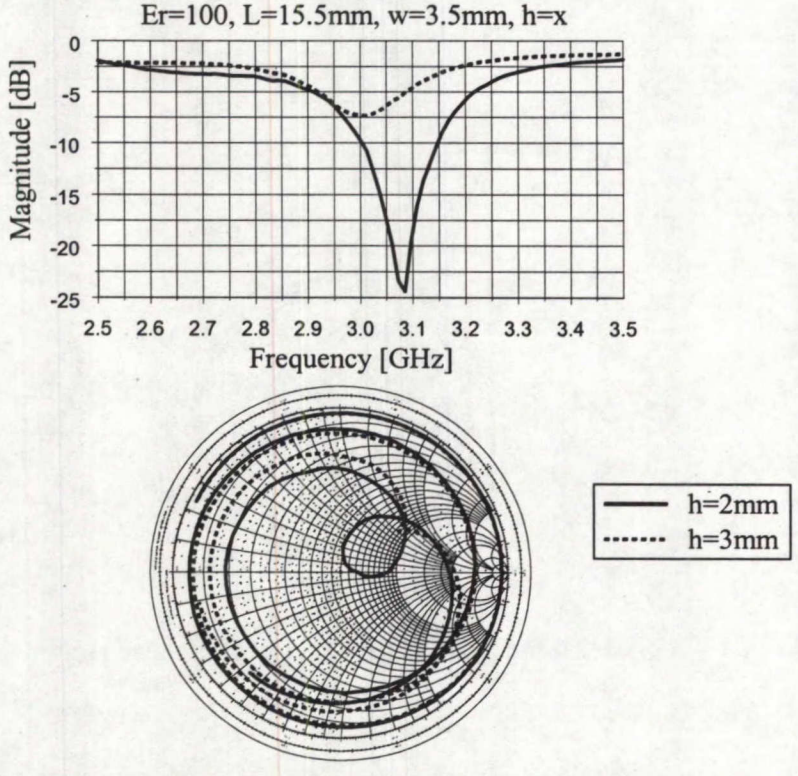

Figure 4.14: Measured Results of Varying Dielectric Height with E_r=100

4.4.2.2 Dielectric Width

Increasing the width of the sample caused the Smith chart resonant loop to enlarge for cases of E_r =20 and 40 and move clock-wise (CW) on a constant radius circle away from the capacitive section of the chart, towards and often into, the inductive region. As the relative permittivity increased, this movement became more pronounced and covered a larger distance. Also, as the permittivity increased, the size of the loop began to decrease with increasing sample width such that, when E_r=100, the loops had become very small. This effect is illustrated in Figures 4.15 through 4.17. The size of the resonant loop is important since it is an indication of the impedance bandwidth.

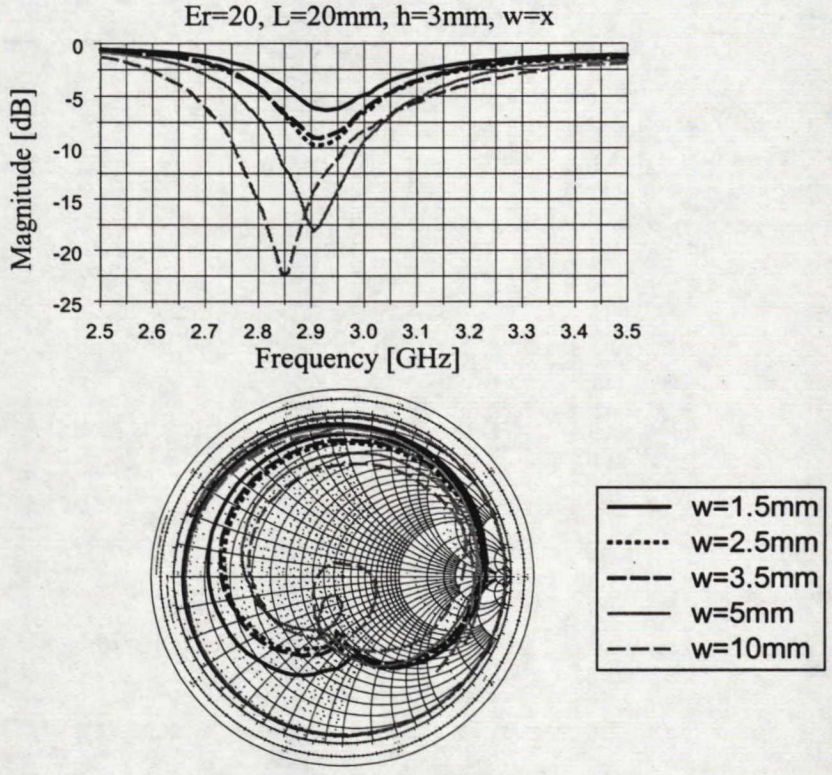

Figure 4.15: Measured Results of Varying Dielectric Width with E_r=20

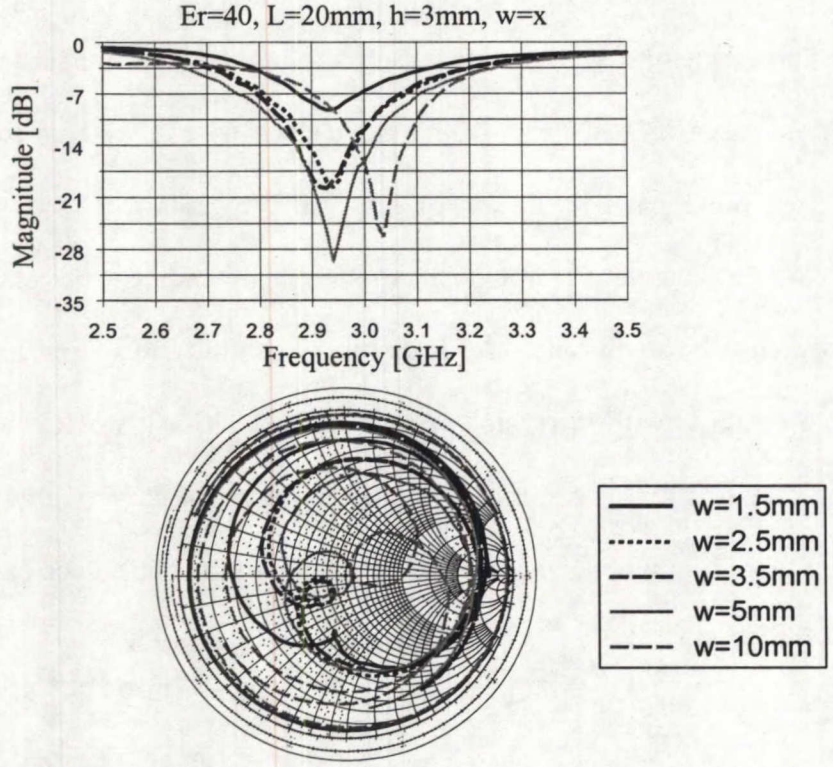

Figure 4.16: Measured Results of Varying Dielectric Width with E_r=40

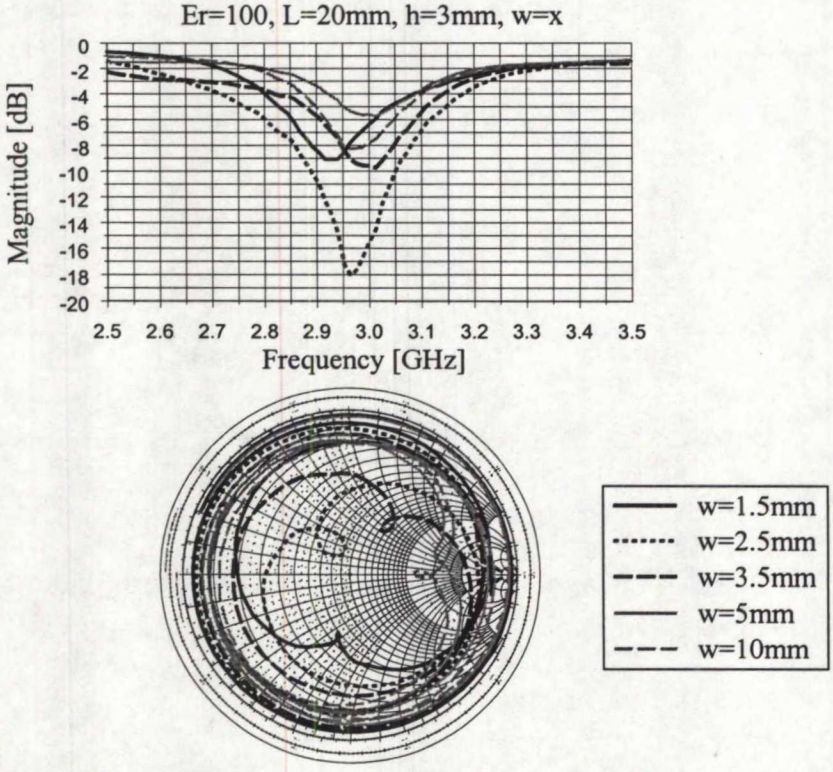

Figure 4.17: Measured Results of Varying Dielectric Width with E_r=100

4.4.2.3 Dielectric Length

An increase in the length of a sample caused the Smith chart resonant loop to rotate slightly CCW on a constant radius circle while tending to decrease in the process. This effect was minimal when E_r =20 but, with increasing relative permittivity, it became far more noticeable such that, when E_r=100, the resonant loop rotation with increasing length was significant. This effect is shown in Figures 4.18 through 4.20.

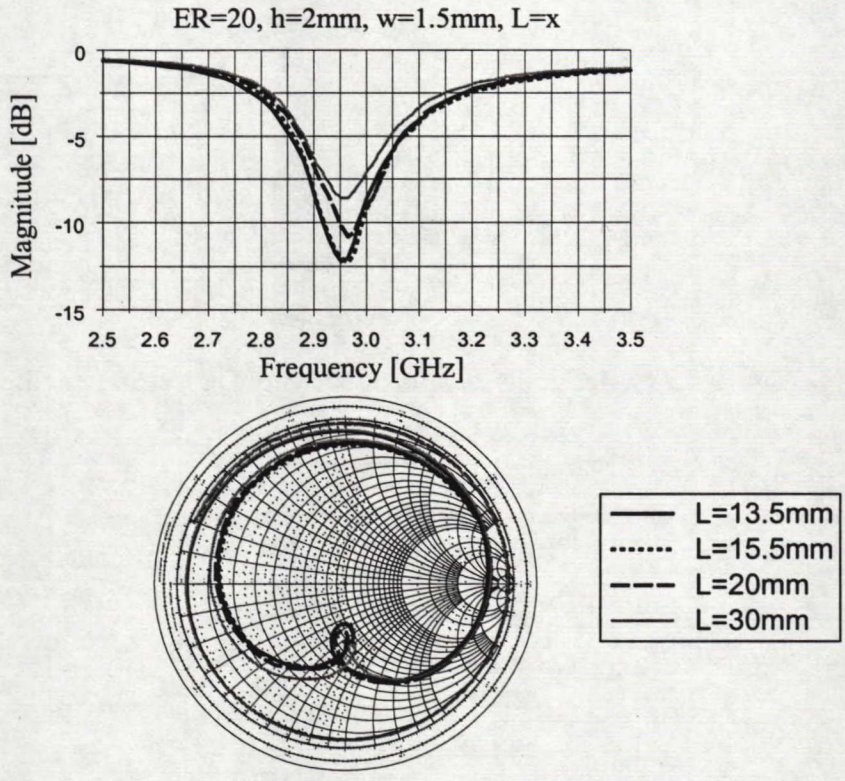

Figure 4.18: Measured Results of Varying Dielectric Length with E_r=20

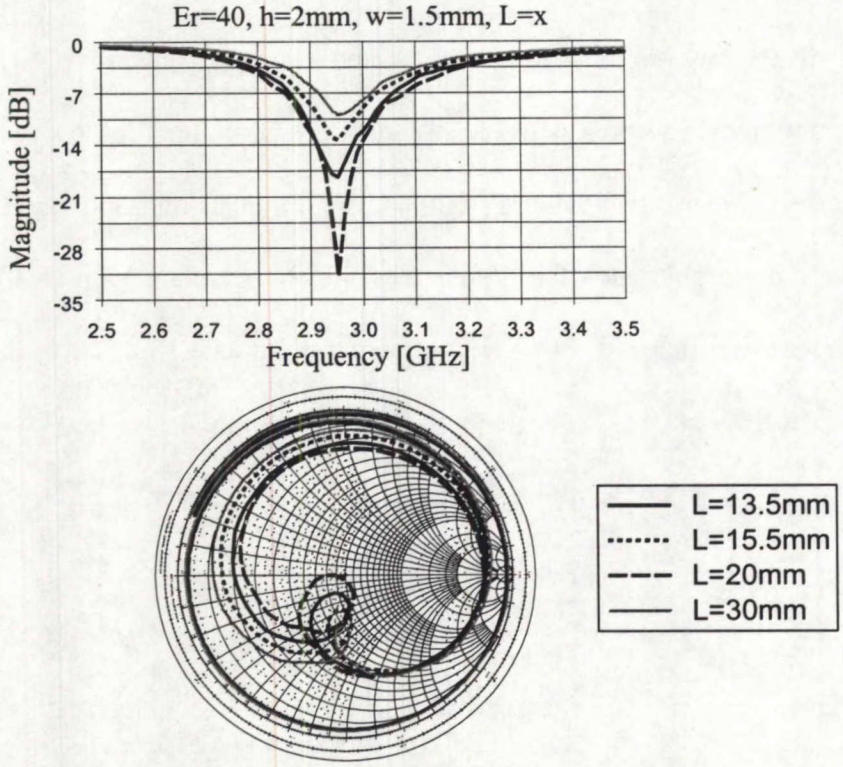

Figure 4.19: Measured Results of Varying Dielectric Length with E_r=40

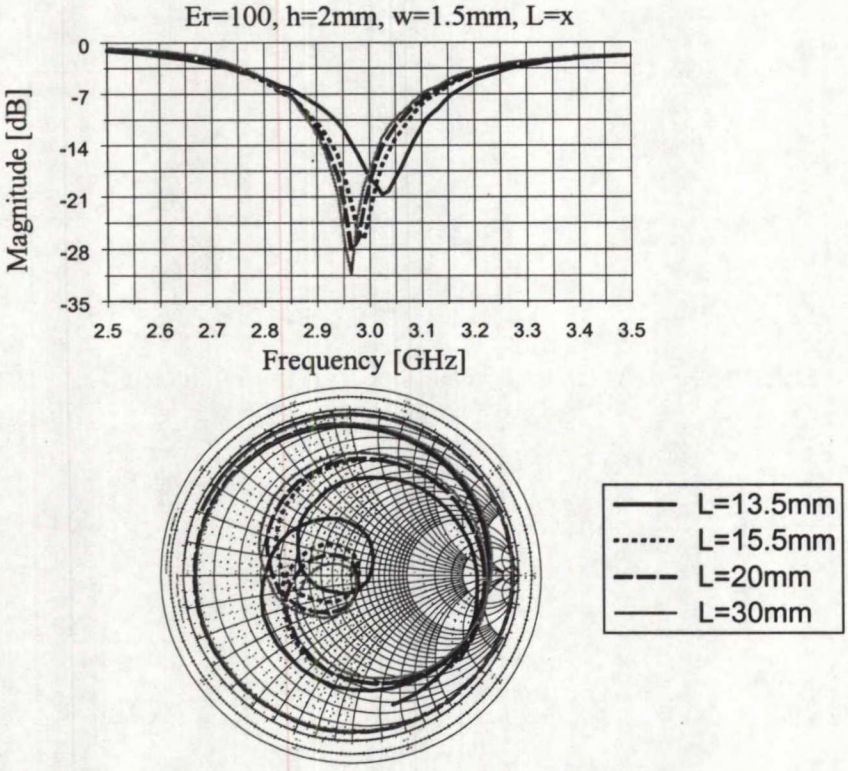

Figure 4.20: Measured Results of Varying Dielectric Length with E_r=100

4.4.2.4 Relative Permittivity

Figures 4.21 through 4.23 represent three selected cases that illustrate the effect of the slot sample's relative permittivity. It was found that samples with relative permittivities of 20 and 40 caused the Smith chart resonant loop to rotate CW on a constant radius circle toward the middle of the chart. When E_r=100 the resonant loop also rotated CW but much farther into the inductive region and well away from the middle. In general, the resonant loop increased in size when going from E_r =20 to E_r =40 but became very small at E_r=100.

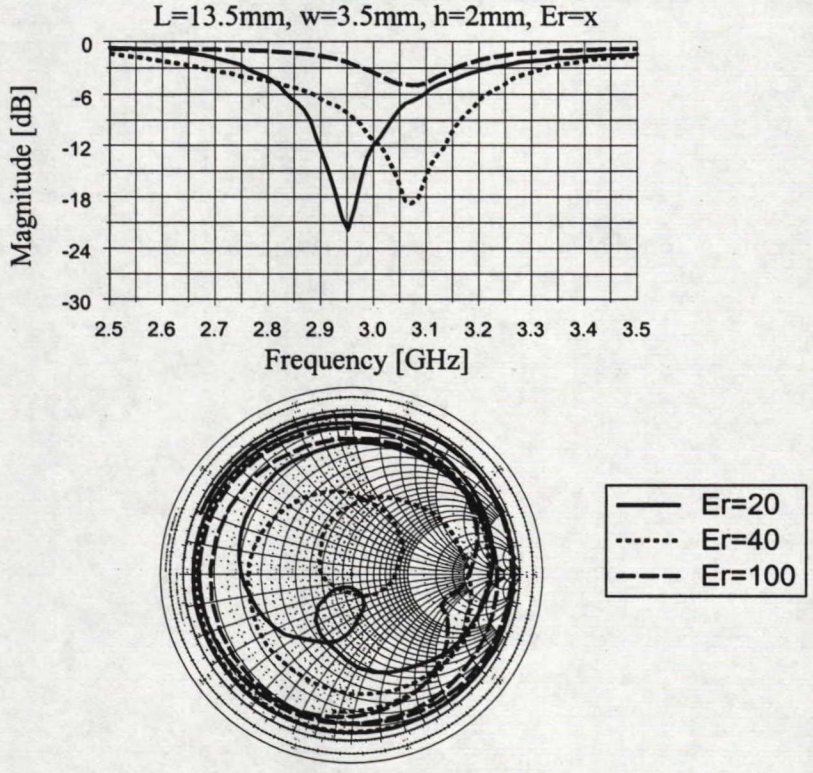

Figure 4.21: Measured Results of Varying Dielectric Relative Permittivity

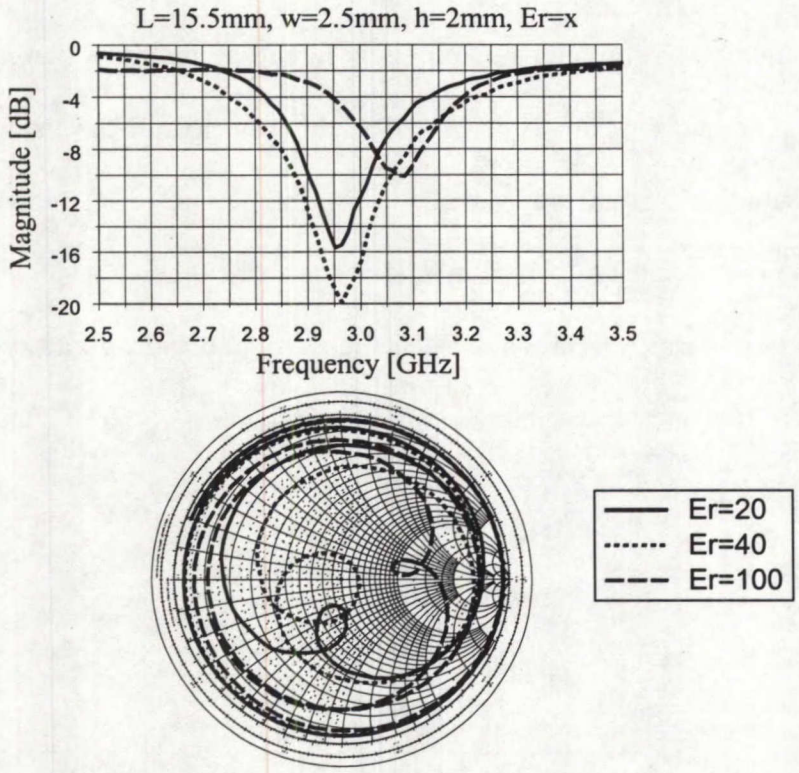

Figure 4.22: Measured Results of Varying Dielectric Relative Permittivity

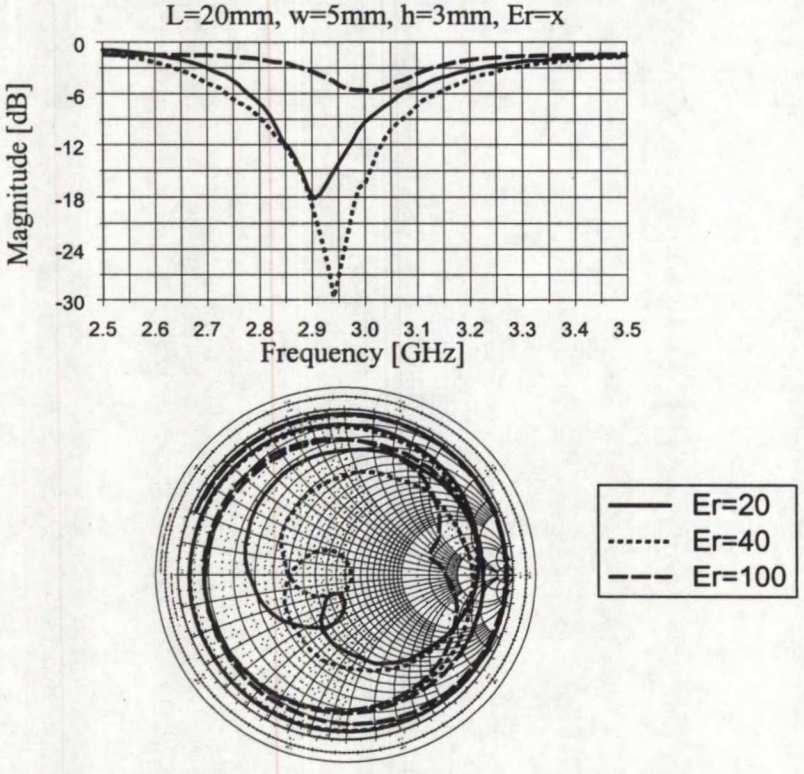

Figure 4.23: Measured Results of Varying Dielectric Relative Permittivity

4.4.2.5 Air above the Dielectric Pieces

Increasing the amount of air above the dielectric samples caused both the resonant frequency and the bandwidth of the patch to increase. This was only true up until a certain point, though, since the coupling between the patch and the slot would degrade significantly with too much additional air.

The amount of air was controlled by the thickness of the spacers used in the measurements. Since they were made in 1 mm increments, the accuracy of these measurements was only within 1 mm.

4.4.2.6 General Remarks

As expected, slot loading had little effect on the resonant frequency of the patch which remained at about 3 GHz, the reference value predicted by Ensemble for the patch entirely on air. The effect of all variables was to rotate the Smith chart locus either CW or CCW on a circle of constant radius centered between the middle of the chart and the open-circuit point.

All parameters had an effect on the matching ability of the patch. Results indicated that the patch, without side loading, could be matched quite easily to 50 Ω. This was an important observation since aperture-coupling can be used instead of probe-coupling for L-band thick-air substrate patches to overcome the radiation problems of the probe feed.

A slight frequency shift was observed for samples having widths of 10 mm. This was justified since the wide sample would be infringing on an area where the electric fields would no longer be minimum, thus contributing to a frequency reduction according to perturbation theory. Although the effect of the dielectric length became more

noticeable as the relative permittivity increased, varying the widths and thicknesses of the dielectric samples had more pronounced effects.

It is important to note that these results were measured for the specific slot and stub length as originally designed. These dimensions may not have been optimum for the dielectric-loaded patch configuration. The effect of varying the stub length was approximated experimentally by both adding a length of copper tape to the end of the stub and by scratching away part of the existing etched stub. These results showed that the resonant loop would rotate around the Smith chart depending on the amount of length either added or subtracted. The resonant loop did not move laterally so that adjusting the stub length would be only useful for eliminating reactive components of reflections. In order to optimize the slot dimensions, several feed boards would need to be fabricated having slots with incremental size changes. Time did not allow for this work.

4.4.3 Trends Observed with Only Side Loading

This set of measurements was intended to determine the effect of varying the width, height, and relative permittivity of the dielectric pieces that load the edges of the patch. Different from the slot-loaded cases, only two widths and heights were considered for measurement purposes, a decision based on the quantity of material available and the time required for fabrication.

The measurements for these cases were performed both with and without the 1 mm layer of air between the dielectric sample and the patch substrate. The decision to measure without the air was based on the fact that the extra layer of air would effectively reduce the permittivity under the patch edges and result in less of a frequency reduction according to perturbation theory. Since the purpose of examining side loading without

slot loading was to observe the lowest frequency reduction possible, this would be prohibited by the extra air.

The major observations describing the effect of each parameter are outlined below with an example of these results being illustrated in the plots of Figure 4.24. In this case, no air was between the patch and load pieces and the pieces had a permittivity of 100, a width of 10 mm, and a height of 4 mm. The trends shown in the plots as the permittivity increases from 20 to 100 were as expected, regardless of the height or width of the sample. Also, the relative location of the resonant frequencies shown on the graphs were the same for each height with varying width and were also the same for each width with varying height.

4.4.3.1 Dielectric Height and Width

Increasing the sample height from 2 mm to 4 mm and the width from 5 mm to 10 mm caused the Smith chart locus to rotate CW on a constant radius circle from the capacitive to the inductive sides of the chart. The resonant frequency decreased with this increase in height and width and a similar effect was observed to occur for all relative permittivities. Both results can be explained by perturbation theory and were as expected.

4.4.3.2 Dielectric Relative Permittivity

Although similar effects were observed for all relative permittivities, it was noted that higher order resonances appeared for the samples with h=4 mm and E_r =100. This was expected since the large dielectric pieces tended to radiate at frequencies within the band of interest. These resonances were spaced more than 1 GHz away from the resonant frequencies of interest and therefore were assumed to not cause any problems. Another

observation for increasing relative permittivities was that the resonant loops became more narrow band. This was clear from the degrading smoothness quality of the resonant loops on the Smith charts indicating that fewer frequency points were contained in the loops.

4.4.3.3 Air Above the Side Loading

As predicted, a much larger reduction in frequency was obtained when the 1 mm of air was removed from between the sample and patch substrate. Without the air, the lowest frequency reduction achieved was 1.42 GHz for the case when E_r =100, L=37mm, w=10 mm, and h=4 mm. The measured results shown in the Figure 4.24 include the results both with and without the air. The Smith chart resonant loops tended to be a little larger in the cases without the air since the coupling would improve with the patch being closer to the slot.

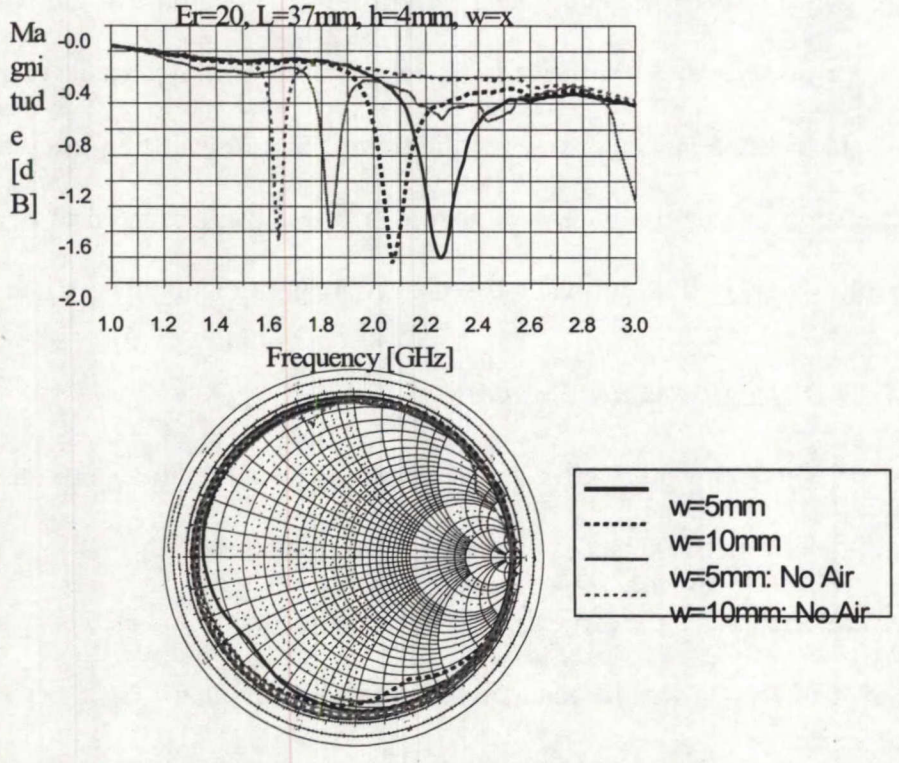

Figure 4.24 (a): Measured Results of Varying Dielectric Width (h=4 mm) for E_r=20

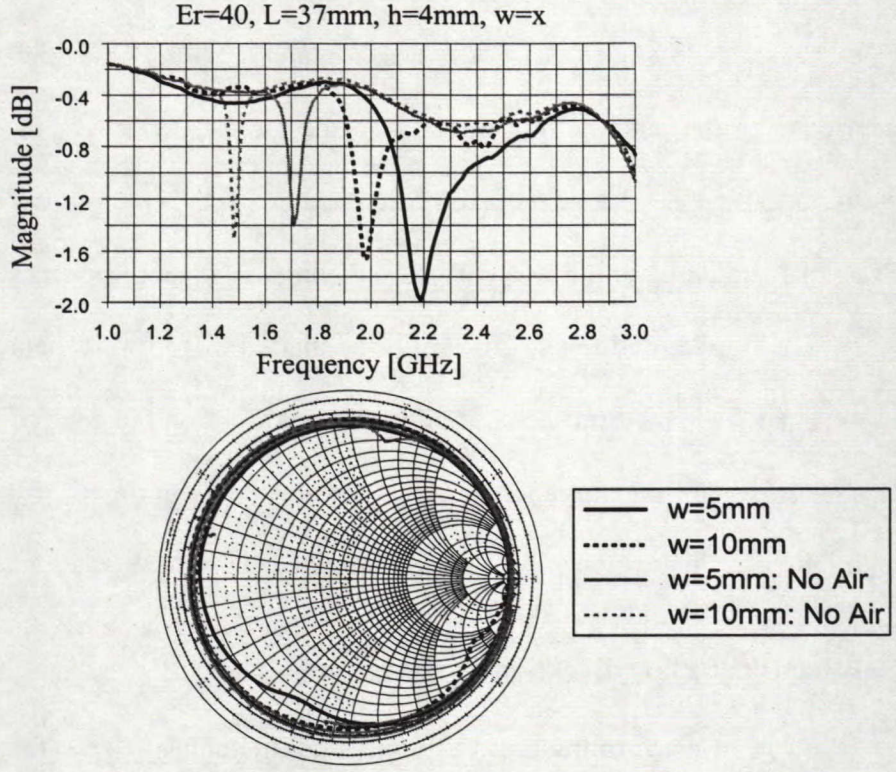

Figure 4.24 (b): Measured Results of Varying Dielectric Width (h=4 mm) for E_r=40

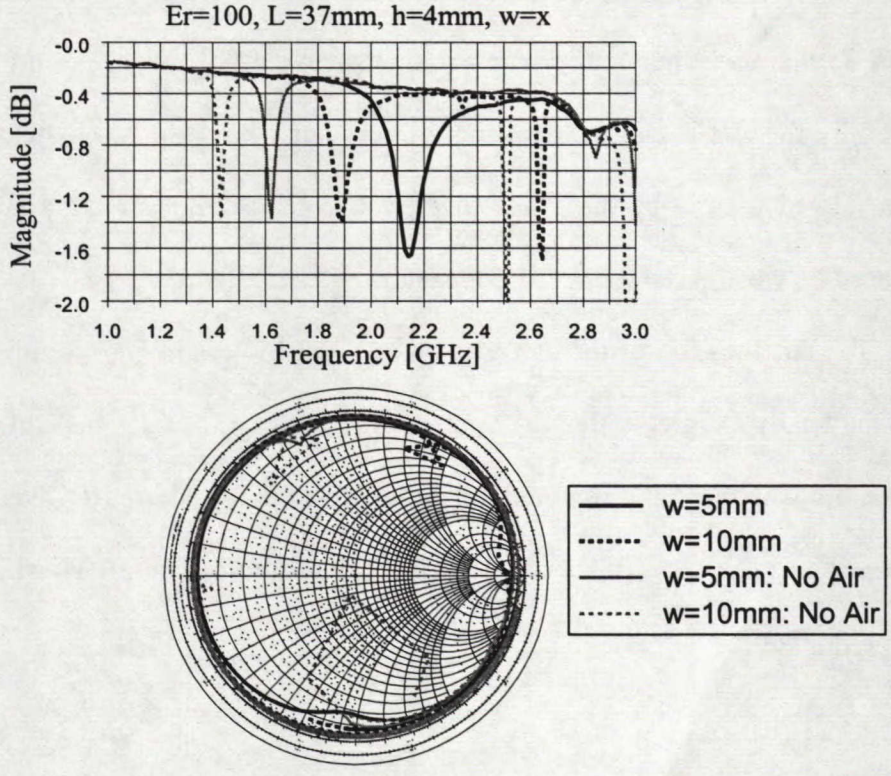

Figure 4.24 (c): Measured Results of Varying Dielectric Width (h=4 mm) for E_r=100

4.4.3.4 General Remarks

Of the side-loaded cases, the best frequency reduction achieved was 53% and it occurred with the patch sitting directly on the largest dielectric pieces (w=10 mm and h=4 mm) having E_r =100. The patch resonated at 1.42 GHz, representing a reduction of 53% when compared to the reference case having a resonant frequency of 3 GHz.

These measured results also revealed that, at this low frequency, the antenna was not matched since the Smith chart resonant loops were on the edge of the chart and were very small. Again, the slot and stub may not have been optimal for these configurations and might result in a better match when optimized.

4.4.4 Reference Plane Location For Matching

Prior to performing any experimental matching, the reference plane of the network analyzer had to be moved from the default location at the connector pin to the slot. In this way, the locus on the Smith chart would be displayed in the correct phase as seen by the slot. This was especially important when external matching networks were considered as will be discussed in section 4.4.5.4 since the extra stubs could then be placed between the slot and the connector.

The location of the slot was determined by looking at the time-domain response of the feed structure, without the patch. Figure 4.25 illustrates this structure. Achieving a time-domain response required a frequency-domain calibration over a wide range of frequencies from 0.04 GHz to 40 GHz to allow for an accurate Fourier Transform to the time-domain.

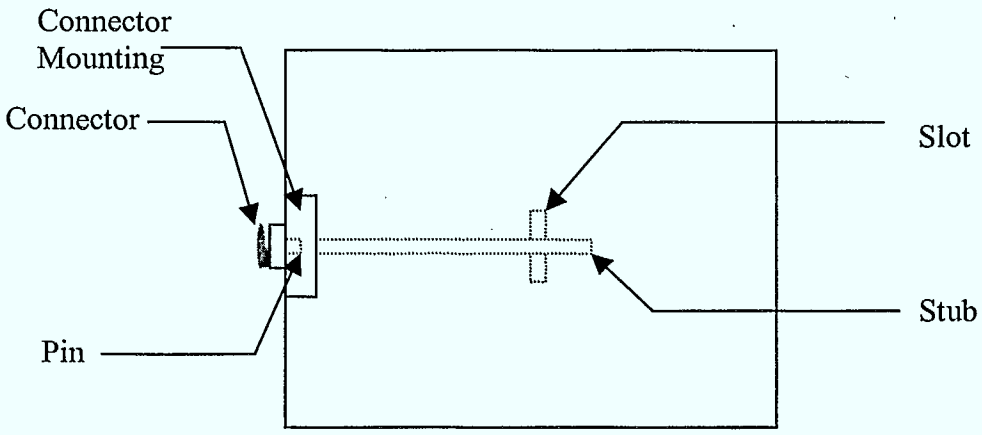

Figure 4.25: Feed Structure with Exaggerated Dimensions

The time-domain response showed the location of all of the discontinuities in the feed structure. From the plot shown in Figure 4.26, the discontinuities located at the connector, pin, slot, and microstrip stub are all visible and labeled. The slot was located at 9.016 cm from the default reference, a value that was very close to the expected distance between the slot and the connector. This offset was applied to all network analyzer results displayed in the remainder of the chapter.

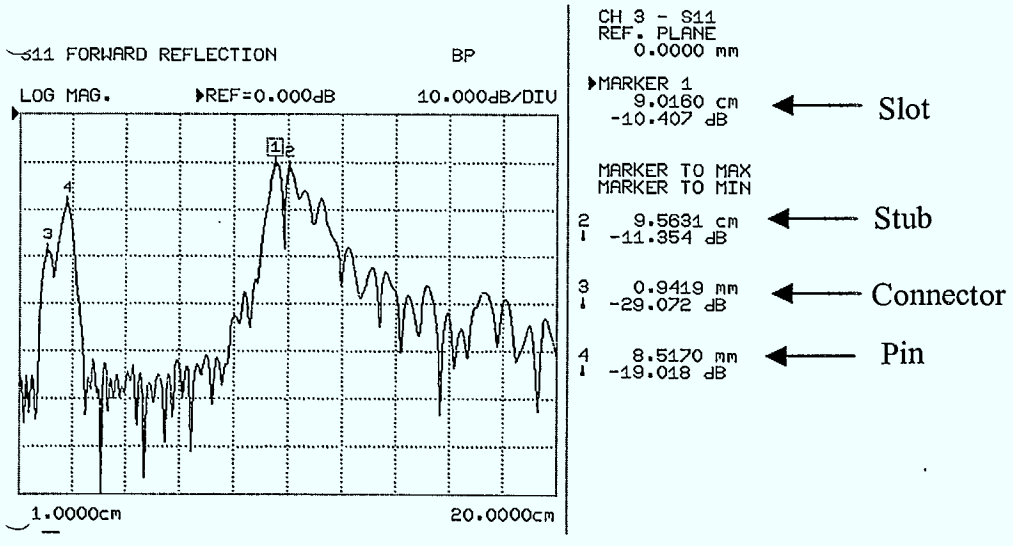

Figure 4.26: Time-Domain Reference Plane Determination

4.4.5 Matching Without Extra Air

4.4.5.1 Matching Procedure

The process of impedance matching involved cycling through various dielectric pieces over the slot for each set of side load pieces in an attempt to obtain a match at that frequency reduction. The trends observed from slot loading only were applied and found to assist greatly in the matching process. The location of the resonant loop on the Smith chart was observed and then moved as near as possible to the 50 Ω point by changing the slot load piece. In all cases, the patch was placed directly on the side load pieces since this was found to enable the largest frequency reduction.

4.4.5.2 Matching Observations

Matching without extra air was an interesting challenge since, with only side loading, the resonant loop was on the edge of the Smith chart and was very small. Loading the slot would rotate the loop according to the previously observed trends but lateral movement toward the center of the chart was limited.

Attempting to match while side loaded with dielectric pieces having relative permittivities of 100 proved to be the most difficult regardless of the piece over the slot. The lower the permittivity of the side loading, the better the ability to match and hence the larger the resonant loop on the Smith chart. In fact, using pieces over the slot that had permittivities higher than that of the side loading consistently generated large resonant loops on the Smith chart. It was ineffective, for example, to be side loaded with pieces having E_r=100 since the highest permittivity available to load the slot was 100. The compromise was that lowering the permittivity of the side load pieces to achieve a match

caused the resonant frequency of the antenna to increase and reduced the degree of miniaturization.

The plots of Figure 4.27 illustrate the differences between having side loading with permittivity of 100 versus 40 and 20. The different resonant loop sizes on the Smith chart and the resonant frequency changes can be observed.

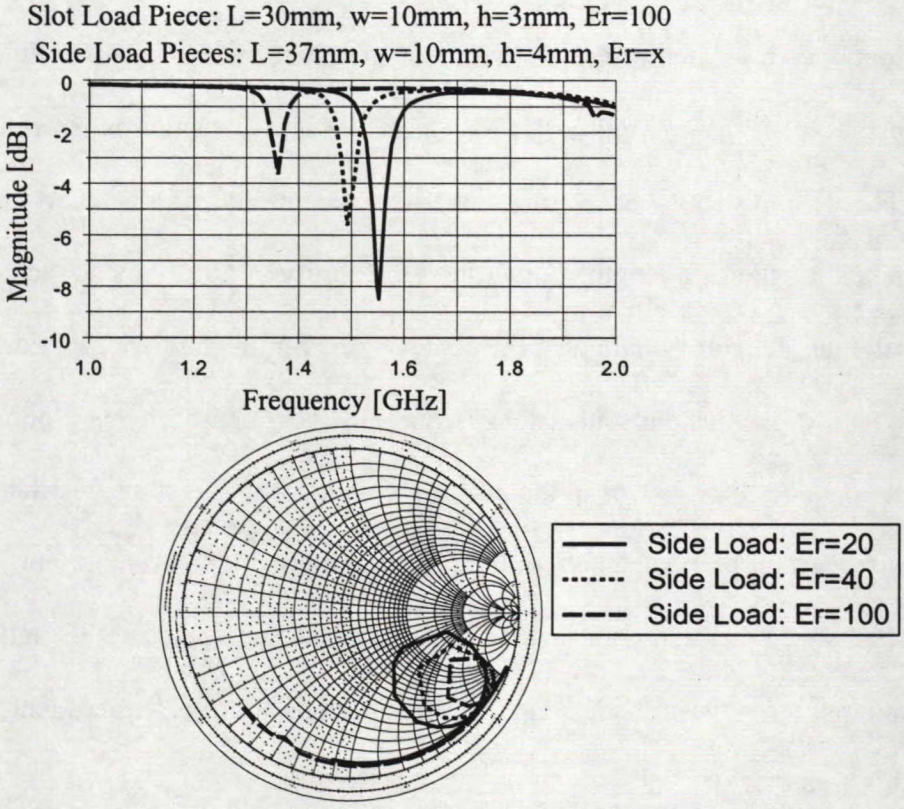

Figure 4.27: Attempting to Match with Side Loading with E_r=100, E_r=40, E_r=20

It was found that side load pieces having the largest dimensions (10 mm wide and 4 mm thick) were the most effective at providing both a good frequency reduction as well as a resonant loop with a fair number of frequency points such that the loop curvature was smooth. Similarly, matching with slot load samples having widths less than 3.5 mm was not as effective as when the widths were larger since the width of the larger pieces

actually contributed to the frequency reduction by infringing on areas of higher electric fields beneath the patch.

4.4.5.3 General Summary

It was difficult to match this antenna to 50 Ω without tuning the stub length and with the patch sitting directly on the side load pieces without any extra air. The resonant loops were located at the perimeter of the chart as illustrated in Figure 4.27, generally close to the open circuit point but in the capacitive region, when referenced to the slot. These loops could easily be moved to the middle of the chart, hence matched, by adjusting the stub length. But without the ability to tune the stub, achieving a case with a resonant loop anywhere near the center of the Smith chart was very difficult.

Also, these resonant loops contained very few frequency points as shown in the non-smooth loop curves in the plots of Figure 4.27. This indicated that a small bandwidth would result once matched with an external network. It is important to realize that these results were based on one set of slot dimensions and a fixed stub length which may not be optimum for these loaded patch configurations. Further experimentation is required in this area.

4.4.5.4 External Matching

In order to get an approximate idea of the impedance bandwidth for these non-matched cases, it was decided to simulate an external matching network using the HP Libra circuit modeling software. Since the data was referenced to the slot, the external network would be located between the connector and the slot.

The first of two matching techniques investigated was a simple quarter-wave transformer. A series microstrip line was used to rotate the Smith chart resonant loop close to the real axis, then the transformer shifted the loop to the 50 Ω point. The second method involved using an open-circuit shunt stub to cancel the reactive part of the impedance. The resonant loop was first moved to the g=1 location with a small series transmission line; then, by adjusting the open-circuit stub dimensions, the loop was rotated along the g=1 circle until it reached the 50 Ω point. When optimized, it was found that there was very little difference between these two techniques.

The impedance bandwidths obtained after external matching varied depending on the original resonant loop sizes. Once matched and centered on the 50 Ω point, the initially large resonant loops became even larger such that S_{11} would often never cross the –10 dB line resulting in zero bandwidth. The initially small resonant loops also became larger when matched but S_{11} did cross the –10 dB line and bandwidths in the range of 2 to 4% were achieved.

Figure 4.28 displays one of the cases that was externally matched using a quarter-wave transformer. The non-smooth loop curvature and the resulting 3.7% bandwidth, which was well below the desired 8%, can be noted.

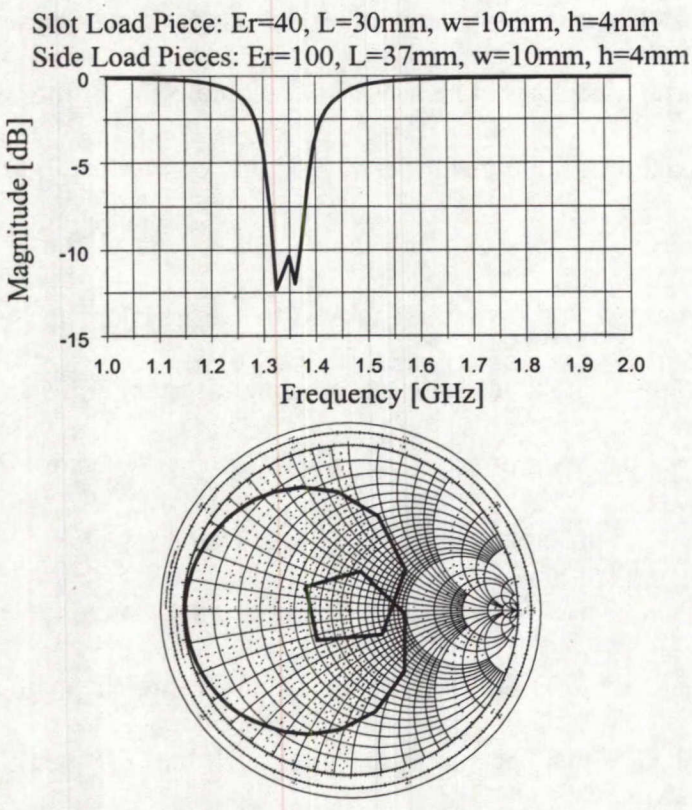

Figure 4.28: Results with λ/4 Transformer as an External Matching Network

4.4.6 Matching With Extra Air

4.4.6.1 Matching Procedure

The objective was to determine how much air was required between the dielectric load pieces and the patch in order to achieve an impedance bandwidth greater than 8%. Since increasing the amount of air beneath a patch increases the resonant frequency of the patch, it was understood that this attempt to increase bandwidth would be at the expense of the frequency reduction.

The measurement process involved cycling through the various slot dielectric pieces for a single set of side load pieces (w=10 mm and h=4 mm) but the amount of air was increased between the samples and the patch until the Smith chart resonant loop

moved to the 50 Ω point. Again, the trends observed from slot loading only were applied and the quantity of air was controlled by inserting the specially fabricated plastic spacers on the alignment screws. Since the smallest spacer thickness was 1 mm, the best match was determined to within this accuracy.

4.4.6.2 Matching Observations

Depending on the particular slot and side load sample being tested, between 2 and 4 mm of air was required to achieve a match, giving the antenna an overall height between 6 and 8 mm. Bandwidths ranged from 8% to nearly 15% with resonant frequencies varying from 2.22 to 2.48 GHz.

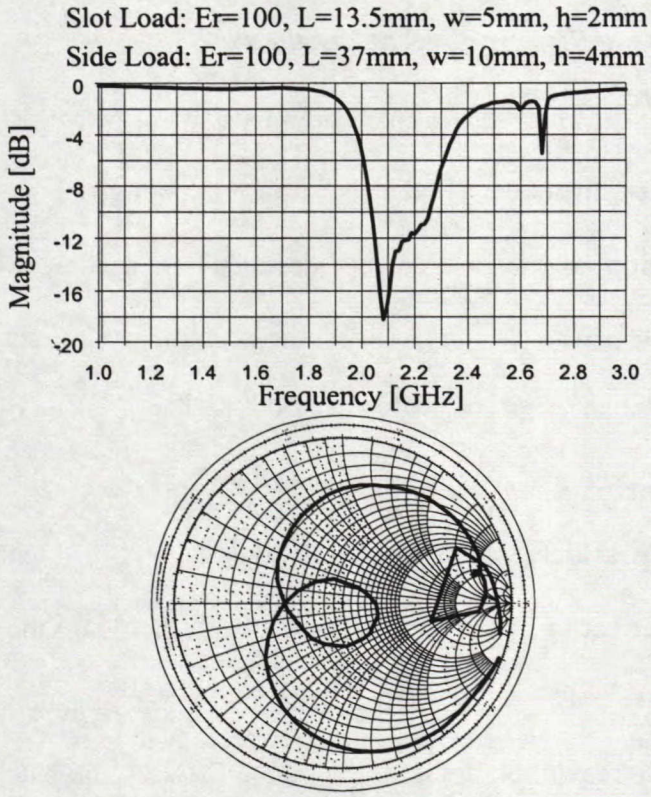

Figure 4.29: Return Loss of the Lowest Resonant Frequency Matched Case

The lowest resonant frequency, when compared to the reference frequencies in Table 4.2, occurred when the patch was 6 mm off the ground plane with a slot and side

load samples having parameters as indicated in Figure 4.29. The impedance bandwidth for this case was 10.8%. Given these values, to obtain an impedance bandwidth greater than 8%, a frequency reduction of 32% (from 3.33 GHz to 2.22 GHz) was approximately all that could be achieved. This was a significant sacrifice, considering 53% was the reduction achieved without matching as described in section 4.4.3.4.

4.4.7 Other Important Return Loss Measurements

Further return loss measurements were performed with the intention of evaluating the effect of air between the slot load dielectric pieces and the patch, the effect of the side loading location, and the effect of loading only one side of the patch.

4.4.7.1 Air Between the Dielectric Pieces and the Patch

The purpose of this set of measurements was to confirm the decision of maintaining 1 mm of air above the dielectric pieces loading the slot, without any side loading, in the return loss measurements described in section 4.4.2. As previously explained, this number was chosen based on the preliminary investigation where it was observed that more than 1 mm of air between the dielectric piece over the slot and the patch would cause the coupling to degrade excessively.

This set of measurements involved selecting several different dielectric samples and observing the effect of increasing the air between them and the patch. The general trend observed was consistent with the original measurements and confirmed that 1 mm of air was the maximum amount acceptable between the patch and the dielectric before losing coupling. The same effect was observed for the other samples.

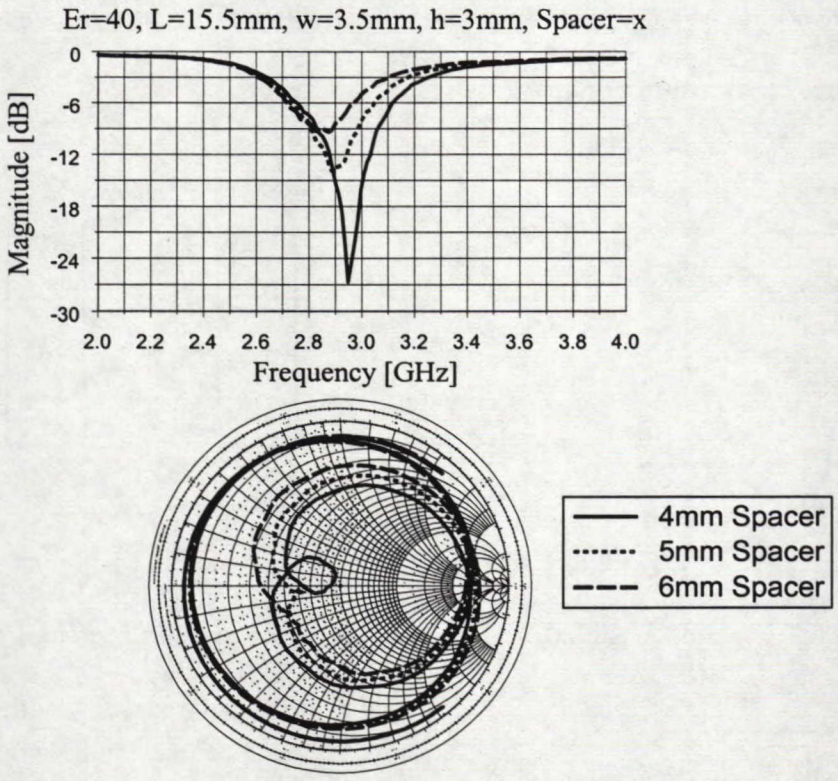

Figure 4.30: Example of the Effect of Air above the Slot Loading

The curves in Figure 4.30 show an example of these results where each represents an increase in the spacer height. This height was measured from the ground plane up to the patch. The actual amount of air between the patch and the dielectric sample was thus the spacer thickness minus the sample thickness.

4.4.7.2 Locations of the Side Loading Dielectric Pieces

This set of return loss measurements was intended to determine the best placement of the side-loaded dielectric samples. Three locations were chosen for the measurements and are illustrated in Figure 4.31. The dielectric samples were initially placed completely within the bounds of the patch with their outer edges being aligned with the outer edges of the patch, as shown in Figure 4.31(a). They were then moved out

of these bounds about halfway and finally three-quarters of the way past the patch bounds as shown in Figure 4.31(b) and (c) respectively.

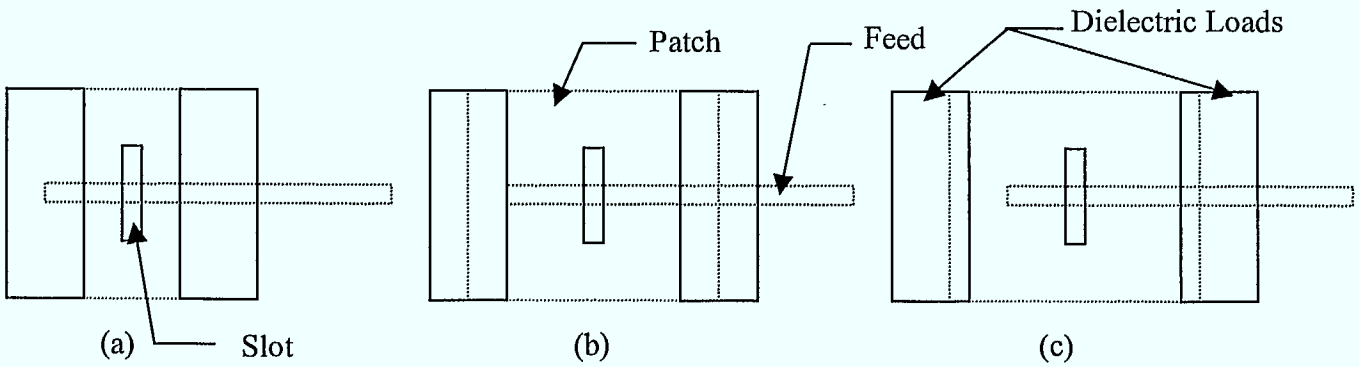

Figure 4.31: Location of Side Loading Samples

It was not feasible to move the pieces toward the center of the patch since that space would be occupied by the slot load pieces. Only samples with 10 mm widths and 4 mm heights with varying relative permittivity were used.

The basic trend observed during these measurements was that moving the dielectric samples out of the patch bounds increased the resonant frequency, regardless of the relative permittivity of the dielectric load pieces. This trend is illustrated in Figure 4.32 where the locations are referenced to the diagram in Figure 4.31.

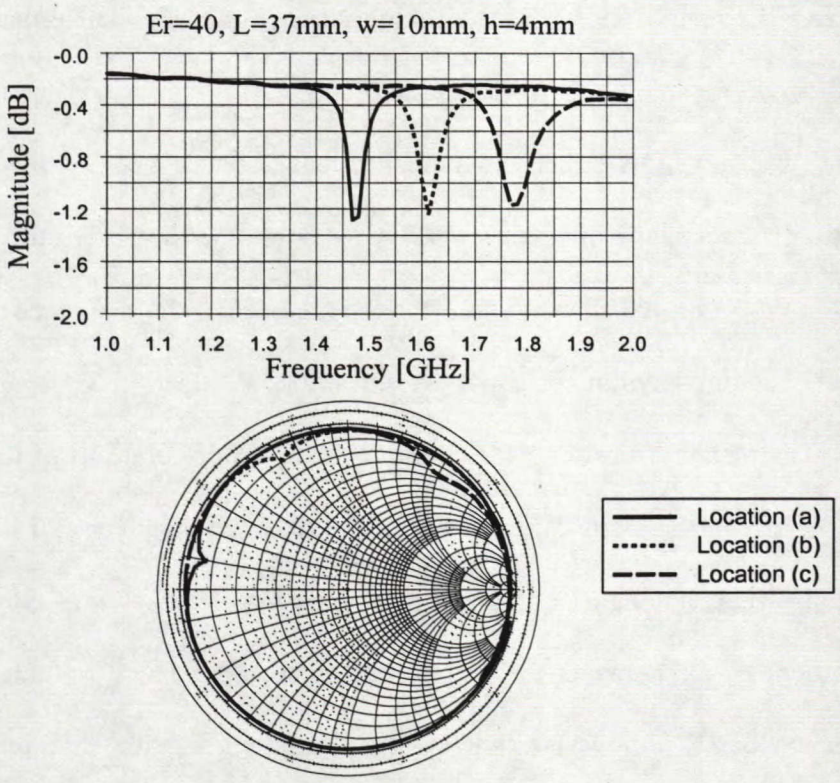

Figure 4.32: Example of the Effect of the Location of the Side Loading

Based on these results, it was found to be more beneficial from a frequency reduction point of view to keep the side loading dielectric pieces within the patch bounds. The fields under the patch edges are stronger than the fields outside the patch, thus enabling a bigger perturbation to occur when the dielectric sample covers the region under the edge of the patch.

4.4.7.3 Dielectric Loading under One Side of the Patch Only

Dielectric loading only one side of the patch was intended to observe the loading effects expected with a circularly polarized, dual-slot feed configuration. This type of structure would likely have each slot located near one edge of the patch instead of in the middle. In these cases, dielectric loading would only be feasible on the two other sides or one side per mode. Although the principle will be tested on an actual dual-feed circularly

polarized antenna (Chapter 5), these measurements were performed with the current patch by loading only one side instead of both.

To observe this effect, the dielectric-loaded patch was first arranged in a matched condition, as described in section 4.4.6, with both side load dielectric pieces, a slot load piece, and the required air below the patch. One of the side load pieces was then removed without changing anything else and the return loss was measured.

The results, from several randomly chosen configurations of loading, all revealed the same effect, this being an increase in the resonant frequency of the patch. With this change in frequency came a degradation of the match which was corrected by reducing the amount of air between the patch and the loading. Once re-matched, however, the impedance bandwidth was much smaller than when both side loading pieces were present. An example of this result is displayed in Figure 4.33.

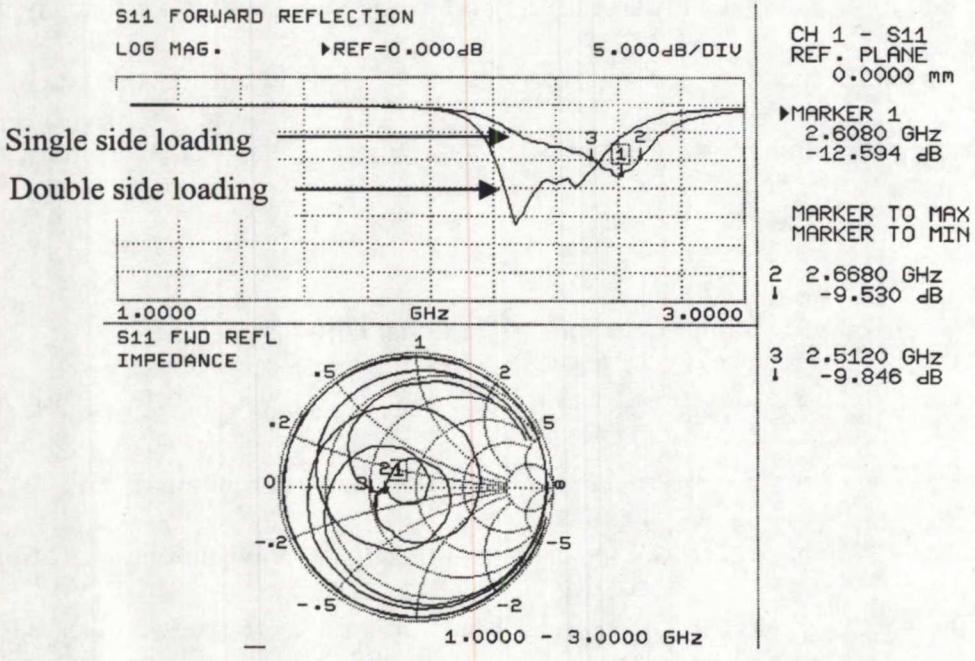

Figure 4.33: Example of the Effect of Loading Only One Side of the Patch

4.5 Radiation Pattern Measurements

4.5.1 Overview

Radiation pattern measurements were also performed on selected configurations of the dielectric-loaded patch antenna. Both double and single side loading was investigated with the intention being to observe the effect of loading on the patterns. A comparison between these patterns and an equivalent case with probe-coupling was also performed to highlight the benefits of the slot-loaded aperture feed.

4.5.2 Both Patch Sides Loaded

Radiation patterns were measured for six dielectric-loaded structures in which the load pieces were placed on both sides of the patch as well as over the slot. The return loss characteristic of each structure was tested prior to pattern measurement to ensure that each was well matched having an impedance bandwidth greater than 8%. The properties of each loading case are listed in Table 4.3 and the measured results are summarized in Table 4.4.

Sample	E_r	Length (mm)	Width (mm)	Thickness (mm)
100-10	100	13.5	5	2
100-11	100	13.5	5	3
100-40	100	20	5	2
100-41	100	20	5	3
100-58	100	30	10	2
40-15	40	13.5	10	2
40-29	40	15.5	10	3
40-30	40	15.5	10	4
100s-4	100	37	10	4
40s-4	40	37	10	4
20s-4	20	37	10	4

Table 4.3: Dielectric Loading Sample Properties

Loading Cases [slot]/[sides]-[spacer]	Resonant Frequency (GHz)	E-Plane Gain (dB)	E-Plane Beamwidth (degrees)	Cross-Polarization Level (dB:-180° to 180°)
[100-10]/[100s-4]-[6mm]	2.10	7.34	81.23	20 dB below CoPol
[100-58]/[100s-4]-[7mm]	2.30	7.70	74.13	20 dB below CoPol
[100-40]/[40s-4]-[6mm]	2.30	7.43	72.98	20 dB below CoPol
[40-15]/[40s-4]-[8mm]	2.40	7.62	72.26	20 dB below CoPol
[100-41]/[20s-4]-[7mm]	2.40	7.45	73.60	20 dB below CoPol
[40-29]/[20s-4]-[7mm]	2.40	7.47	73.05	20 dB below CoPol

Table 4.4: Results from Pattern Measurements: Both Sides of Patch Loaded

It should be noted that in order to view the patterns in all 360 degrees of azimuth a primitive stand was used to mount the antenna in the anechoic chamber instead of the normal one. This stand was not as accurate since it depended on a visual confirmation of alignment. It is for this reason that the E and H-plane pattern gains do not exactly match at boresight.

The actual radiation patterns for the first loading case in Table 4.4 are displayed in Figure 4.34 at the resonant frequency. The associated return loss for this case was shown previously in Figure 4.29.

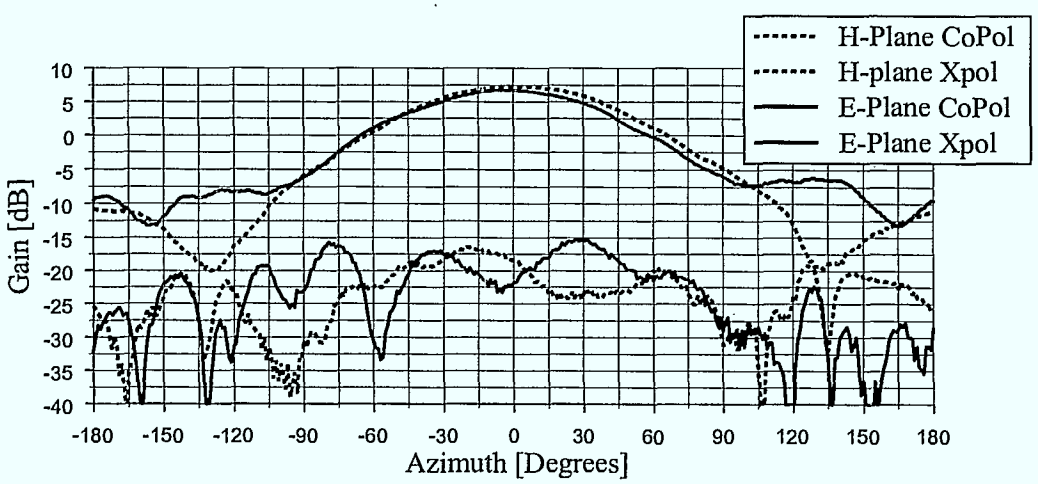

Figure 4.34: Radiation Patterns for [100-10]/[100s-4]-[6mm]

The radiation patterns revealed that no additional losses were incurred because of the loading since they closely matched the patterns of a typical patch antenna. Despite the varying loading conditions (dielectric size and distance between the patch and the ground), the E and H-plane co-polarized patterns were very similar for each structure. Beamwidths were nearly the same and were consistently greater than 72 degrees while gains at the resonant frequency were greater than 7 dB at boresight. Cross-polarization levels were better than 20 dB below the co-polarized levels over the entire azimuth sweep and front-to-back ratios were greater than 10 dB.

To observe the benefits of this aperture-coupled structure the above radiation patterns were compared to those of an equivalent probe-fed patch. This equivalent patch was configured, without dielectric loading, to have the same amount of air between the patch and the ground plane, as in the dielectric-loaded case, and was fed with a probe in a location where a match to 50 Ω was achieved. Though not an exact equivalent structure, it was expected that the radiation patterns would still highlight the important differences.

Comparing these patterns to those of the dielectric-loaded patch structure with aperture-coupling revealed some significant differences. As shown in Figure 4.35, the H-plane cross-polarization levels were much higher with the probe-coupling, about 10 dB down from the co-polarized level, and the E-plane co-polarized pattern showed significant distortion with a null around 60 degrees [60]. These effects were due to the unwanted radiation from the relatively tall probe, and significantly degraded the pattern performance. Neither of these effects were present in the loaded patch structure with aperture-coupling.

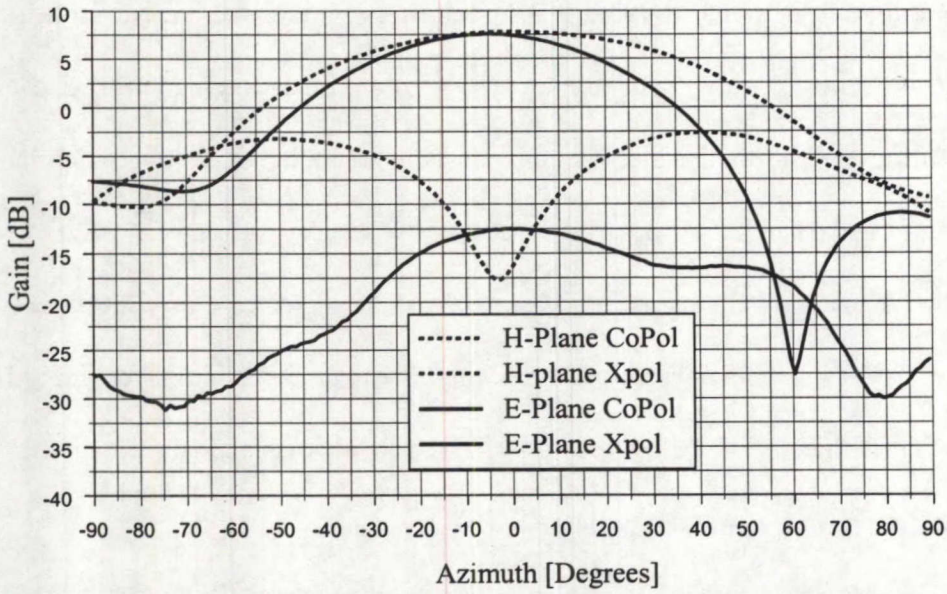

Figure 4.35: Radiation Pattern of an Equivalent Probe-Coupled Patch (from [60])

4.5.3 One Patch Side Loaded

Radiation patterns were also measured for three cases in which the patch was loaded on only one side for the benefit of a later circularly polarized design. The results are summarized in Table 4.5 and the properties of each loading configuration are listed in Table 4.3 of the previous section.

Loading Cases [slot]/[sides]-[spacer]	Resonant Frequency (GHz)	E-Plane Gain (dB)	E-Plane Beamwidth (degrees)	Cross-Polarization Level (dB:-180° to 180°)
[100-11]/[100s-4]-[6mm]	2.40	6.97	71.14	13 dB below CoPol
[40-30]/[40s-4]-[8mm]	2.60	7.55	78.16	17 dB below CoPol
[40-30]/[20s-4]-[7mm]	2.60	7.27	78.76	17 dB below CoPol

Table 4.5: Results from Pattern Measurement: Single Side Loading

The actual radiation patterns for the first loading case listed in Table 4.5 are displayed in Figure 4.36 at the resonant frequency.

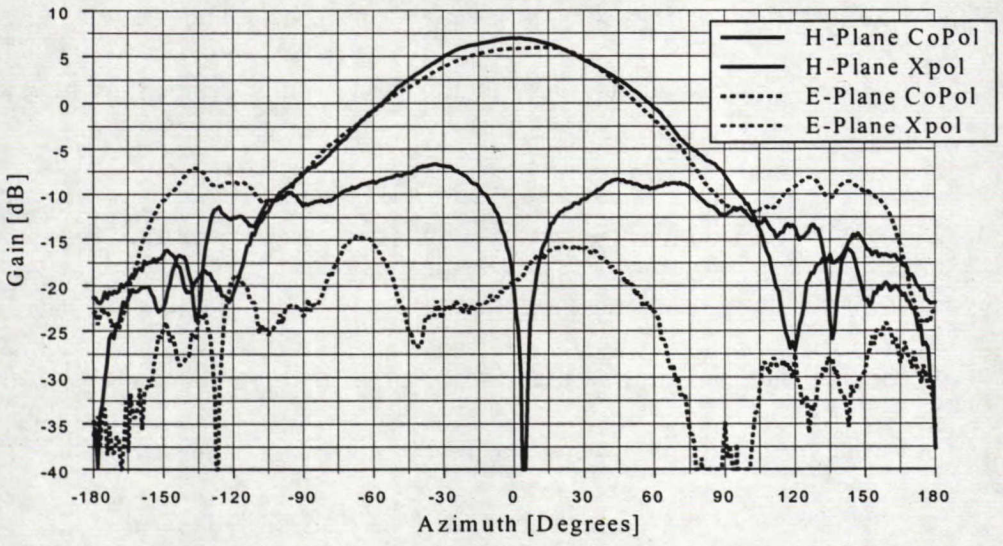

Figure 4.36 Radiation Pattern for [100-11]/[100s-4]-[6mm]

The pattern shapes for each structure were essentially the same as what was observed before except for the H-plane cross-polarization pattern. Having the dielectric loading only on one side caused the H-plane cross-polarization levels to be higher and to make a large dip at boresight, similar to the pattern of a probe-fed patch. This occurrence confirmed the non-symmetry of the structure in that the electric fields at each end of the patch were not equal and did not cancel each other out, hence contributing to the overall cross-polarization of the antenna.

4.6 HFSS Simulated Results and Trends

4.6.1 Simulation Background and Structure

As outlined in Appendix 2, modeling of the dielectric-loaded patch structure in HFSS was a very time consuming and frustrating process. Many modeling issues were encountered which, even with assistance from the HP technical support people, could not be resolved. The lengthy simulation time involved in analyzing each structure was the

most serious problem hindering the progress with HFSS. The double resonance phenomenon was also an issue but, despite this, the results seemed to be in good agreement.

Over the course of this thesis, many simulations were performed following the same process as with the measurements. Although only some of the slot-loaded cases were completed (and none of either side loading or matching), there was a sufficient amount of information to comment on some of the observed trends. In order to make these observations as well as comparisons with the measured results, the double resonance was ignored.

The HFSS modeled structure was set to have the same dimensions as the actual structure in every way possible. The same size dielectric pieces were used as well as the exact same dimensions of the substrates, slot, and microstrip line. The HFSS model did not include the alignment screws, spacers, nuts, the transparency with the alignment lines, nor the silicone glue. Each was shown to have very little effect on the measured results and were thus not modeled.

4.6.2 Measured versus Simulated Results

By ignoring the double resonance, a comparison between the simulated and measured results revealed a significant amount of similarities. In almost all cases, the simulated structure predicted the correct resonant frequency and generally showed the same impedance bandwidth as the measured structure, although the latter was difficult to tell given the double resonance. The plots of Figure 4.37 show three examples of the HFSS return loss results overlaid with measured results.

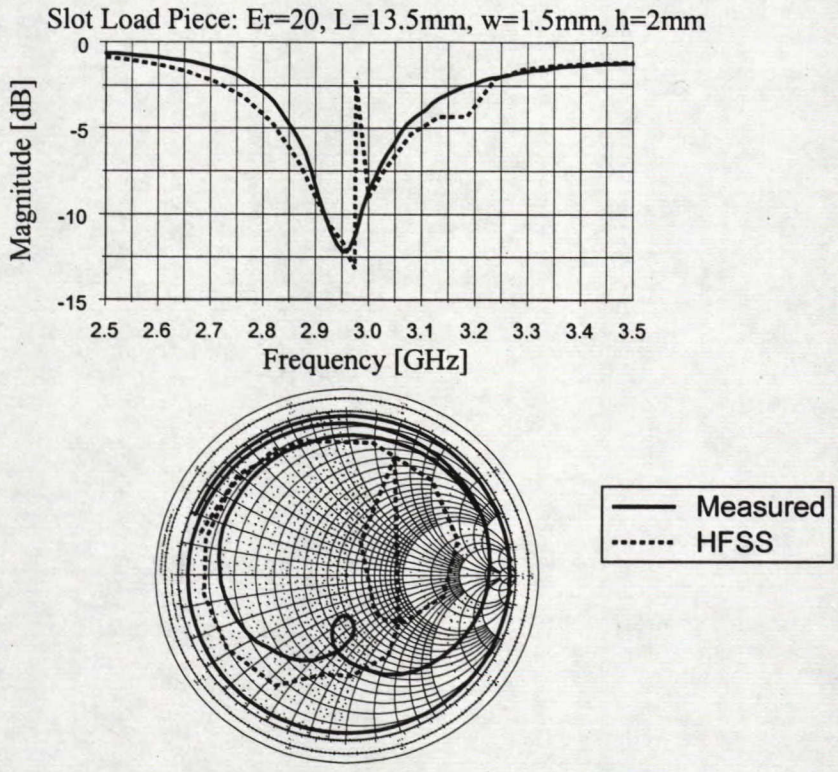

Figure 4.37 (a): HFSS Return Loss Results Compared to Measured Results

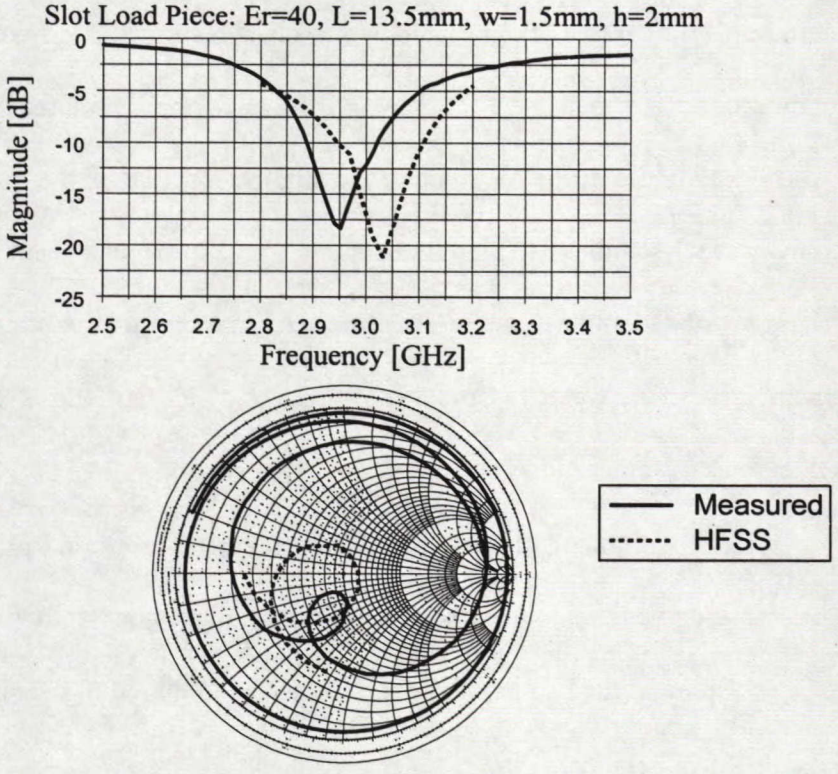

Figure 4.37 (b): HFSS Return Loss Results Compared to Measured Results

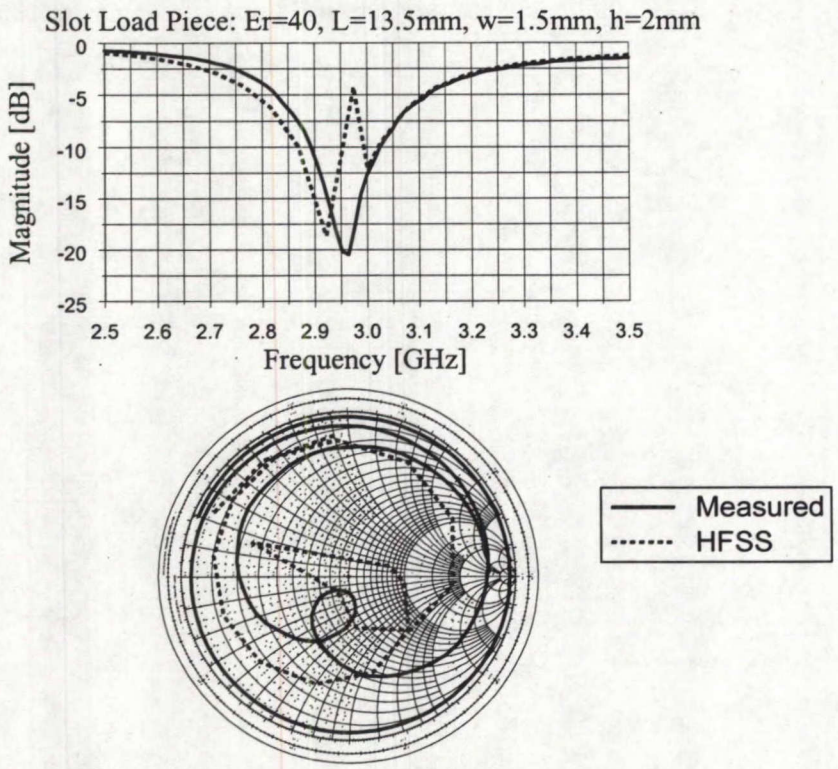

Figure 4.37 (c): HFSS Return Loss Results Compared to Measured Results

In almost all cases, the simulated Smith chart resonant loops were rotated slightly CCW compared to the measured loops. Also, some of the simulated loops were shifted more toward the middle of the chart and were slightly larger than the measured ones.

These results indicated that there were some impedance and phase differences between the simulated and measured structures. In an attempt to explain these results, the physical differences between the measured and simulated structures were more closely analyzed and are summarized as follows:

- The simulated structure had an infinitely thin ground plane and hence slot thickness. This implied that the small air gap normally present between the slot and the ground plane would not be included in the simulation.

- The simulated structure had a very accurate amount of air set between the dielectric load pieces and the patch substrate. This would not be as accurate in the measured structure since the spacers used to control the amount of air had a manufacturing tolerance and the substrate had a small amount of sag in the middle.
- The dielectric piece in the simulated structure would be placed exactly without any glue whereas the placement of the pieces in the measured structure was not as accurate and a thin layer of glue was used.

Considering that the simulated and measured results were fairly closely matched, these physical differences could certainly account for the slight variance observed. An attempt was made to include the finite ground-plane effect into the model but was unsuccessful for unknown reasons.

Another interesting observation was that the simulated results, when slot loaded with pieces having a relative permittivity of 100, were quite different from the measured ones. Although the resonant frequency was close to the correct value, the magnitude of the return loss was slightly greater than –2 dB whereas it was less than –20 dB when measured. The only explanation available for this behavior was that the alignment of these pieces was very sensitive and, in measurement, it was unknowingly placed slightly off center such that a better match was obtained.

With regard to simulated trends, those that were observed were similar to those measured. For example, enough simulations were performed to note that increasing the length of a dielectric piece with E_r=20 had little effect while there was a greater effect when E_r=40. It was also confirmed that varying the height and width of the dielectric

pieces had similar effects to those measured, although not enough simulations were performed to know exactly.

CHAPTER 5: L-Band Dielectric-Loaded Patch Designs

5.1 Introduction

A detailed trend analysis of the basic dielectric-loaded patch structure has been performed and a significant amount of insight into the antenna operation and its dependence on various loading parameters has been acquired. This information, however, was in a raw form and thus not particularly useful to the average designer. The primary purpose of this chapter is therefore to collate the trend data into a concise set of design guidelines which, when implemented, will lead to a functional dielectric-loaded antenna.

Another linearly polarized dielectric-loaded patch was designed, fabricated, and tested. The design strictly followed each step of the guidelines starting from a specific frequency and then attempted to achieve a match at that frequency. The goal was to minimize the amount of experimental tuning required but, in such a process where the overall antenna structure could not be accurately simulated with a 3D electromagnetic tool, optimizing in an experimental manner could not be avoided.

To complete the experimental work of this thesis, a circularly polarized dielectric-loaded patch antenna was designed and tested. Since the theoretical benefit of miniaturizing a patch with dielectric loading lies in the ability to achieve circular polarization, experimental confirmation was warranted. Two design iterations were required in this investigation, both of which are documented in detail.

5.2 Development of Design Guidelines

Based on the trends observed in the previous chapter, a set of guidelines was proposed for the design of a linearly polarized, aperture-coupled, dielectric-loaded patch antenna. These guidelines are intended for use as a starting point in a dielectric-loaded patch design, and are especially useful in the absence of a suitable 3D electromagnetic simulator, where the patch and feed network have to be separated from the loading in the design phase. Following the guidelines results in an approximate solution which will inevitably require experimental optimization to meet any required specifications.

These specific guidelines were developed in conjunction with the Ensemble patch simulator but using the equations outlined in Chapter 3 will lead to the same results. The guidelines are as follows:

1. Choose the desired operating frequency (f_o) of the dielectric-loaded patch antenna and select the substrate materials for the patch and microstrip feed.
2. Assume a 30% frequency reduction and calculate the patch resonant frequency required to achieve the desired one:

$$f_x = \frac{f_o}{1-0.3} = \frac{f_o}{0.7} \qquad (5\text{-}1)$$

3. Assume an air substrate with thickness $0.035\lambda_o$ ($\lambda_o = c/f_o$, $c=3\text{x}10^8$ m/s), to achieve the desired 8% impedance bandwidth, and calculate the required patch dimensions at f_x.
4. Using the actual patch substrate, as chosen in step 1, and the patch dimensions calculated in step 3, determine the resulting resonant frequency (f_{feed}) by working

backwards. Design the feed network (slot dimensions, stub length, and microstrip line) at this frequency.

5. Choose dielectric pieces to cover the slot that have a relative permittivity of about 100 and that cover nearly the whole length of the patch. These pieces should have a width starting at about $0.05\lambda_o$ but varying with slot width. The height of these pieces requires some experimentation but being different from the height of the side load pieces tends to yield better results.
6. The side load pieces should cover the entire length of the patch. The higher they are in relative permittivity, the better the frequency reduction. They should be at least $0.02\lambda_o$ high and $0.05\lambda_o$ wide. Aligning these pieces with the edge of the patch such that they are completely within the confines of the patch produces the best results.
7. Adjusting the height of the patch above the dielectric load pieces affects the bandwidth and matching ability of the antenna. Start with a spacing of $0.035\lambda_o$ from the ground plane to the patch (as used in step 3) and then experiment with other heights close to this value. Very small changes in this parameter, on the order of $0.0025\lambda_o$, have large effects on the return loss characteristic so a precise way to control the height down to $0.0025\lambda_o$ increments is important.
8. Experimentally tuning the slot dimensions and microstrip stub length are important to optimize the match of this antenna if the match cannot be achieved with the correct combination of loading.

These guidelines can effectively be separated into two sections. Steps one through four are very precise, describing exactly how to design the patch and feed network. The

remaining steps are less specific and describe, qualitatively, how to perform the dielectric loading. These last steps should be used as starting points in the experimental optimization process with the understanding that they are dependent on factors such as the slot dimensions and the patch size. Following these guidelines should yield results near the desired ones and it is expected that fine tuning will certainly be required.

5.3 Linearly Polarized Patch Design

This antenna design was intended to confirm the validity of the above guidelines by achieving a match at the desired frequency with an impedance bandwidth greater than 8%. The first four steps of the proposed guidelines will be followed in the patch design section with the remaining steps being completed in the return loss measurement section. Radiation patterns were not measured for this antenna since they would be the same as before.

5.3.1 Patch Design and Fabrication

The design and fabrication of this patch was straight-forward and strictly followed the guidelines. Each of the first four steps of the process will be reviewed in detail to outline how the guidelines were intended to be used.

Step 1:

The desired operating frequency was f_0=1.5 GHz and the substrate materials were chosen to be the following:

- Microstrip substrate: Rogers 4003, E_r=3.38, t=0.762 mm (0.030"), tan δ=0.0027

- Patch substrate: Rogers 3003, E_r=3, t=1.524 mm (0.060"), tan δ=0.0013

Rogers 3003 was adopted for the patch substrate due to its higher gain and bandwidth potential. To avoid material sagging issues, the thickness was doubled from 30 mil to 60 mil.

Step 2:

The frequency required to give the 30% reduction:

$$f_x = \frac{f_o}{0.7} = \frac{1.5}{0.7} = 2.14\,\text{GHz}$$

Step 3:

The patch dimensions sitting on $0.035\lambda_o$=7 mm of air were obtained using the Ensemble estimator tool and found to be L=W=54.82 mm at f_x=2.14 GHz, VSWR=2, and Z_{in}=50 Ω.

Step 4:

Using the above determined patch dimensions, the air substrate was removed and replaced with the actual substrate (Rogers 3003). With the patch dimensions from step 3 the Ensemble estimator tool calculated that the resonant frequency would be around 1.57 GHz. The feed network was thus designed, in Ensemble, at this frequency.

The final patch design is illustrated in Figure 5.1 and a summary of the designed characteristics is shown in Table 5.1. The simulated return loss result is shown in Figure 5.2 of the next section overlaid with the measured results of the patch without loading.

The patch antenna was layed out in DW2000, similar to the original linearly polarized patch, with the microstrip substrate having dimensions of 17 cm x 17 cm and the

patch substrate having dimensions of 10 cm x 10 cm. The design was then fabricated along with several new dielectric pieces, for side loading purposes, since the patch dimensions were longer than before and the old pieces could not be used.

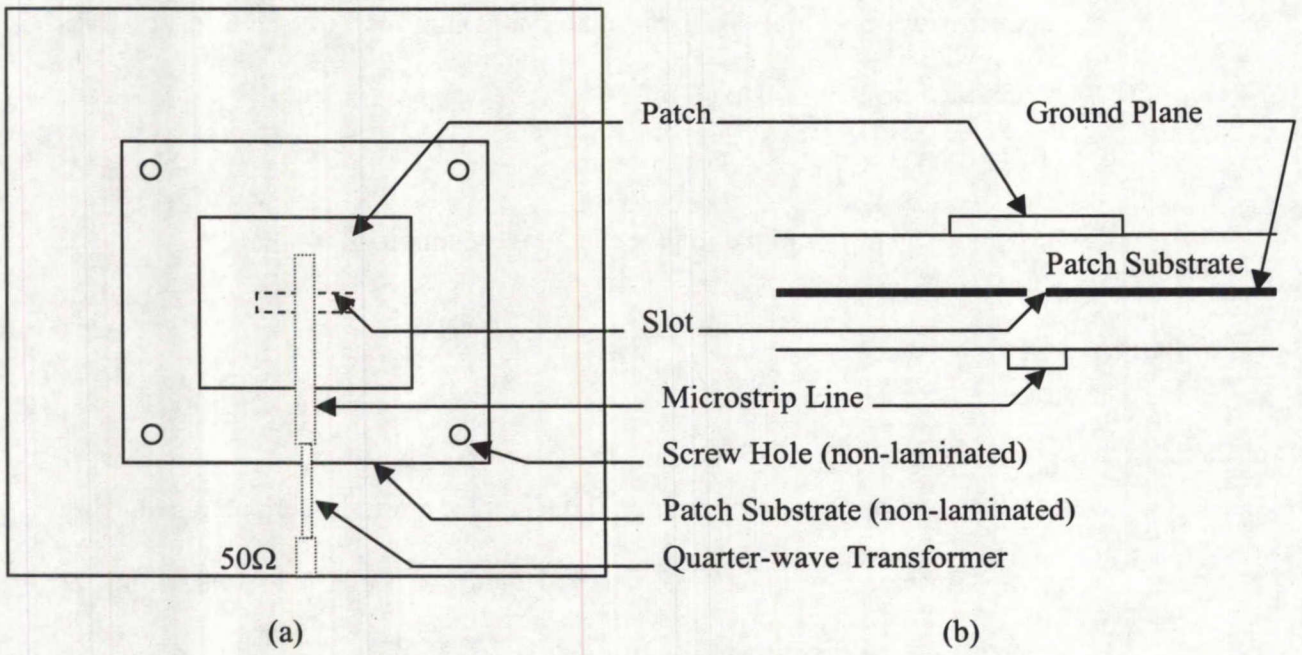

Figure 5.1: Linearly Polarized Microstrip Patch Antenna, a) top view and b) side view

Resonant Frequency	1.563 GHz
Patch Dimensions	53.6 mm x 53.6 mm
Slot Width	1.8 mm
Slot Length	12 mm
Stub Length	12.6 mm
Impedance Bandwidth	1.4%
Gain	5.7 dB
Front to Back Ratio	31 dB

Table 5.1: Ensemble Simulated Patch Results

5.3.2 Return Loss Measurements

5.3.2.1 Laminated versus Non-Laminated Results

Return loss measurements of the laminated patch indicated that the results were quite similar to those predicted by Ensemble, resonating at 1.55 GHz and having a very narrow impedance bandwidth. The non-laminated patch behaved similarly, though with a slight increase in resonant frequency due to the small air gap present between the patch and the feed substrate layers. Figure 5.2 shows the return loss of both the simulated and measured antennas without loading.

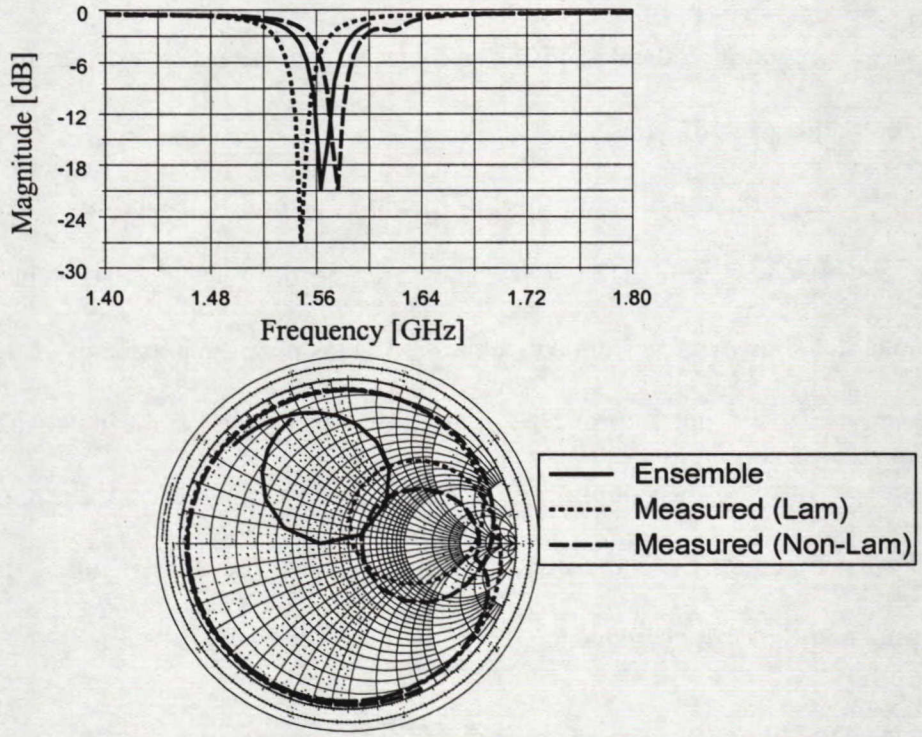

Figure 5.2: Simulated and Measured Return Loss Characteristic

5.3.2.2 Initial Tests Following the Guidelines

Initially, dielectric pieces were placed over the slot alone to confirm that the impedance transformations and general parameter trends would occur similarly to the original dielectric-loaded patch antenna. It was shown that resonant loops on the Smith chart

were achievable and that they tended to vary in a similar manner to the trends observed with the original patch.

Matching was next performed by loading both the slot and the sides of the patch. The suggestions in the guidelines were followed to determine the initial dimensions and permittivities of the dielectric pieces. The initial piece chosen to load the slot had E_r=100, was $0.05\lambda_o$=10 mm wide, and covered about half the length of the patch. The side load pieces also had E_r=100 and were $0.05\lambda_o$=10 mm wide but they covered the whole length of the patch. The height of the side load pieces was chosen to be $0.02\lambda_o$=4 mm and the height of the slot load piece was initially set to be slightly lower, at 3 mm. The pieces were aligned as indicated in the guidelines and the patch was set to be $0.035\lambda_o$=7 mm above the ground plane.

The measured return loss of this loading configuration revealed that the operating frequency was around 1.6 GHz, close to the desired 1.5 GHz. The patch was poorly matched, however, since the resonant loop was near the perimeter of the Smith chart. The bandwidth did not improve by increasing the height of the patch above the dielectric pieces. Instead, the coupling degraded and the resonant loop disappeared on the chart. Experimentation with the dielectric loading was therefore required in order to obtain a match at the correct frequency.

5.3.2.3 Experimental Optimization

After trying several combinations of loading and patch heights above the ground plane, the desired resonant frequency of 1.5 GHz was achieved. The Smith chart shown in Figure 5.3 reveals a resonant loop centered on the zero reactance line around the r=2

circle, when referenced to the slot. Though the antenna was not perfectly matched at this frequency, tuning of the slot and stub dimensions may result in a better match.

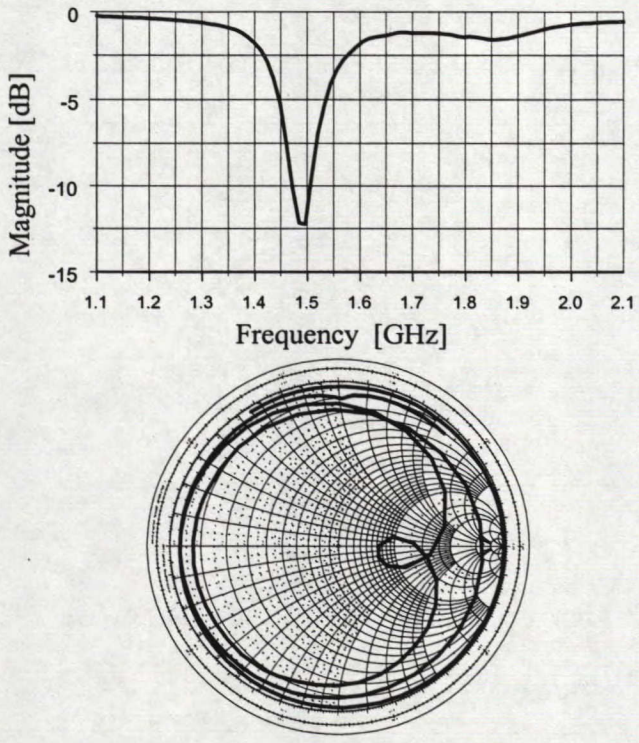

Figure 5.3: Return Loss Results at 1.5 GHz

During the course of this optimization process, it was found that the antenna could be very well matched at frequencies in the range of 1.7 to 1.9 GHz with bandwidths ranging from 9 to 12%. The return loss plot of Figure 5.4 illustrates one of these cases. The main difference between this loading condition and the previous one was primarily in the height of the loading. The well matched case had side load pieces with E_r=100 that were stacked to about 7 to 8 mm high while the slot load piece had an E_r=40 and was about half the height. The opposite was true for the 1.5 GHz case where the side load pieces were 4 mm high and E_r=100 while the slot load piece was 6 mm high and also E_r=100.

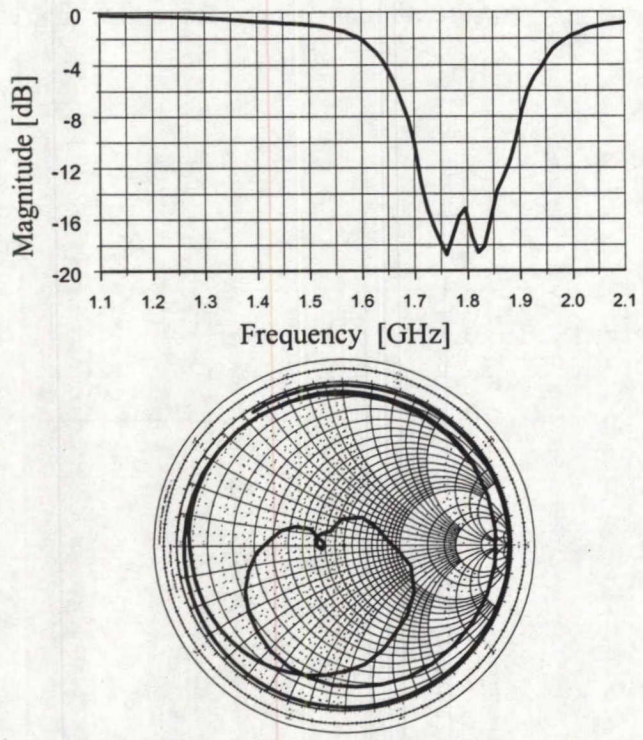

Figure 5.4: Return Loss Results at 1.8 GHz

5.3.2.4 Discussion of Results

To summarize, the guidelines were effective at predicting the approximate resonant frequency of the dielectric-loaded patch antenna, but experimental manipulation of the dielectric loading condition (dielectric size and distance between patch and ground) was required in order to achieve a better match at the desired frequency. The antenna was very well matched around 1.8 GHz with a bandwidth on the order of 10%.

These measurements were conducted with a limited amount of available dielectric pieces having varying heights and lengths. A more accurate experimental process might have yielded a better match at 1.5 GHz but it is also possible that the slot and stub length were not optimal for this configuration.

5.4 Circularly Polarized Patch Design

A final dielectric-loaded patch antenna was designed, fabricated, and tested with the intention of observing the effect of dielectric loading on the quality of the CP. It was important to confirm CP operation since this is a major mobile satcom specification and one of the theoretical advantages of the dielectric-loaded structure compared to other miniaturization techniques.

Two design iterations were required in this investigation since the results of the first one were not entirely satisfactory. Several issues emerged regarding the feed network, primarily related to maintaining the correct phase at the operating frequency of the loaded structure. The second iteration feed design incorporated a Wilkinson power divider to ensure that there would be no unwanted reflections contributing to a phase degradation.

5.4.1 CP Prototype Development

At this stage, it was uncertain as to how much frequency reduction to expect with the CP structure since the feed network had not been selected and was expected to set the loading configuration. Choosing a dual-feed versus a single-feed, for example, would mean loading either one or both radiating edges, thus having a direct impact on the loading capability.

Also, since the CP structure was not necessarily compatible with the LP design guidelines, the CP patch and feed were designed to operate at 2 GHz. This was similar to the approach taken in the original design of Chapter 4 and would allow sufficient room for the loading to reduce the resonant frequency down to L-band levels.

5.4.1.1 Patch and Feed Design Attempts

5.4.1.1.1 Rotated Off-Square Patch, Single-Feed

Initially, an attempt was made to obtain circular polarization by rotating the original patch (from Chapter 4) by 45 degrees with respect to the slot. To get the required phase separation, one of the orthogonal modes was perturbed by increasing the length of one dimension of the patch by a small amount such that the patch would appear to be slightly off square.

The structure was simulated in Ensemble with both the microstrip and patch substrates being Rogers 4003, with E_r=3.38, t=0.762 mm (0.030"), and tan δ=0.0027. Simulated results revealed a poor match and a large axial ratio resulting in very narrow impedance and axial ratio bandwidths. Also, the gain peak and axial ratio minimum did not coincide. Tuning the slot dimensions, microstrip stub length, and the length of the perturbation segment were unsuccessful at improving the situation.

In an attempt to increase the bandwidth and promote better gain, the patch substrate was changed to 1.524 mm (60 mil) Rogers 3003 as was done in the LP patch design at the beginning of this chapter. Although these changes did succeed in slightly improving the gain and axial ratio, both were still unacceptable and matching was difficult. Adjusting the impedance of the line feeding the patch would still not result in a better match.

5.4.1.1.2 Square Patch with Truncated Corners, Single-Feed

Changing the perturbation segment to having two diagonally opposite corners truncated instead of increasing the length of a patch dimension yielded results that were even worse than before. Tuning was again unsuccessful.

5.4.1.1.3 Square Patch, Dual-Feed

In order to get both a better match and a better axial ratio, a two-feed structure was implemented. The patch dimensions were made square with a length of 42.84 mm at 2 GHz according to the Ensemble estimator tool. The substrate material was kept the same as last defined.

The feed structure still incorporated aperture-coupling but this time from two slots in the ground plane. The two slots were located as shown in Figure 5.5, fairly close to the edges of the patch to ensure minimal coupling between the two. The 90-degree time-phase difference between the two modes required for circular polarization was achieved by making one of the two feeds longer than the other by 90 degrees in electrical length.

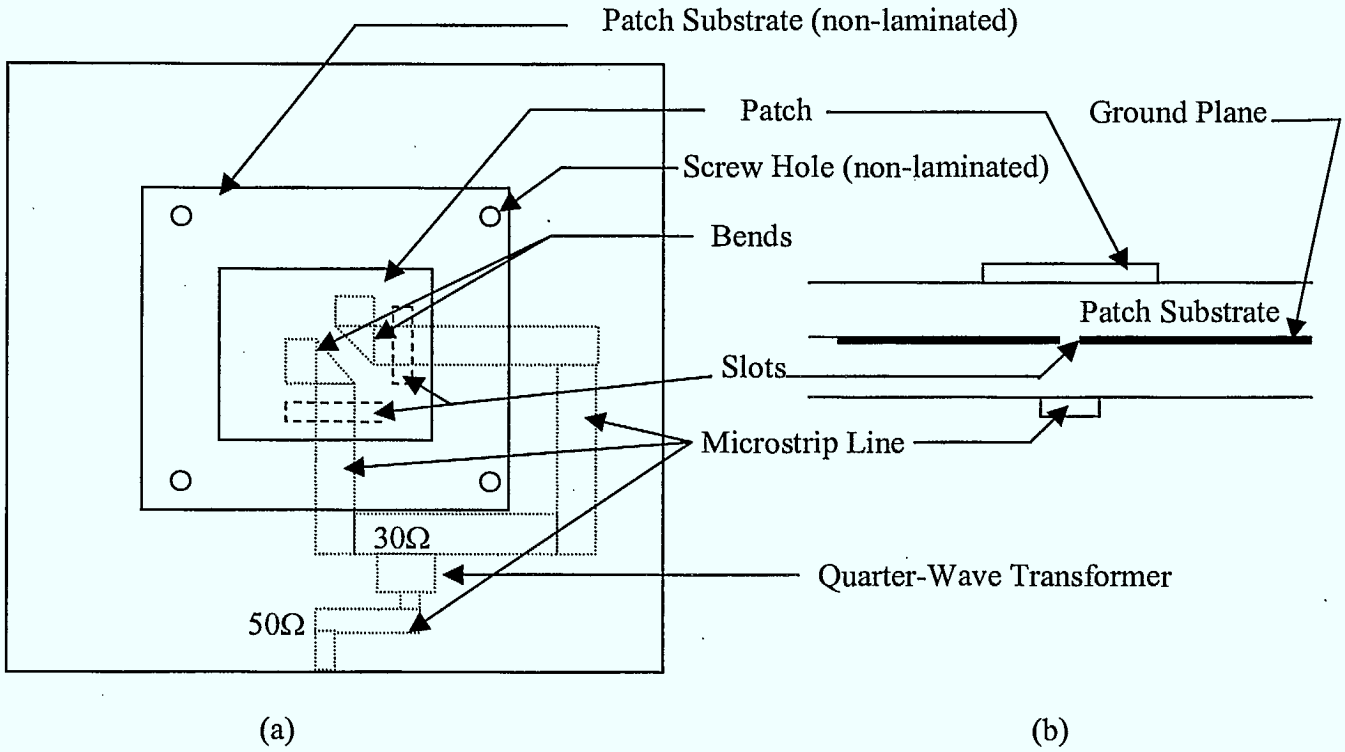

Figure 5.5: Approximate Diagram of CP Patch Antenna: a) top view and b) side view

Initial simulations of this structure yielded better results than with the other feeding methods. The axial ratio at boresight was just under 2.5 dB but the 3 dB bandwidth was very small and the structure was not matched. Of the feed techniques attempted, this one seemed to be the best and thus was further pursued and optimized.

5.4.1.2 Design Optimization

To determine the best position for the slots, the feed network was cut as shown in Figure 5.6 with each microstrip line representing a port. Using the substrate materials described above and varying the slot positions, simulations were performed until the isolation between the two ports was better than -20 dB.

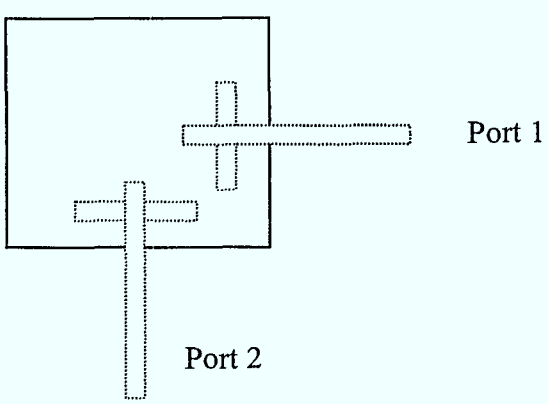

Figure 5.6: Feed Network for Isolation Test

Both slots were given the same dimensions and were placed in the same respective locations to maintain antenna symmetry. They had to be well away from the center of the patch and made relatively short. The length of the microstrip stub also had an effect on the isolation between the two ports; the shorter these lines, the better the isolation. When the isolation was acceptable, the feed network was returned to the configuration shown in Figure 5.5 with the two paths being joined and one being 90 degrees longer in electrical length than the other.

By adjusting the width of the slots, the microstrip stub lengths, and the patch dimensions, an attempt was made to match the antenna to 50 Ω. This was found to be quite difficult since the resonant loop on the Smith chart encircled 30 Ω instead of 50 Ω. It was decided to therefore match the patch to 30 Ω and the junction of the two 30 Ω lines, which is a 15 Ω line, was transformed into a 50 Ω line with a quarter-wave transformer. The 50 Ω line was then extended to the connector as was roughly illustrated in Figure 5.5.

The entire structure was simulated in Ensemble with the final design characteristics being displayed in Table 5.2. A plot of the simulated return loss is illustrated in Figure 5.7 along with the measured results.

Resonant Frequency	1.952 GHz
Patch Dimensions	42.84 mm x 42.84 mm
Slot Width	1.2 mm
Slot Length	14.4 mm
Width of 50 Ω line	1.764 mm
Width of 30 Ω line	3.764 mm
λ/4 Transformer Impedance	27 Ω
λ/4 Transformer Width	4.138 mm
λ/4 Transformer Length	22.15 mm
Impedance Bandwidth	2%
Axial Ratio (min)	0.5 dB @ 1.95 GHz
Axial Ratio 3 dB Bandwidth	0.72%
CP Gain	5.7 dB @ 1.95 GHz
Front to Back Ratio	<-20 dB

Table 5.2: CP Patch Design Characteristics

It was observed during the optimization process that extending the length of the microstrip stubs had a positive effect on the match. The stubs could not be made very long, however, since they would be too close to each other and degrade the isolation. A solution to this problem was achieved by bending the two lines away from each other. In

this way, they could be as long as necessary and not lead to poor isolation. These bends also had an effect on the phase in the feed lines, enabling the axial ratio to be minimized. The bending is shown on the schematic in Figure 5.5.

5.4.1.3 Structure Fabrication

Similar to before, two versions of this patch were prepared for fabrication. The first one consisted of the patch and microstrip substrates being laminated together where both substrates were of the same dimensions (15 cm x 15 cm). The second version involved the two substrates not being laminated together. In this case, the patch substrate was cut smaller (9 cm x 9 cm) and aligned over the slot with plastic screws as in the original design. The patch substrate dimensions were larger than necessary to avoid having one of the screw holes directly over the feed network.

Many new dielectric load pieces had to also be fabricated to accommodate both the new patch and slot dimensions as well as the second slot. Since the loading was intended to be symmetrical, the load pieces for the second slot were made to be the same dimensions as those already made for the first slot.

5.4.2 Results and Discussion

5.4.2.1 Laminated versus Non-Laminated Return Loss Results

Return loss measurements of the laminated CP patch indicated that the results were quite similar to those predicted by Ensemble. It actually resonated at 1.936 GHz compared to the simulated resonant frequency of 1.952 GHz. The non-laminated patch behaved similarly but only after applying pressure to the patch substrate to eliminate the small air gap present between the patch and the feed substrate layers. This small gap had

a much more significant effect on the resonant frequency of this patch than it did in the previous designs. Figure 5.7 shows the return loss of both the simulated and measured antennas without loading.

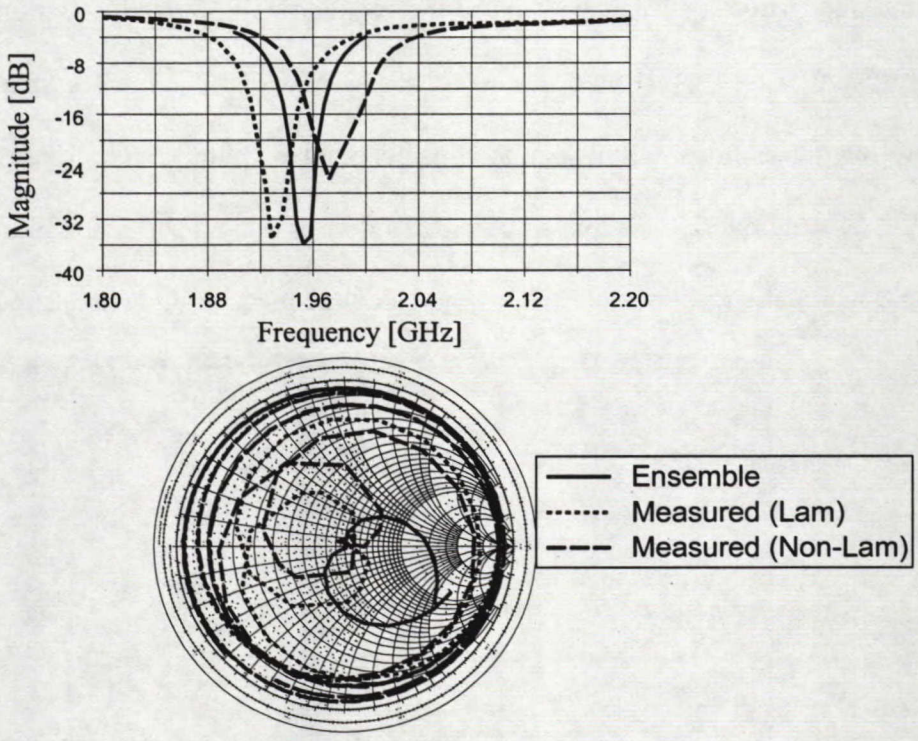

Figure 5.7: Simulated and Measured Return Loss Results

5.4.2.2 Measured Results of the CP Loaded Patch

5.4.2.2.1 Overview

With a dual-aperture feed configuration, dielectric loading of the patch structure would be performed differently from before. The dielectric load pieces would be placed under only one of the radiating edges of the patch per orthogonal mode and the loading over the slots would no longer be in a region of minimum electric fields. The effect of this new arrangement on the frequency reduction, matching ability, and bandwidth was the focus of these measurements.

Results from Chapter 4 indicated that having only one radiating edge of the patch loaded would cause the resonant frequency of the patch to increase and require an entirely new matching condition. These same results also indicated that having only one radiating edge loaded would cause the E-plane co-polarized radiation pattern to have a null and cause high H-plane cross-polarization levels. The measurements described in the following sections will investigate this behavior with the CP configuration.

The overall CP loaded patch structure is illustrated in the photographs of Figure 5.8 where the locations of the slot and side load pieces can be identified.

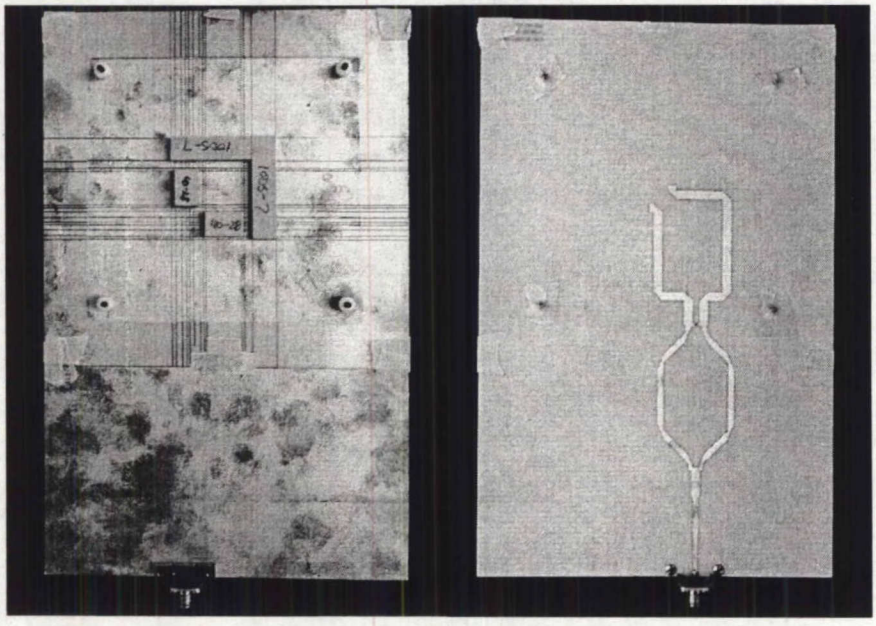

Top view without Patch Bottom view

Figure 5.8(a): Photographs of the CP Loaded Patch Antenna

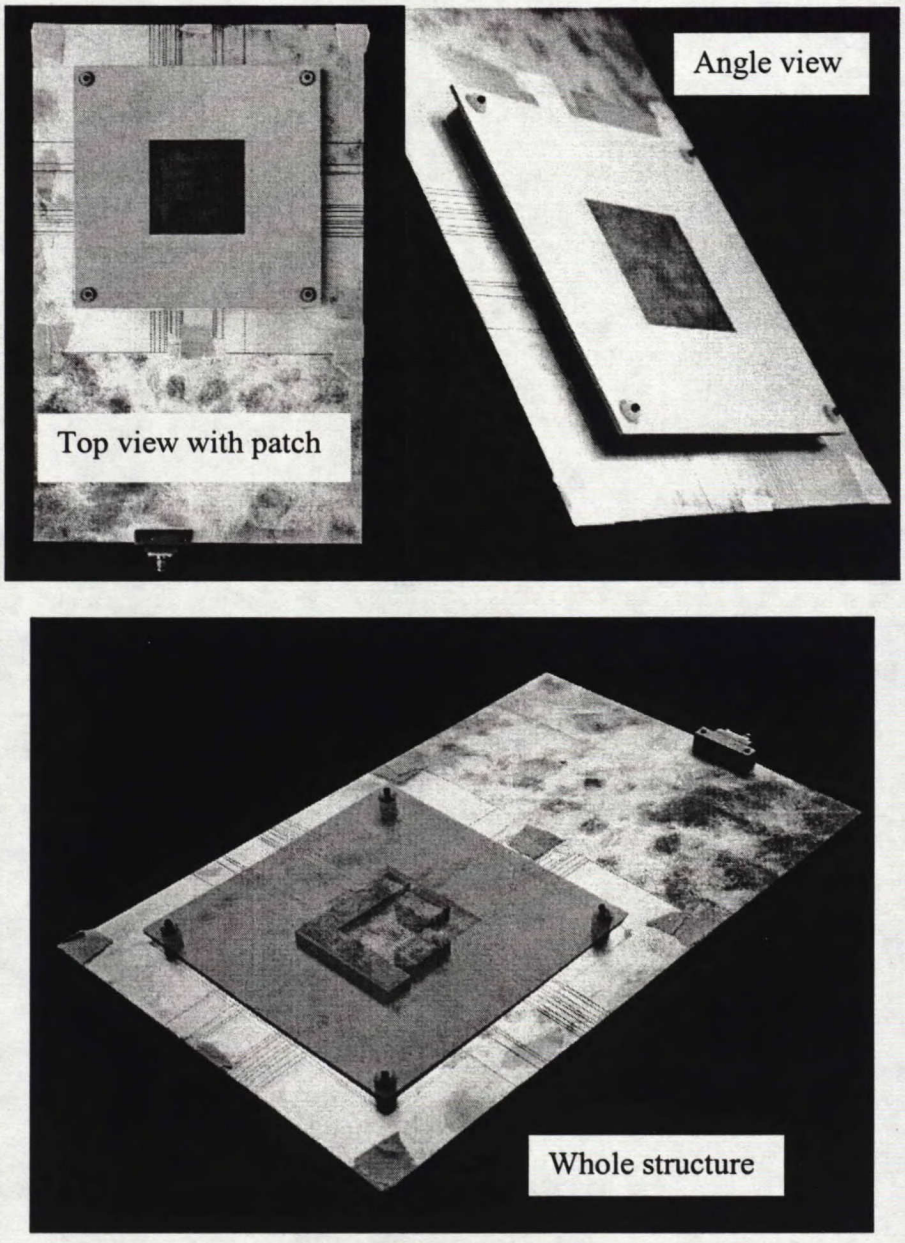

Figure 5.8(b): Photographs of the CP Loaded Patch Antenna

The return loss measurements of the CP dielectric-loaded structure were performed in a similar manner to those outlined in Chapter 4 with slot loading being investigated alone, followed by matching. However, a full characterization of the parameters was not performed since not enough dielectric pieces were available. The intention of

these measurements was to simply observe the important trends and the associated patterns.

5.4.2.2.2 Return Loss Results

The slot loading only measurements were performed with 1 mm of air between the patch and load pieces as done before and each slot was loaded with the exact same piece of dielectric. These return loss measurements confirmed that the same general trends observed with the linearly polarized loaded patch still applied. Achieving a match to 50 Ω was shown to be quite possible depending on the pieces of dielectric used to load the slots. Figure 5.9 shows an example of a well-matched case.

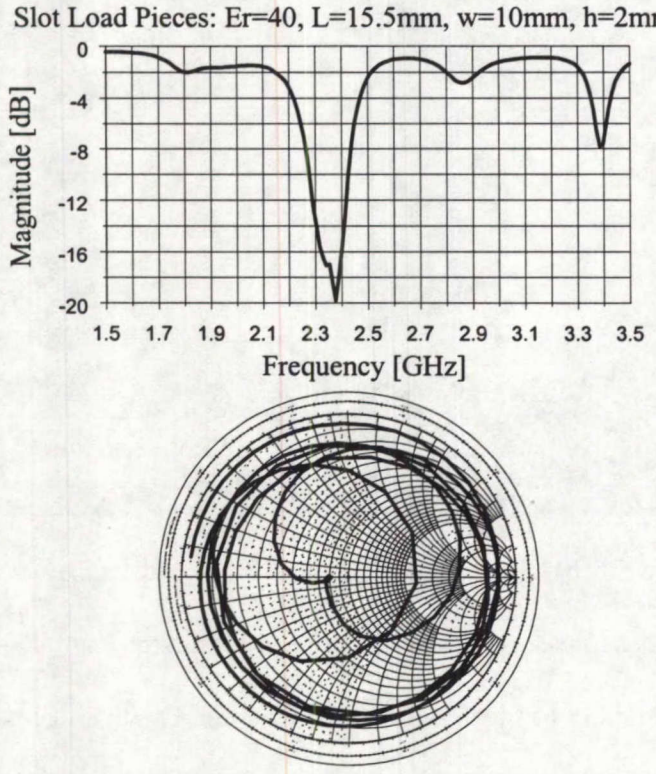

Figure 5.9: Return Loss of Well Matched Slot Loading Case

The proximity of the two slots to the radiating edges of the patch seemed to have little effect on the matching results but caused the resonant frequency to decrease. This was expected since these slot load pieces would now be acting as small side load pieces in an area of maximum electric fields. The resonant frequency varied depending on the loading condition, but was generally between 2.2 and 2.4 GHz. The total height of the patch in these cases varied from 3 to 5 mm off the ground plane and, when compared to the reference frequencies listed in Table 5.3, the typical frequency reduction achieved with slot loading only was on the order of 15%. This was an important result since frequency reductions were not achieved with only slot loading in the linear polarization designs due to the location of the slot.

Total Height of Air (mm)	Resonant Frequency (GHz)
3	2.74
4	2.73
5	2.70
6	2.66
7	2.63
8	2.58

Table 5.3: Reference Resonant Frequencies for CP Patch

By loading both the slots and the radiating edges of the patch, significant frequency reductions were achievable while maintaining a good match. Depending on the loading condition, frequency reductions on the order of 35% could be achieved with impedance bandwidths greater than 8%. Shown in Figure 5.10 is an example of a case with an 8.5% bandwidth and a center resonant frequency of 1.78 GHz. The patch is 6 mm above the ground plane and therefore has a frequency reduction of 33% when compared to the reference.

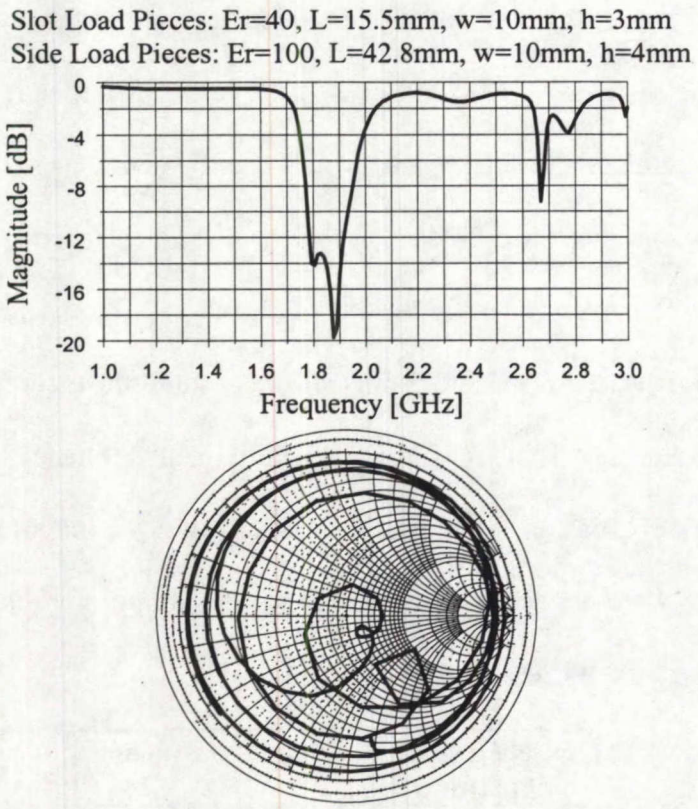

Figure 5.10: Example of Return Loss for the Loaded CP Structure

5.4.2.2.3 Radiation Pattern Results

Radiation pattern measurements were performed for several of the well matched CP dielectric-loaded structures. The resulting patterns revealed that the loaded structures were not generating good quality CP; axial ratios were very large with 10 dB being near the minimum.

To confirm that the patch alone was generating CP as designed in Ensemble, the patterns were also measured for the laminated structure. Though shown to have a very narrow 3-dB axial ratio bandwidth, good quality CP was achieved at 1.93 GHz with a minimum axial ratio of about 2.5 dB at boresight and even less in the 90-degree cut. Figure 5.11 illustrates these patterns for both the 0 and 90-degree cuts of the device under test (DUT).

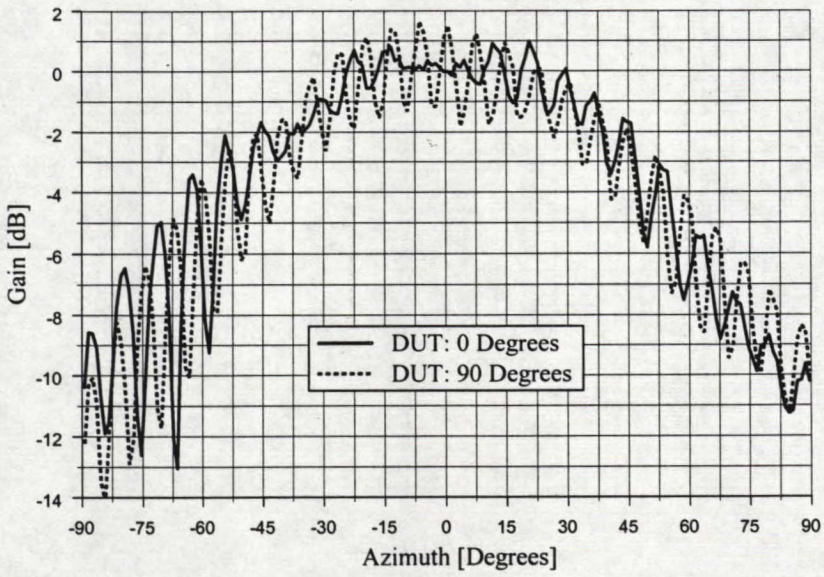

Figure 5.11: Laminated CP Patch Radiation Patterns

During these investigations, it became apparent that the phase in the feed network was likely not the required 90 degrees. Since the feed was designed at 2 GHz and the loaded structure actually operated around 1.8 GHz, the phase would certainly be incorrect at the operating frequency. Reviewing the simulation, it was determined that the 90-degree phase bandwidth was very small and would certainly not encompass frequencies below 1.95 GHz.

In an attempt to confirm that the phase issue was a cause of the poor circular polarization, patterns were measured with the loading set such that the resonant frequency of the structure was nearly 2 GHz, the designed frequency of the feed. These results revealed good circular polarization with a minimum axial ratio at boresight of about 2 dB, but the 3-dB axial ratio bandwidth was again narrow, on the order of 0.02 GHz. Figure 5.12 shows these patterns for both the 0 and 90-degree cuts at 2.03 GHz.

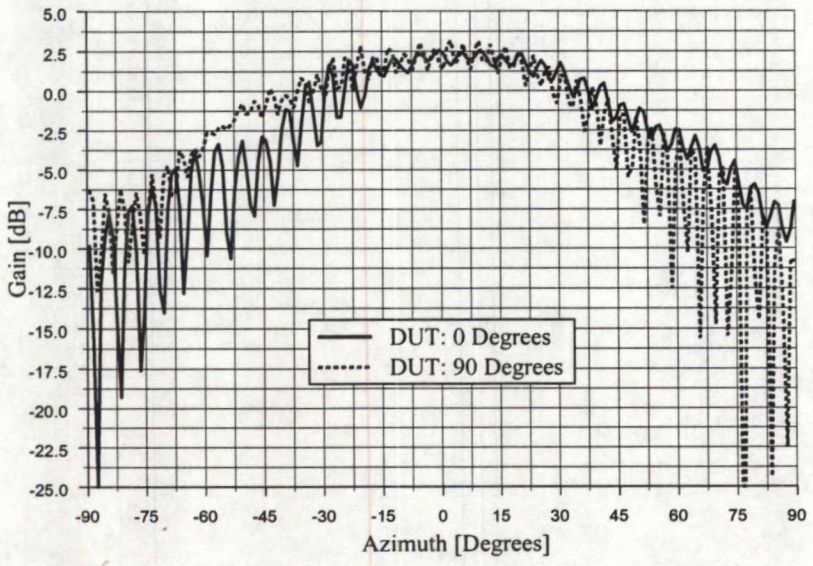

Figure 5.12: Slot-loaded Patch Radiation Pattern at Feed Frequency

Based on these measurements, it became clear that the feed network, when dealing with circular polarization, must operate at the same frequency as the loaded structure in order to maintain the correct phase relationship between the two feeds. This problem was not encountered in the linearly polarized structure since phase was not an issue in the feed network and designing it at a higher frequency was acceptable.

5.4.3 Re-Design of Feed Network

The feed network was re-designed to operate around 1.87 GHz, a frequency where several loading configurations would enable a match. The patch and slots were not altered and a Wilkinson power divider was added into the feed network to ensure that there would be no reflections from the two paths.

The Wilkinson divider was designed in the 30 Ω system and a 62 Ω resistor was used to absorb the reflections. The quarter-wave transformer was placed on the left of the

Wilkinson divider, as shown in the layout of Figure 5.13. The new feed structure was optimized in HP's Advanced Design System (ADS), and layed out in DW2000.

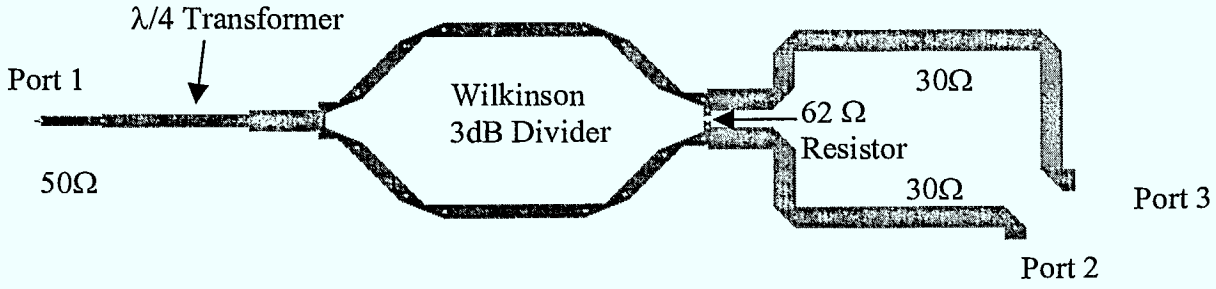

Figure 5.13: New Feed Network with Wilkinson Divider

Two versions of the feed network were fabricated. The first was as shown in Figure 5.13 and was to be used with the patch and dielectric loading. The second one had the lines at ports two and three extended to a connector and was to be tested on its own to confirm the correct phase and power split.

5.4.4 Final Results and Discussion

5.4.4.1 Results of CP Loaded Patch with New Feed

Prior to connecting the resistor to the Wilkinson, the correct loading and matching configuration had to be determined such that the structure would operate near 1.87 GHz, the optimum frequency of the feed network. The patch was thus loaded such that a match was found at 1.9 GHz, which was close enough to the desired value. The impedance bandwidth was about 5% but could have been improved with a different loading condition. Figure 5.14 shows this return loss.

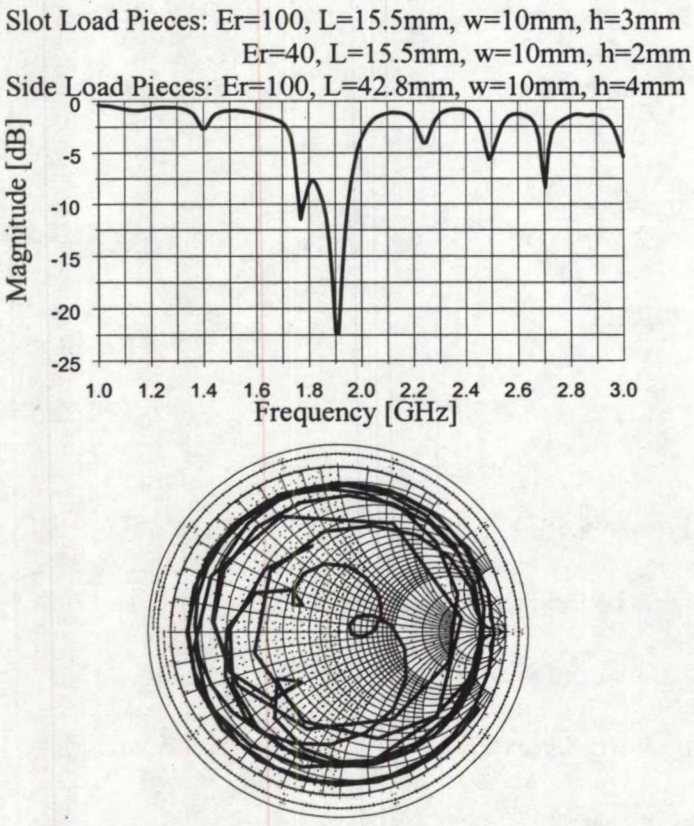

Figure 5.14: Return Loss of CP Loaded Patch without Resistor in Wilkinson Feed

When the resistor was mounted, the return loss was again measured. The overall level of the curve shifted down since the resistor absorbed some of the reflections thus yielding a better match, as expected, and several other resonances appeared. A resonance was still present at the location where the match was previously; therefore, the Wilkinson divider appeared to be performing correctly. Figure 5.15 illustrates this return loss characteristic.

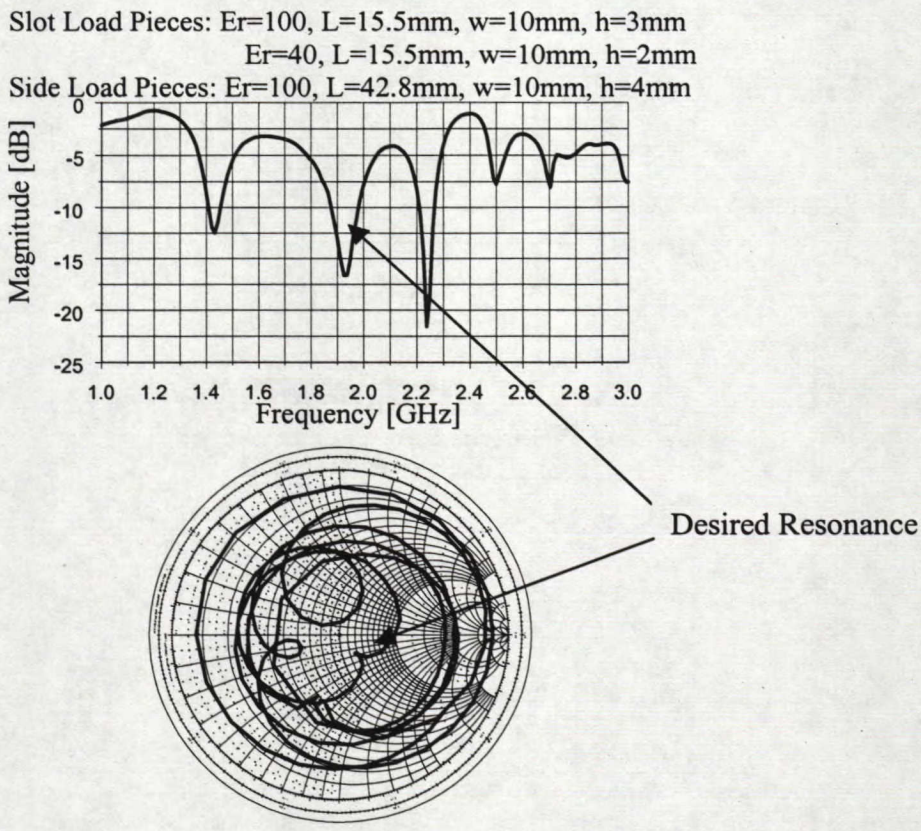

Figure 5.15: Return Loss of CP Loaded Patch with Resistor in Wilkinson Feed

The radiation pattern of this structure was measured with three cuts of the DUT, these being 0, 45, and 90 degrees. The results indicated that the structure was generating circular polarization with a minimum axial ratio of about 4 dB. The best axial ratio occurred at 1.78 GHz even though the best match was closer to 1.9 GHz. The patterns for the three cuts are shown in Figure 5.16 at 1.78 GHz. The axial ratios off boresight were different in each of the cuts indicating that the ground plane was likely causing scattering.

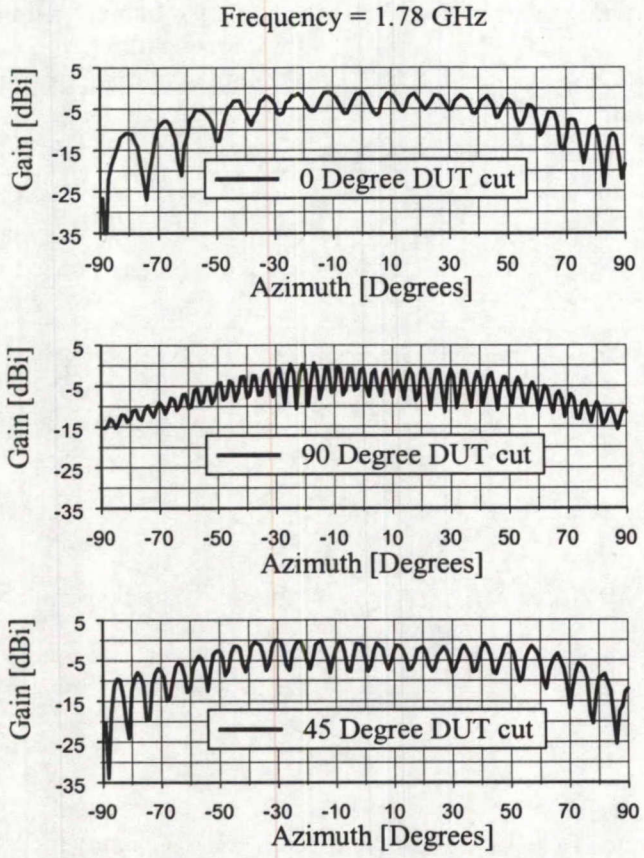

Figure 5.16: Radiation Patterns for CP Loaded Patch with Wilkinson Feed

The axial ratio bandwidth was small but larger than what was observed in the original set of CP measurements. Figure 5.17 illustrates the boresight axial ratio and associated CP gains as frequency increases. A sample calculation of the CP gain is shown in Appendix 3. The fluctuations in the curves are due to the inaccuracies involved in approximating the axial ratio off the pattern plots.

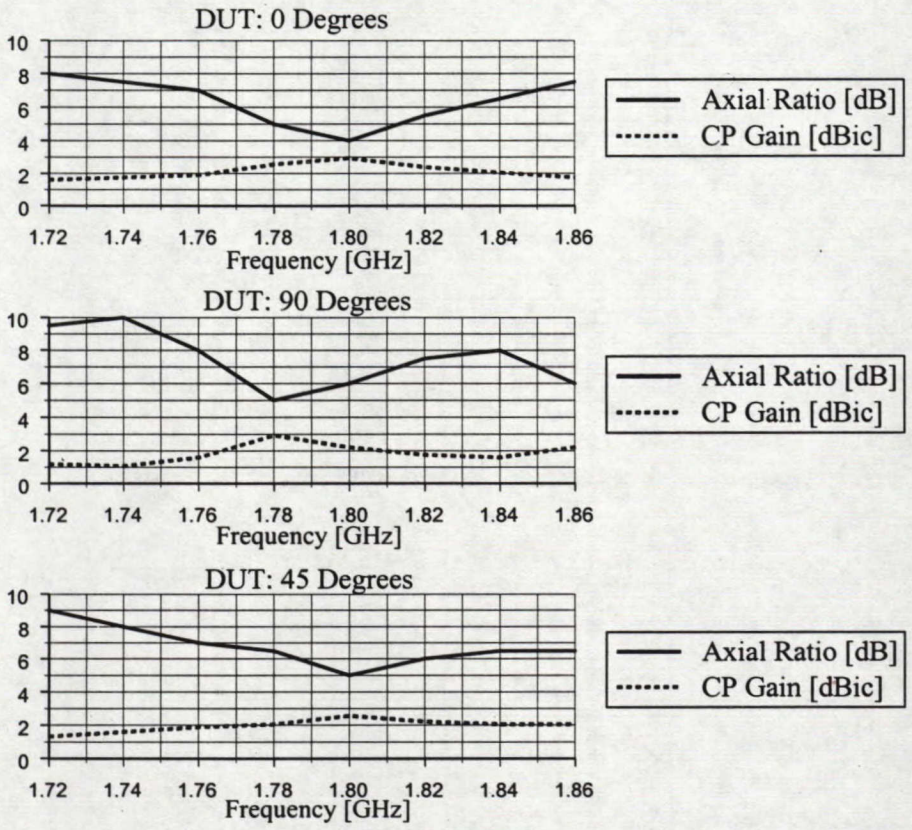

Figure 5.17: Axial Ratio and CP Gain at Boresight

5.4.4.2 Results of Feed Alone

Testing of the Wilkinson feed alone revealed that it was working as designed. The return loss at port 1 was below –15 dB as shown in Figure 5.18 and the transmission measured with S_{21} and S_{31} revealed that the power split was about –3.6 dB with a 95-degree phase difference at 1.87 GHz. At 1.78 GHz, the frequency where the axial ratio was the best in the previous measurements, the power split was about the same but the phase was closer to 90 degrees. These transmission results are illustrated in Figure 5.19 and 5.20. Since the feed network was designed to give a –3-dB power split and a 90-degree phase difference, it was clearly working well.

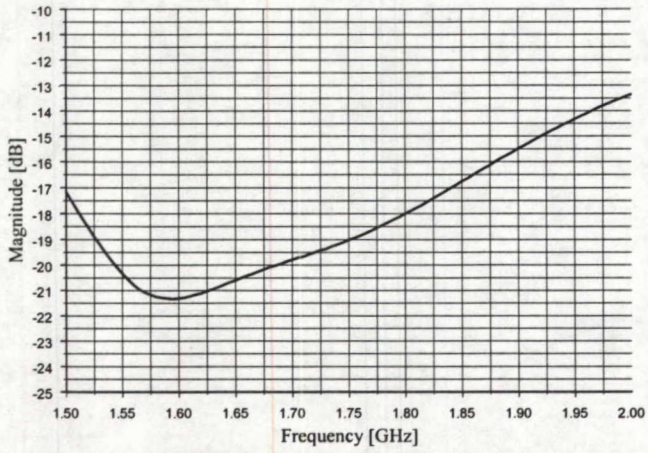

Figure 5.18: Wilkinson Feed Return Loss

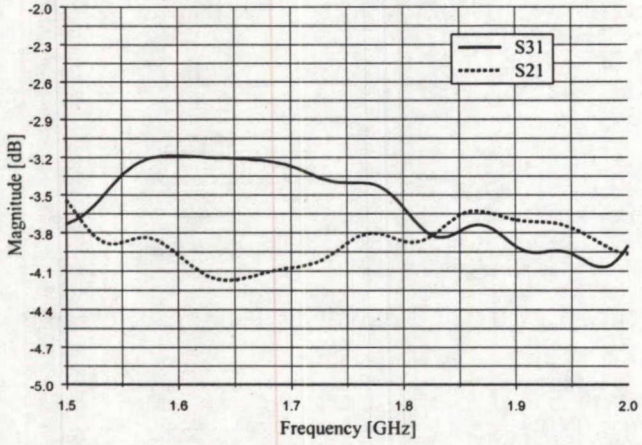

Figure 5.19: Wilkinson Feed Transmission Power

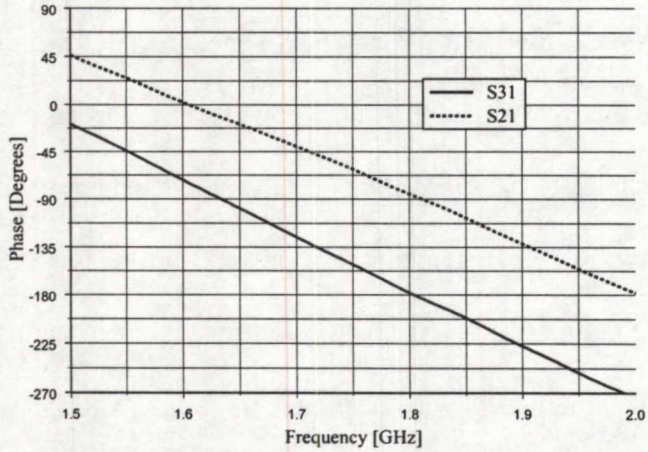

Figure 5.20: Wilkinson Feed Transmission Phase

The slight difference between the two curves in Figure 5.19 indicated that the power split is not identical between the two paths. This could lead to a slight degradation in the quality of the circular polarization.

5.4.4.3 Discussion

The general conclusion from these measurements was that the quality of circular polarization improved when the feed network was designed at the operating frequency of the loaded structure. It was uncertain as to whether or not the addition of the Wilkinson divider contributed to this improvement, but the feed was operating properly and not generating any excessive reflections.

The fact that the three cuts had different axial ratios indicated that ground plane effects were likely contributing to the CP degradation by altering the phase. Future testing of the same structure with different size ground planes is required in order to evaluate these effects.

Finally, the loading was found to have an effect on the phase in the feed network as indicated by the fact that the frequency of the best axial ratio did not coincide with the frequency of the best match. The 90-degree phase shift generated by the feed network was not optimum for the structure when loaded and matched. To improve this, the feed should be tuned to compensate for the loading and maintain the 90 degrees once loaded. The best way to investigate this would be with a simulation tool like HFSS. The patch would have to be fed with two excitations from Ports 2 and 3 such that the phase between them could be controlled. In this way, the phase on each port could be varied and the effect on the quality of CP could be observed. This same test could also be performed experimentally although feeding from two ports is typically a challenge.

CHAPTER 6: Discussion and Recommendations

6.1 Synopsis

6.1.1 Summary of Work

This thesis has investigated dielectric loading as a technique to miniaturize a wide band microstrip patch antenna and hence make it a better alternative to helices and crossed-drooping dipoles for mobile satcom applications.

A detailed characterization of the linearly polarized dielectric-loaded patch antenna was presented and the effect of each physical parameter was described. Trends were recorded to document how the loading was used to control the frequency reduction as well as the matching and impedance bandwidth of the structure. These observations were collated into a concise set of design guidelines which were successfully tested. The results from these tests highlighted the fact that meeting an exact set of specifications requires time since significant experimental manipulation was required.

Circular polarization was also investigated and it was shown how two design iterations were required in order to improve the quality of the CP. Several issues were identified for further investigation, including an analysis of how the feed phasing is altered with the dielectric-load pieces.

6.1.2 Major Thesis Accomplishments

This investigation into dielectric-loaded patch antennas has demonstrated the potential for the dielectric-loaded patch antenna as a suitable candidate for mobile satcom applications. The major results of this work are the following:

- A compact LP dielectric-loaded patch antenna was achieved.
- Aperture-coupling was shown to reduce cross-polarization and pattern distortion that are typical with probe-coupled patches at L-band.
- A compact CP dielectric-loaded patch antenna was investigated.

A linearly polarized structure was shown to achieve a 32% reduction in frequency with an impedance bandwidth better than 8%. The patch dimensions were on the order of 5.5 cm by 5.5 cm with a height between 6 and 10 mm, depending on the desired bandwidth. These dimensions are more compact than any of the antennas currently under consideration and also smaller than those of a probe fed patch which is approximately 8 cm by 8 cm.

Achieving a match to 50 Ω with an aperture-coupled thick-air patch at L-band frequencies was demonstrated. Placing dielectric over the slot enabled the coupling to reach the patch and hence provide the match which, until now, was difficult. This was an important result since aperture-coupling can now be used to overcome the probe radiation problems that have been characteristic with L-band patches on thick-air substrates.

Finally, a circularly polarized structure was shown to achieve a frequency reduction on the order of 35% with an impedance bandwidth just under 8%. The quality of the circular polarization was acceptable but, with further investigation, it may be improved. The minimum axial ratio at boresight was 4 dB and the maximum CP gain was 3 dBic. The axial ratio bandwidth was relatively small but could likely be improved.

6.2 Discussion of Future work

There is a great deal of work that remains in the realm of dielectric-loaded patch antennas. Such work might include the following:

- A detailed investigation of the slot and stub dimensions in the linearly polarized structure should be pursued. All measurements in this thesis were performed at one set of slot and stub dimensions and, as noted on many occasions, it may not have been optimal for the loaded structure.
- Further work on the circularly polarized structure needs to be performed. The emphasis should be on the phase required in the feed network and on analyzing the ground plane effects. To be effective for mobile satcom applications, the quality of the circular polarization must be improved.
- Numerical modeling of the structure should be continued such that better models are achieved and simulation times are decreased. Other simulation packages should also be considered since some of the new software may be more user-friendly. A reliable simulation tool is needed to eliminate the tedious experimental optimization that is currently required to design these structures.

- Dual-band and dual polarization possibilities should be explored. Varying the loading seen by each mode of the CP patch presents a number of interesting scenarios including the possibility of controlling the frequency of each mode and hence their separation. Different polarizations may also be achieved in this manner.

APPENDIX 1

DRA Equations for $TE_{11\delta}$ Mode:

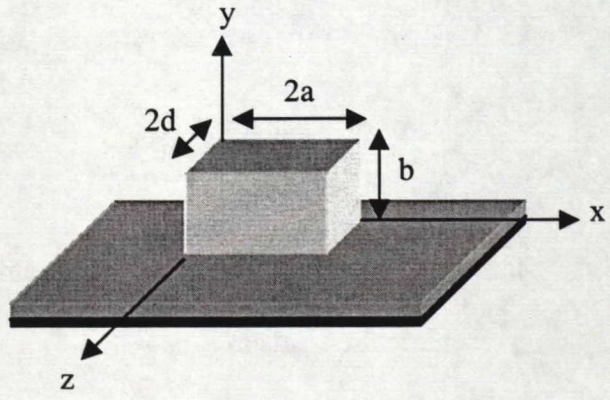

$$k_o = \frac{2\pi \cdot f_o}{c}$$

$$k_x = \frac{\pi}{2a}$$

$$k_y = \frac{\pi}{2b}$$

$$k_z = \sqrt{E_r k_o^2 - k_x^2 - k_y^2}$$

$$k_z \tan(k_z d) = \sqrt{(E_r - 1)k_o^2 - k_z^2}$$

$$\delta = \frac{k_z 2d}{\pi}$$

where c=3.8x10^8 m/s and f_o is the resonant frequency of the DRA in Hz.

Sample Calculation:

Chosen values:

2d = 50 mm
2a = 50 mm
b = 32 mm
E_r = 10

Calculated results:

$k_x = 98.17$ rad/m
$k_y = 62.83$ rad/m
$k_z = 59.03$ rad/m
$k_o = 33.73$ rad/m
$\delta = 0.601$ rad
$f_o = 1.61$ GHz

APPENDIX 2:

A2.1 High Frequency Structure Simulator (HFSS)

Hewlett Packard's HFSS version 5.3 is an EM modeling tool for arbitrarily-shaped, passive, 3D structures. The engine uses the finite element method to solve Maxwell's equations by dividing the problem space into thousands of smaller regions and representing the fields in each with a local function.

There are many issues involved in the correct modeling of any given structure which demands that the user have a firm grasp of how the solver works. As will be described in detail, it is for these reasons that HFSS will remain a tool outside of the normal design process.

A2.1.1 Modeling Considerations for the Dielectric-Loaded Patch Antenna

Modeling of the dielectric-loaded microstrip patch structure was a challenging problem that required significant consultation with the HP HFSS technical support staff. The idea was to have the modeled structure be as close to the actual design as possible for later comparisons with the measured results. This task was far more involved than simply drawing the objects correctly. Setting the boundary conditions and optimizing the mesh density in critical areas were two of the most important HFSS modeling issues.

A2.1.1.1 Boundary Conditions

Defining boundary conditions properly in HFSS structures is essential to the success of the simulation. By default, the structure is assumed to be completely encased in a conductive shield, also known as the background. No energy is allowed to propagate to or

from the background unless specific boundary conditions that allow propagation are applied somewhere within the structure. The three most important conditions to establish are the port, ground plane, and radiation boundaries.

Port boundary conditions allow energy to enter and leave the structure. They have to be exposed to the background and thus cannot be on the interior of the structure. Since the dielectric-loaded patch antenna structure is a radiation problem, it was only necessary to define one port. It covered the region from the air above the microstrip line to the ground plane, as shown in the gray region of Figure A2.1 where the bottom half of the structure is illustrated in a front view.

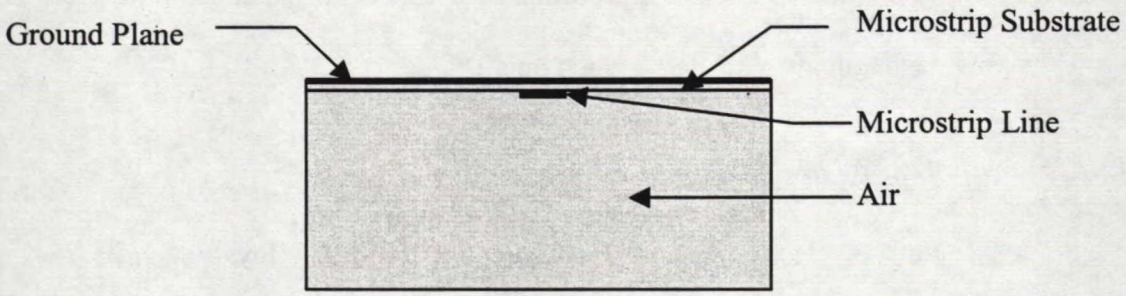

Figure A2.1: Port Boundary Location

The ground plane boundary acts as a perfect conductor that is infinite in size and infinitely thin. It must be coincident with the background and can only be applied to a 2D plane. This had serious implications when it came to defining the dielectric-loaded patch antenna structure since both sides of the ground plane were in contact with part of the structure; the microstrip substrate was underneath the ground plane and the dielectric loading as well as the patch antenna were above it. Since this boundary needed to be coincident with the background, it was unacceptable and not used.

The ground plane had to be finite in size and defined as a conductor boundary, analogous to assigning a "lossy" metal material to an object. Although it was possible to model a finite thickness ground plane, it was decided to initially keep it as a 2D plane to avoid the complications that will be discussed in section A2.1.2.

The radiation boundary is important in antenna problems to allow the waves to radiate into infinite space. This boundary must be an exterior object that is exposed to the background and located at least one-quarter of a wavelength away from the radiating source to allow the evanescent fields to decay.

The radiation boundaries in the dielectric-loaded patch antenna structure were defined as the sides and top of a box placed around the patch. The final location of the box was about a wavelength away from the patch on all sides.

A2.1.1.2 Mesh Density in Critical Areas

To generate an electromagnetic field solution, HFSS employs the finite element method. The general premise of this method is the division of the problem space into thousands of smaller regions with the fields in each region being represented by a local function.

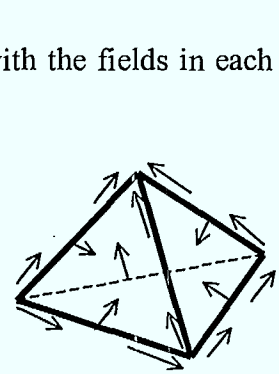

Figure A2.2: Field Quantities on a sample Tetrahedron

In HFSS, the problem space division is performed automatically and the subdivided elements are tetrahedra, each formed by four equilateral triangles as shown in Figure A2.2. A mesh is thus defined as the group of tetrahedra. The value of the vector field

quantity at points inside each tetrahedron is interpolated from the field quantities at the vertices. HFSS stores the components of the fields that are tangential to the three edges of the tetrahedron at each vertex.

Since the tetrahedra of the mesh in HFSS are located based on the vertices of the objects in the structure, it follows that more vertices in a given area would lead to a denser mesh in that area. Additional vertices were added in two ways, the first being the drawing of virtual boxes around the objects in the critical area. A virtual box is a box filled with air, that does not change the physical structure of the antenna. In the dielectric-loaded patch antenna configuration, a virtual box was placed around the slot area to ensure that a denser mesh would be formed near those critical fields.

The second way to increase the number of vertices was to divide some of the objects into multiple pieces and then stack them to recreate the original object, as illustrated in Figure A2.3. The material properties of the divided objects would all be the same and there would be no physical change to the structure. However, HFSS would place more tetrahedra in the area because it would see more vertices. This technique was used for all the dielectric load pieces that were placed under the patch with particular attention given to the piece placed over the slot.

Figure A2.3: Division of Objects for Increased Mesh Density

A2.1.2 Modeling Problems and Limitations

Throughout the course of modeling the dielectric-loaded patch antenna, several problems were recognized and most remained unresolved. These problems revealed the obvious limitations of the HP HFSS software and indicate how it is ineffective as an optimization tool.

The following problems were encountered:

- ground plane thickness,
- double resonance phenomena,
- lengthy simulation times.

A2.1.2.1 Ground Plane Thickness

In the earlier simulations, both the ground plane and the slot were simulated as being infinitely thin whereas they have an actual finite thickness, 0.017 mm. This extra thickness would cause a small air gap to be present between the dielectric load piece and the microstrip feed.

It was expected that this air gap would have a large impact on the effective relative permittivity beneath the patch and would shift the resonant frequency slightly. This effect is shown mathematically in the following example:

> *A 0.017 mm air gap combined with an E_r=40 dielectric piece over the slot will reduce the effective permittivity over the slot to 30. These numbers were obtained by considering the structure to be a sort of parallel-plate capacitor with two dielectric layers, as shown in Figure A2.4.*

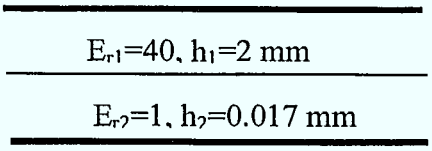

***Figure A2.4**: Parallel-Plate Capacitor Representation of Structure*

The two dielectric layers behave as two capacitors in series and thus would add according to:

$$\frac{1}{C_T} = \frac{1}{C_1} + \frac{1}{C_2} \qquad (A2\text{-}1)$$

where C_T is the total capacitance and C_1 and C_2 are the capacitances of layers one and two respectively. By replacing the capacitances with the appropriate version of the expression:

$$C = \frac{E_o E_r A}{h} \qquad (A2\text{-}2)$$

where h is the thickness of the dielectric layer and A is the area, then the following relationship for the effective relative permittivity results:

$$E_{reff} = \frac{h_1 + h_2}{\frac{h_1}{E_{r1}} + \frac{h_2}{E_{r2}}} \qquad (A2.3)$$

Filling in the correct values for the layer thickness and dielectric constant results in $E_{reff} = 30$.

Including the 0.017 mm thickness into the simulations effectively stopped the patch from resonating within a span of 5 GHz. The problem was speculated to be due to how the slot was defined inside the ground plane and the structure is currently being re-viewed by the HP technical support staff for possible modeling flaws.

A2.1.2.2 Double Resonance Phenomenon

From the very beginning, nearly all simulations of the dielectric-loaded patch antenna resulted in two resonant frequencies within 0.1 GHz of each other, near the correct resonant frequency. Figure A2.5 illustrates an example of this effect by showing the HFSS simulated return loss results overlaid on the measured results for the exact same loading configuration (the magnitude of S_{11} is plotted on the vertical axis). With the exception of the anomaly at the resonant frequency, the curves are fairly similar.

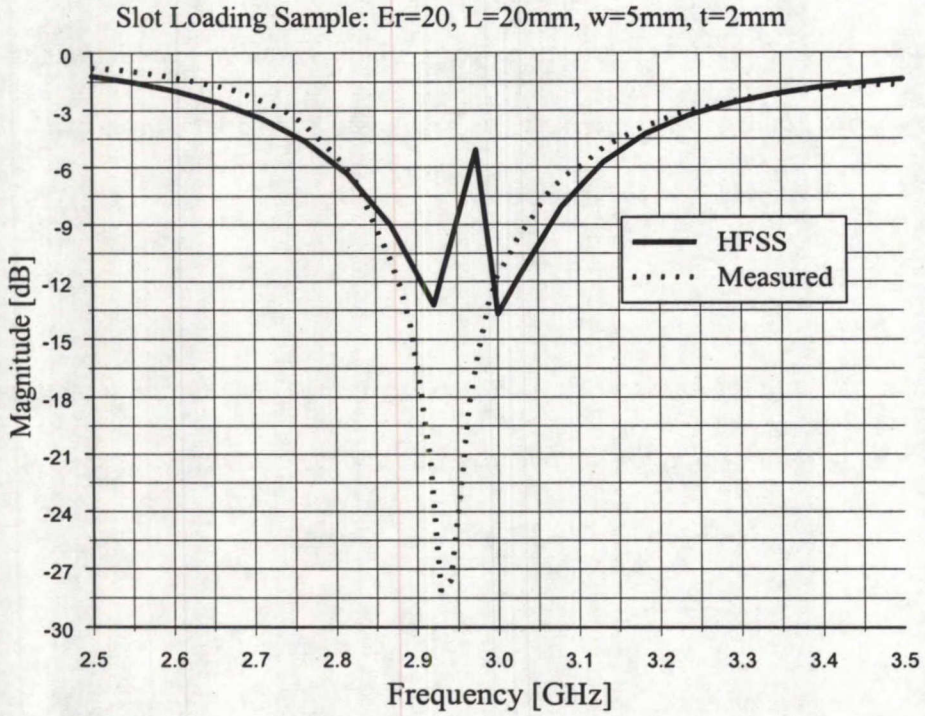

Figure A2.5: HFSS versus Measured Return Loss Characteristic

Initially, the cause of the double resonance was assumed to be due to a lack of points used in the generation of the plots, but a significant increase in the number of frequency points had no effect other than to further smooth the curves. Much time was spent investigating the reason for this double resonance phenomenon and several theories were proposed:

- *Excitation of a degenerate mode?*
- *Radiation box size?*
- *Mesh Density?*

Excitation of a degenerate mode was a possibility since the patch was square and, with the proper perturbation of the fields, a degenerate mode could be excited. This theory was disproved since a closer look at the fields underneath the patch indicated that only one mode was excited. Also, the co-polarized radiation patterns were quite different in the E and H planes where they would have been nearly the same had a degenerate mode been excited.

HP recommends that the radiation box be at least a quarter wavelength away from the radiating structure. It was thought that the double resonance could be due to the radiation box not being far enough away and thus picking up some energy from the evanescent fields that were not completely decayed. Simulations were performed with the radiation box placed nearly a full wavelength away. This was successful in reducing the degree of the double resonance but was unsuccessful in its elimination. After a certain size, the effect of the larger radiation box diminished as expected.

Significant investigations were performed to determine if the mesh density around the thinner objects was the cause of the double resonance. Virtual boxes were placed around the dielectric inserts and some of the thinner objects were divided and stacked but the results did not improve. Changing the seeding (increasing or decreasing the amount of extra points added to the coarse mesh) of some of the structures which initially displayed double resonances did have a positive effect and seemed to eliminate the problem. Other structures, however, were not affected by the increased seeding.

This double resonance was a recurring problem most probably related to the complexity of the structure and the many differences in field strength beneath the patch that required fine meshing. Achieving a fine mesh was difficult with the large aspect ratios inherent to the modeled structure. The problem remains unresolved and the HP technical support staff are currently reviewing the modeled structure.

A2.1.2.3 Lengthy Simulation Time

The most important reason that HFSS is not suitable as an optimization tool is the lengthy amount of time required to complete a simulation. For the dielectric-loaded patch structure under consideration, each simulation lasted for an average of about three to four days. These types of simulation times were due to the fine discretization required in the finite element mesh. The majority of this simulation time was spent refining the mesh with a comparatively smaller portion involved in actually solving for the fields at each frequency point.

APPENDIX 3:

Procedure to Calculate the Gain of a Circularly Polarized Antenna [61]:

Since circularly polarized standard-gain antennas do not exist, an accurate gain procedure using linearly polarized standard-gain antennas must be used. This procedure is equally applicable to antennas that are linearly or circularly polarized since both are degenerate cases of elliptical polarization. This method makes a direct comparison between signal levels of a known, standard-gain antenna and the antenna under test where the standard-gain antenna is referenced to an isotropic-source. The procedure is as follows:

1. Plot the antenna-radiation patterns as shown in Figure A3.1.

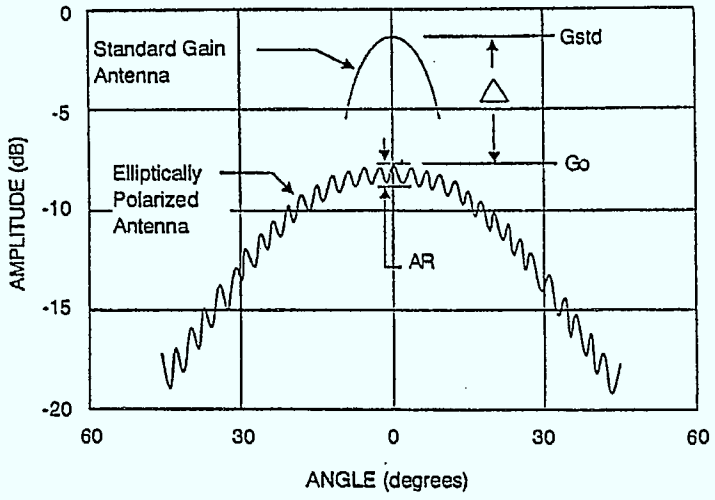

Figure A3.1: Radiation Pattern of an Elliptically Polarized Antenna (from [61])

2. Find the gain to linear polarization at the peak of the axial ratio (G_o) by subtracting delta (Δ) from the standard-gain antenna value (G_{std}).

$$G_o = G_{std} - \Delta \,\text{dBiL} \quad \text{(A3.1)}$$

3. Determine the axial ratio (AR) of the antenna under test, in dB.

4. Calculate the gain-correction factor (G_c) to account for the axial ratio effects:

$$G_c = 20\log\left(\frac{1}{2}\left[1+10^{-(AR/20)}\right]\right)\text{dB} \quad \text{(A3.2)}$$

5. The gain of the antenna under test can then be found from:

$$G_A = G_o + G_c + 3\,\text{dBic} \quad \text{(A3.3)}$$

Sample Calculation:

Based on results shown in Chapter 5, Figures 5.16, 5.17:

Given:

0 Degree Cut
f = 1.78 dB
G_{std}=7.7 dB at boresight
AR = 5 dB at boresight
Δ=6 dB

Calculated:

$G_o = 7.7 - 6 = 1.7$ dBiL
$G_c = -2.145$ dB
G_A = 2.55 dBic

REFERENCES

[1] G. Heftman, "The Wide World of Wireless Heads for Generation 3," *Microwaves & RF*, pp. 31-39, August 1998.

[2] P. Horkin, "Air Traffic Management System Design Using Satellite Based Geo-Positioning and Communications Assets," *Proceedings of 4th International Mobile Satellite Conference (IMSC)*, Ottawa, Canada, June 1995, pp. 198-203.

[3] D. Bell, "Global Tracking and Inventory of Military Hardware via LEO Satellite: A System Approach and Likely Scenario," *Proceedings of 4th International Mobile Satellite Conference (IMSC)*, Ottawa, Canada, June 1995, pp. 204-211.

[4] R. Cochetti, *Mobile Satellite Communications Handbook*, Quantum Publishing Inc., California, 1995.

[5] S. Ohmori, H. Wakana, S. Kawase, *Mobile Satellite Communications*, Chapters 1 & 4, Artech House, Boston, 1998.

[6] S. Ohmori, "Vehicle Antennas for Mobile Satellite Communications," *IEICE Transactions*, vol. E 74, No. 10, pp. 3210-3221, October 1991.

[7] W.J. Vogel, J. Goldhirsh, "Mobile Satellite System Propagation Measurements at L-band using MARECSB2," *IEEE Trans. Antennas and Propag.*, AP-38, pp.259-264, 1990.

[8] Y. Hase, W.J. Vogel, J. Goldhirsh, "Fade/Non-fade Characterisitics in Land Mobile Satellite Communications," IEEE Trans. Commun., vol. 39, no.5, May 1991.

[9] K. Woo, "Performance of a Family of Omni and Steered Antennas for Mobile Satellite Applications," *Proceedings of International Mobile Satellite Conference (IMSC)*, Ottawa, Canada, June 1990, pp. 540-546.

[10] B. Pattan, *Satellite-Based Cellular Communications*, McGraw-Hill, New York, 1998.

[11] A.T. Adams, "The Quadrifilar Helix Antenna," *IEEE Trans. Antennas and Propag.*, AP-22, pp. 173-178, March 1974.

[12] K. Fujimoto, J. R. James, *Mobile Antenna Systems Handbook*, Artech House, Norwood, MA, 1994.

[13] R.B. Waterhouse, "Small Microstrip Patch", *Electron. Lett.*, vol. 31, pp. 604-605, 1995.

[14] I. Park, R. Mittra, "Aperture-coupled Small Microstrip Antenna," *Electron. Lett.*, vol. 32, pp. 1741-1742, 1996.

[15] T.K. Lo, "Miniature Aperture-Coupled Microstrip Antenna of Very High Permittivity," Electron. Lett., vol. 33, pp.9-10, 1997.

[16] D.M. Kokotoff, R.B. Waterhouse, J.T. Aberle, "An Annular Ring Coupled to a Shorted Patch," *IEEE Trans. Antennas and Propag.*, AP-45, pp.913-914, 1997.

[17] R.B. Waterhouse, "Printed Antennas Suitable for Mobile Communication Handsets," *Electron. Lett.*, vol. 33, pp.1831-1832, 1997.

[18] J. George, "Dielectric-Resonator-Loaded Microstrip Antenna for Enhanced Impedance Bandwidth and Efficiency," *Microwave and Optical Tech. Lett.*, vol.17, no. 3, February 20 19998.

[19] A. Petosa, "Dielectric Resonator Antennas for Mobile Satellite Applications," Proceedings of 5th International Mobile Satellite Conference (IMSC), Pasadena, CA, June 1997, pp. 363-368.

[20] M. Cooper. M. Eng. Thesis: Investigation of Current and Novèl Rectangular Dielectric Resonator Antennas for Broadband Applications at L-band Frequencies, Carleton University, Canada, 1997.

[21] C.A. Balanis, *Antenna Theory Analysis and Design*: Second Edition, John Wiley &Sons, New York, 1997.

[22] I.J. Bahl, P. Bhartia, *Microstrip Antennas*, Artech House, Dedham MA, 1980.

[23] G.A. Deschamps, "Microstrip Microwave Antennas," *Proceedings of the 3rd USAF Symposium on Antennas*, 1953.

[24] J.Q. Howell, "Microstrip Antennas," *IEEE AP-S Int. Symp. Digest*, 1972, pp.177-180.

[25] R.E. Munson, "Conformal Microstrip Antennas and Microstrip Phased Arrays," *IEEE Trans. Antennas and Propag.*, AP-22, pp. 74-78, 1974.

[26] J.R. James, P.S. Hall, C. Wood, *Microstrip Antenna: Theory and Design*, Peter Peregrinus Ltd., New York, 1981.

[27] C.A. Balanis, *Advanced Engineering Electromagnetics*, John Wiley & Sons, New York, 1989.

[28] H. Pues, A, Van de Capelle, "Accurate Transmission-Line Model for the Rectangular Microstrip Antenna", 1984 IEE Reprinted in: K.C. Gupta, A. Benalla, *Microstrip Antenna Design*, Artech House Inc, Norwood MA, c1988.

[29] A.K. Bhattacharyya, M. Tech, R. Garg, "Generalized Transmission –Line Model for Microstrip Patches," 1985 IEE Reprinted in: K.C. Gupta, A. Benalla, *Microstrip Antenna Design*, Artech House Inc, Norwood MA, c1988.

[30] D.M. Pozar, "Microstrip Antenna Aperture-Coupled to a Microstrip Line," *Electron. Lett.*, vol. 21, pp. 49-50, 17 January 1985.

[31] P. Bhartia, K.V.S. Rao, R.S. Tomar, *Millimeter-wave Microstrip and Printed Circuit Antennas*, Chapter 5, Artech House Inc., Norwood MA, 1991.

[32] D.H. Schaubert, "A Review of Some Microstrip Antenna Characteristics," printed in: D. Pozar, D. Shaubert, *Microstrip Antennas*,

[33] P.L. Sullivan, D.H. Schaubert, *Analysis of an Aperture-Coupled Microstrip Antenna*, Dept. Elect. Comput. Eng., Univ. Massachusetts, Amherst, MA, ANTLAB Rep. No. 8501, July 1985.

[34] A. Ittipiboon, "A Modal Expansion Method of Analysis and Measurement on Aperture-Coupled Microstrip Antennas," *IEEE Trans. Antennas and Propag.*, AP-39, pp.1567-1574, 1991.

[35] K.R. Carver, "Microstrip Antenna Technology," *IEEE Trans. Antennas and Propag.*, AP-29, pp.2-24, 1981.

[36] Y. Hwang, Y.P. Zhang, "Planar Inverted F antenna Loaded with High Permittivity Material," *Electron. Lett.*, vol. 31, pp. 1710-1712, 1995.

[37] T.K.Lo, "Miniature Aperture-Coupled Microstrip Antenna of Very High Permittivity," *Electron. Lett.*, vol. 33, pp. 9-10, 1997.

[38] N.G. Alexopoulos, D.R. Jackson, "Fundamental Superstrate (cover) Effects on Printed Circuit Antennas," *IEEE Trans. Antennas and Propag.*, AP-32, pp.807-815, 1984.

[39] M. Sanad, "Effect of the Shorting Posts on Short Circuit Microstrip Antennas," *Proc. IEEE Antenna Propag. Symp.*, 1994, pp. 794-797.

[40] R. Waterhouse, "Small Microstrip Patch Antenna," *Electron. Lett.*, vol. 31, pp. 604-605, 1995.

[41] I. Park, R Mitra, "Aperture-Coupled Small Microstrip Antenna," *Electron. Lett.*, vol. 32, pp. 1741-1742, 1996.

[42] G. Kossiavas, A. Papiernik, "A Quarter-Wavelength Antenna with Superposed Square Patches," *Microwave Journal*, pp.82-86, June 1998.

[43] R.B. Waterhouse, "Stacked Shorted Patch Antenna," *Electron. Lett.*, vol. 34, pp. 612-614, 1998.

[44] R.B. Waterhouse, "Broadband Stacked Shorted Patch," *Electron. Lett.*, vol. 35, pp. 98-100, 1999.

[45] J. Ollikainen, M. Fischer, "Thin Dual-Resonant Stacked Shorted Patch Antenna for Mobile Communications," *Electron. Lett.*, vol. 35, pp. 437-438, 1999.

[46] R.B. Waterhouse, "Small Printed Antennas with Low Cross-Polarized Fields," *Electron. Lett.*, vol. 33, pp. 1280-1281, 1997.

[47] K. Wong, Y. Lin, "Small Broadband Rectangular Microstrip Antenna with Chip-Resistor Loading," *Electron. Lett.*, vol. 33, pp. 1593-1594, 1997.

[48] C. Huang, J. Wu, "Gain-enhanced Compact Broadband Microstrip Antenna," *Electron. Lett.*, vol. 34, pp. 138-139, 1998.

[49] V. Palanisamy, R. Garg, "Rectangular Ring and H-Shaped Microstrip Antennas-Alternatives to Rectangular Patch Antennas," *Electron. Lett.*, vol. 321, pp. 874-876, 1985.

[50] D. Singh, P. Gardner, P.S. Hall, "Miniaturized Microstrip Antenna for MMIC Applications," *Electron. Lett.*, vol. 33, pp. 1830-1831, 1997.

[51] J. George, M. Deepukumar, "New Compact Microstrip Antenna," *Electron. Lett.*, vol. 32, pp. 508-509, 1996.

[52] S.A. Bokhari, "A Small Microstrip Patch Antenna with a Convenient Tuning Option," *IEEE Trans. Antennas and Propag.*, AP-44, pp.1521-1527, 1996.

[53] C. Huang, J. Wu, "High-Gain Compact Circularly Polarized Microstrip Antenna," *Electron. Lett.*, vol. 34, pp. 712-713, 1998.

[54] K. Wong, J. Wu, "Single-Feed Small Circularly Polarized Square Microstrip Antenna," *Electron. Lett.*, vol. 33, pp.1833-1834, 1997.

[55] H. Iwasaki, "A Circularly Polarized Small-Size Microstrip Antenna with a Cross Slot," *IEEE Trans. Antennas and Propag.*, AP-44, pp.1399-1401, 1996.

[56] W. Chen, C. Wu, K. Wong, "Compact Circularly Polarized Microstrip Antenna with Bent Slots," *Electron. Lett.*, vol. 34, pp.1278-1279, 1998.

[57] R.F. Harrington, *Time-Harmonic Electromagnetic Fields*, McGraw-Hill Book Company, New York, 1961.

[58] Hewlett Packard, *High Frequency Structure Simulator 5.0*, User's Reference, HP part no. 85180-90123, August 1997.

[59] Boulder Technologies Inc., *Ensemble*, User's Guide, March 1997.

[60] A. Petosa, A. Ittipiboon, N.Gagnon, "Suppression of Unwanted Probe Radiation in Wide-Band Probe-Fed Microstrip Antennas," *IEE Electron. Lett.*, vol. 35, pp.355-357, Mar. 1999.

[61] D. S. Dunn, E. P. Augustin, "Measuring the Gain of Circularly or Elliptically Polarized Antennas," *IEEE Antennas and Propag. Magazine*, vol. 36, no. 1, pp.49-51, 1994.